

# Domain wall fermions

Thomas Blum<sup>a</sup> and Yigal Shamir<sup>b</sup>

<sup>a</sup>Department of Physics, University of Connecticut, Storrs, CT 06269, USA

<sup>b</sup>Raymond and Beverly Sackler School of Physics and Astronomy,  
Tel Aviv University, 69978, Tel Aviv, Israel

We introduce the formulation of domain wall fermions in the context of lattice QCD. We prove the recovery of exact chiral symmetry in the limit of an infinite fifth direction, and derive the effective four-dimensional operator satisfying the Ginsparg-Wilson relation obtained in this limit. We discuss the residual breaking of chiral symmetry for finite extent of the fifth direction, and how it is affected by spectral features of the Wilson kernel. We also discuss various improvements of domain wall fermions including notably Möbius fermions. These notes are a chapter contributed to the on-line book “Lattice QCD at 50 years” (*LQCD@50*).<sup>\*</sup>

---

<sup>\*</sup>*LQCD@50* is edited by Tanmoy Bhattacharya, Maarten Golterman, Rajan Gupta, Laurent Lellouch, and Steve Sharpe.

# 1 Introduction

From the beginning of lattice field theory in the mid 1970s it was realized that putting fermions on the lattice is a difficult problem. The simplest way to see this is to note that continuum fermions obey a first-order differential equation, which is linear in the momentum. For example, in one spatial dimension the dispersion relation of a single-component massless fermion is  $E = \pm p$ . If we discretize space (keeping the time coordinate continuous), we have to replace the continuum derivative by a difference operator. Using the nearest-neighbor lattice difference operator yields the dispersion relation  $E = \pm(1/a) \sin(ap)$  where  $a$  is the lattice spacing. This dispersion relation conforms to the periodicity of the lattice's Brillouin zone,  $0 \leq p \leq 2\pi/a$ . For  $ap \ll 1$ , the lattice dispersion relation is  $E = \pm p(1 + O(ap)^2)$ , which reproduces the linear continuum dispersion relation up to small discretization effects. The problem is that now  $E(p)$  vanishes not only for  $p = 0$  but also for  $p = \pi/a$ . In the vicinity of the latter point,  $E = \mp q(1 + O(aq)^2)$  where the momentum is effectively  $q = p - \pi/a$ . Hence the dispersion relation is again linear up to discretization effects, but with an opposite slope, hence, opposite chirality.<sup>1</sup> Instead of the single massless fermion of definite chirality we initially had in the continuum theory, the lattice theory describes two massless fermions with opposite chiralities. This is the well-known *doubling problem*.

Alternatively, one can understand fermion doubling by considering the implications of anomalies for a lattice theory. The basic rule is very simple. The lattice is a non-perturbative regulator. Hence, any symmetry that is exact on the lattice will remain so in the continuum limit. It follows that the lattice theory *must not* have exact chiral symmetry (if the chiral transformation has the same form as in the continuum) otherwise it will be impossible to reproduce the axial anomaly in the continuum limit!

The doubling problem was formalized in a series of “no go” theorems [1, 2, 3, 4, 5], which clarify the conditions under which doubling is unavoidable. We comment that fermion doubling can be avoided by using non-local lattice difference operators. However, this invariably leads to various inconsistencies when the fermions are coupled to a gauge field (see, *e.g.*, Ref. [6] and references therein).

Early on, two basic strategies emerged for dealing with the doubling problem. The first strategy is to live with it but to try to minimize it. This leads to staggered fermions, a single-component lattice field which, in four dimensions, yields four Dirac fermions in the continuum limit. Apart from describing several, and not just one, Dirac fermions, also the flavor symmetry structure of the resulting continuum theory is not manifest in the lattice theory. For an introduction to staggered fermions we refer to a companion chapter of the *LQCD@50* book by Golterman [7], as well as to Ref. [8].

The alternative strategy avoids doubling by breaking chiral symmetry explicitly on the lattice, and restoring it only in the continuum limit. This is how Wilson fermions work. The advantage over staggered fermions is that vectorial flavor symmetries remain manifest, the same as in the continuum. The price is that in the

---

<sup>1</sup>In one spatial dimension, the  $\pm$  chirality corresponds to the fermion being a right-mover or a left-mover.

absence of a chiral symmetry to protect it at the lattice level, the bare mass suffers a large  $O(1/a)$  additive renormalization. Other chirally sensitive observables suffer similarly large discretization effects. For an introduction to Wilson fermions we refer to a companion chapter of the *LQCD@50* book by Dalla Brida.

Domain wall fermions were introduced by Kaplan much later, in the early 1990s [9]. A posteriori, one might loosely describe the *raison d’être* of domain wall fermions as “maximum chiral symmetry at minimal doubling.” To what extent this goal has been achieved depends on whether the target continuum gauge theory is a vector-like theory like QCD; or, alternatively, a chiral gauge theory.

For QCD the goal has been fully achieved. Using domain wall fermions for QCD, or for QCD-like theories, is the subject of this introduction. In this case a single domain-wall fermion field gives rise to a single quark field in the continuum limit. The vector flavor symmetry is fully preserved as for Wilson fermions. Chiral symmetry is also fully preserved when a suitable limit is taken, leaving “just enough” room to reproduce the axial anomaly, as in the continuum. The main price to pay is that numerical simulations of domain wall fermions are more costly.

For chiral gauge theories (Kaplan’s original motivation) the situation is much more complicated. Chiral gauge theories are outside the scope of the *LQCD@50* book, and so we will only comment briefly on this topic in the concluding section.

Earlier texts on fermion methods, including in particular domain wall fermions, can be found for example in the book by DeGrand & DeTar [10].<sup>2</sup> Domain wall fermions are also discussed in a set of lecture notes by Kaplan [13]. For the closely related overlap fermions, once again we refer to the DeGrand & DeTar book, as well as to a review talk by Niedermayer [14]. Overlap fermions are also covered in a companion chapter of the *LQCD@50* book, written by DeGrand [15]. We refer to his chapter in particular for a more detailed discussion of the Ginsparg-Wilson relation [16] and its consequences.

## 2 Why domain wall fermions

Domain wall fermions are a system in which a light fermion field is attached to a  $d$ -dimensional “defect” of a massive fermion theory in  $d + 1$  dimensions. For  $d < 4$ , domain wall fermions play a role in condensed matter physics. In this introduction we will consider only the case  $d = 4$  relevant for elementary particle physics. We begin in this section by introducing domain wall fermions in continuum  $(4 + 1)$ -dimensional euclidean space. In the next section we will turn to the lattice formulation of domain wall fermions.

Consider the following Dirac equation

$$(i\not{p} + \gamma_5 \partial_5 + m(s))\chi = 0 , \tag{2.1}$$

where we work in momentum space for the four physical coordinates, and in coordinate space for the fifth coordinate  $s$ . At this stage the fifth coordinate can take any

---

<sup>2</sup>See also Refs. [11, 12].

value,  $-\infty < s < \infty$ . We assume that the mass profile is

$$m(s) = \begin{cases} -M' & s \leq 0, \\ M & s \geq 0, \end{cases} \quad (2.2)$$

where  $M, M' > 0$ . The discontinuity of the mass profile at  $s = 0$  is called a domain wall.

The Dirac equation (2.1) has a right-handed (RH) zero mode. This homogeneous solution of the equation is a normalizable function of the fifth coordinate  $s$ , which is bound to the “domain wall” at  $s = 0$ ,

$$\chi(s) = e^{-m(s)} = \begin{cases} e^{M's} & s \leq 0, \\ e^{-Ms} & s \geq 0. \end{cases} \quad (2.3)$$

Notice the absence of a similar left-handed (LH) zero mode: the homogeneous solution  $e^{+m(s)}$  is not normalizable. Had we flipped the signs of  $M$  and  $M'$  simultaneously, the LH homogeneous solution would be normalizable, hence, a zero mode, whereas the RH homogeneous solution would be non-normalizable.

The five-dimensional fermion system has a conserved fermion number symmetry. This symmetry is neither vectorial nor axial: these notions exist only for an even number  $d$  of dimension, where one can construct a chirality matrix  $\propto \gamma_1 \gamma_2 \cdots \gamma_d$ , which anti-commutes with each of the individual  $d$ -dimensional Dirac matrices. However, let us consider the effective low-energy theory associated with a five-dimensional domain wall fermion. For the (free) domain-wall fermion system introduced above, this will be a (free) four-dimensional theory consisting of a single RH massless fermion. The effective four-dimensional theory inherits the fermion number symmetry; but since this symmetry has now only a RH fermion to act on, it effectively becomes a chiral symmetry!

Kaplan’s original idea was the realization that, since chiral symmetry does not exist in a continuum five-dimensional system, it should be possible to put this theory on the lattice using Wilson fermions without giving up on any (internal) symmetry of the continuum theory and without encountering fermion doubling. As long as the transition to the lattice preserves the zero mode that is bound to the domain wall, one expects that chiral symmetry will emerge in the low-energy effective theory on the lattice, just as it does in the continuum.

Infinites can be elusive, however. Before we turn to the lattice, let us try to recover the fermion system with an unbounded  $s$  coordinate introduced above as a limit of a finite-extent fifth dimension. To this end we will assume that the fifth coordinate takes values  $-L_5 \leq s \leq L_5$  with periodic boundary conditions in the fifth direction. The question is whether the limit  $L_5 \rightarrow \infty$  reproduces the system discussed above, or not. The mass profile introduced in Eq. (2.2) describes a single domain wall at  $s = 0$ . But, once we impose periodic boundary conditions in the  $s$  direction on the fermions, this effectively introduces *another* domain wall at  $s = L_5 = -L_5$ . It is easy to see that, if we disregard exponentially small effect on the order of  $e^{-ML_5}$  or  $e^{-M'L_5}$ , we now have not only a RH zero mode bound to the domain wall at  $s = 0$ , but also

a LH zero mode bound to the new domain wall at  $s = L_5 = -L_5$ . For  $L_5 \rightarrow \infty$  both zero modes become exact. The  $L_5 \rightarrow \infty$  system thus has one massless Weyl field of each chirality. This is different from the result of the earlier, formal treatment of the infinite- $s$  case, in which only one of the two zero modes, the one at  $s = 0$ , was “visible.”

As we will briefly discuss in the concluding section, the existence of an opposite-chirality zero mode within a careful treatment of the fifth direction is a major obstacle if the goal is to construct a chiral gauge theory. By contrast, for QCD this is not a problem at all, since each quark field consists of a RH and a LH component—just the light field content of the finite- $L_5$  system. Moreover, as we will see later on, the geometric separation of the RH and LH fields in the fifth direction still allows for global chiral symmetry to emerge in the limit  $L_5 \rightarrow \infty$ .

There is one more observation to make before we turn to the lattice theory. The parameters  $M$  and  $M'$  in the mass profile (2.2) are independent. Since we are ultimately interested in the physics of the light mode(s) bound to the domain wall(s), we can obtain a more economic formulation as follows. Focusing first on the RH zero mode near the  $s = 0$  domain wall, let us examine the effect of increasing  $M$  or  $M'$ . For  $M' \rightarrow \infty$ , the zero mode will be supported on  $s \geq 0$  only, whereas for  $M \rightarrow \infty$  it will be supported on  $s \leq 0$  only. As for the LH zero mode, in the first case it will be supported on  $s \lesssim L_5$ , while in the latter case it will be supported on  $s \gtrsim -L_5$ .

Either way, we can discard half of the range of the fifth coordinate. We end up with fifth coordinate  $0 \leq s \leq L_5$ , or alternatively,  $-L_5 \leq s \leq 0$ , with a RH and a LH zero modes that are now attached to the two four-dimensional boundaries. In the continuum, sending  $M \rightarrow \infty$  or  $M' \rightarrow \infty$  are equally valid choices. But as we will soon see, when we latticeize the system only one of these choices works.

In the next section we turn to the lattice formulation of domain wall fermions. For a more extensive discussion of continuum domain wall fermions, see the lecture notes of Ref. [13].

### 3 Lattice domain wall fermions: free theory

In this section we discuss free domain wall fermions in  $4 + 1$  dimensions, following Ref. [17]. As a first step, in Sec. 3.1 we consider a five-dimensional lattice with a semi-infinite fifth coordinate. We show that a single massless Weyl fermion exists on the four-dimensional boundary, for a suitable range of parameters.

When using a non-perturbative regularization such as the lattice, one must consider carefully not just the continuum limit but also the infinite volume limit. In particular, a semi-infinite fifth direction is an idealization, which must be reached as a suitable limit of a finite but large fifth direction. In Sec. 3.2 we discuss a finite fifth direction, and show that a second Weyl fermion with the opposite chirality exists on the “far” boundary. This is similar to what we already found in Sec. 2 for the continuum theory. We then confirm that the limit of a semi-infinite fifth direction can be reached without a “penalty” in the free theory. This situation will change in Sec. 4, where we consider the interacting theory. We also explain how to combine the

chiral fermions that reside on the two boundaries into a light Dirac fermion with an adjustable mass.

The domain-wall fermion operator is a five-dimensional Wilson operator designed to produce light chiral fields on four-dimensional “defects,” which, in our constructions, are just the four-dimensional boundaries of the five-dimensional bulk. When we speak about the Wilson (or Wilson-Dirac) operator, we will always refer to the four-dimensional operator unless explicitly stated otherwise.

### 3.1 Semi-infinite fifth direction

The domain-wall fermion matrix on a semi-infinite fifth direction is

$$D_{DW} = \begin{pmatrix} D-1 & P_R & 0 & 0 & 0 & \dots \\ P_L & D-1 & P_R & 0 & 0 & \dots \\ 0 & P_L & D-1 & P_R & 0 & \dots \\ 0 & 0 & P_L & D-1 & P_R & \\ \vdots & \vdots & & \ddots & \ddots & \ddots \end{pmatrix}, \quad (3.1)$$

This matrix structure corresponds to the fifth coordinate  $s$ , which we assume to take values  $s = 1, 2, \dots$ . We will mostly work in units of the four-dimensional lattice spacing, equivalently, set  $a = 1$ . For now, we keep the lattice spacing for the fifth direction  $a_5$  equal to the four-dimensional one.<sup>3</sup> Each entry is a  $4 \times 4$  matrix in Dirac space. In addition, if the lattice dimensions are  $L_1 \times L_2 \times L_3 \times L_4$  then each entry is also a  $V \times V$  matrix in four-dimensional space, with  $V = L_1 L_2 L_3 L_4$ .  $P_{R,L} = \frac{1}{2}(1 \pm \gamma_5)$  denote the chiral projectors.  $D$  is the four-dimensional Wilson-Dirac operator

$$D = D_K + M - W, \quad (3.2)$$

where in the free theory

$$D_K(x, y) = \frac{1}{2} \sum_{\mu} [\delta_{x+\hat{\mu}, y} - \delta_{x-\hat{\mu}, y}] \gamma_{\mu}, \quad (3.3)$$

$$W(x, y) = \frac{1}{2} \sum_{\mu} [2\delta_{xy} - \delta_{x+\hat{\mu}, y} - \delta_{x-\hat{\mu}, y}]. \quad (3.4)$$

We use Greek indices for the four physical dimensions, and the sums are over  $\mu = 1, \dots, 4$ . The  $\gamma_{\mu}$  matrices satisfy the euclidean Dirac algebra  $\{\gamma_{\mu}, \gamma_{\nu}\} = 2\delta_{\mu\nu}$ . The four-dimensional coordinates are labeled  $x, y$ , while  $\pm\hat{\mu}$  moves to the next site in the positive or negative  $\mu$  direction. Here  $D_K$  is the usual nearest-neighbor discretization of the massless continuum Dirac operator  $\not{\partial}$ , while the Wilson term  $W$  is a lattice discretization of the continuum laplacian. In momentum space

$$D_K(p) = i \sum_{\mu} \gamma_{\mu} \sin(p_{\mu}), \quad (3.5)$$

$$W(p) = \sum_{\mu} (1 - \cos(p_{\mu})). \quad (3.6)$$

---

<sup>3</sup>For generalizations that allow for  $a_5/a \neq 1$ , see Sec. 7.

We will also use the notation  $D_K(p) = i\vec{\not{p}}$ , with  $\bar{p}_\mu = \sin(p_\mu)$ . Taken alone, the operator  $D_K(p)$  exhibits the familiar doubling problem, as it vanishes in all 16 “corners”  $p_0$  of the Brillouin zone, defined by  $\sin(p_{0,\mu}) = 0$  for all  $\mu$ . The Wilson term is a momentum dependent mass term that gives the 15 doublers a mass proportional to the lattice cutoff at the price of breaking chiral symmetry explicitly, while the fermion at the origin of the Brillouin zone remains massless in the free theory.

Apart from the presence of boundaries, the domain-wall fermion operator is just the Wilson-Dirac operator in five dimensions, whose structure follows immediately by taking the coordinates and the index  $\mu$  in Eqs. (3.3) and (3.4) to be five-dimensional. In any dimension, the most general form of the Wilson-Dirac operator is  $D_K + M - rW$  where  $r$  is the Wilson parameter. For  $r = 1$ , hopping in the fifth direction<sup>4</sup> is constrained by the chiral projectors  $P_{R,L}$ , as seen in Eq. (3.1). When  $r \neq 1$  the hopping in the fifth direction is not constrained by the chiral projectors and the structure of the zero modes gets more complicated [17]. In this introduction we set  $r = 1$  unless otherwise stated.

In the context of domain wall fermions, the Wilson-Dirac operator  $D$  of Eq. (3.2) is often called the *Wilson kernel*. Notice that the Wilson term  $W$  is a positive operator. The parameter  $M$ , called the *domain wall height*, is given by  $M = -m_0$ , where  $m_0$  is the bare Wilson fermion mass in the convention where  $W + m_0 \geq 0$  when  $m_0 \geq 0$ . We recall that because of the explicit breaking of chiral symmetry by the Wilson term, the bare mass  $m_0$  suffers a large additive renormalization when lattice QCD is formulated using Wilson fermions. Features of domain wall fermions which are related to the way the Wilson-fermion bare mass renormalizes will be discussed later on, in Sec. 5.1 and Sec. 6.2.

As we will see next, for domain wall fermions we need positive  $M$ , or equivalently, negative  $m_0$ . This implies that the operator  $W - M = W + m_0$  does not have a definite sign, a property called *super-criticality* of the Wilson kernel. Apart from playing a crucial role in the very existence of the light chiral modes, super-criticality has additional important consequences that we will encounter later in this introduction.<sup>5</sup>

In order to find the spectrum of domain wall fermions we go to momentum space for the four physical dimensions. The domain-wall fermion matrix (3.1) becomes

$$D_{DW}(p) = \begin{pmatrix} -b(p) + i\vec{\not{p}} & P_R & 0 & 0 & 0 & \dots \\ P_L & -b(p) + i\vec{\not{p}} & P_R & 0 & 0 & \dots \\ 0 & P_L & -b(p) + i\vec{\not{p}} & P_R & 0 & \dots \\ 0 & 0 & P_L & -b(p) + i\vec{\not{p}} & P_R & \dots \\ \vdots & \vdots & \ddots & \ddots & \ddots & \ddots \end{pmatrix}, \quad (3.7)$$

where

$$b(p) = 1 - M + W(p). \quad (3.8)$$

The 16 corners of the Brillouin zone are given explicitly by  $p_0 = \pi(n_1, n_2, n_3, n_4)$  where  $n_\mu = 0, 1$ . At each corner of the Brillouin zone  $D_{DW}$  commutes with  $\gamma_5$ ,

<sup>4</sup>Hopping in the physical  $\mu$  direction is similarly constrained by the projectors  $(1 \pm \gamma_\mu)/2$  for  $r = 1$ .

<sup>5</sup>Super-criticality of the Wilson kernel is equally crucial for overlap fermions [18, 14]

$n$	$M$ range	#(z.m.)	chirality
0	(0,2)	1	RH
1	(2,4)	4	LH
2	(4,6)	6	RH
3	(6,8)	4	LH
4	(8,10)	1	RH

Table 1: The zero modes spectrum on a semi-infinite lattice as a function of  $n$ , the number of momentum components equal to  $\pi$ . See text for further explanations.

and the equation  $P_R D_{DW} \chi_R = 0$  has two linearly independent RH homogeneous solutions<sup>6</sup>  $\chi_{(\alpha)}$  given explicitly by

$$\chi_{(\alpha)\beta}(s) = (P_R)_{\alpha\beta} b^s(p_0) , \quad b(p_0) = 1 + 2n - M , \quad (3.9)$$

where  $n$  is the number of components of the momentum  $p_0$  equal to  $\pi$ . The spinor indices take values  $\alpha, \beta = 1, 2$ , consistent with the two degrees of freedom of a four-dimensional Weyl field. Notice the double role of the chiral projector  $P_R$ . The notation  $(P_R)_{\alpha\beta}$  refers to the nonzero diagonal block of  $P_R$  proportional to the  $2 \times 2$  identity matrix. In order for the homogeneous solution to be a zero mode that belongs to the physical spectrum, it must be normalizable. Remembering that the range of the fifth coordinate is semi-infinite, this will be true if and only if  $|1 + 2n - M| < 1$ , which in turn constrains the range of the domain wall height  $M$  as a function of  $n$  [19].

The zero modes spectrum is summarized in Table 1. The first column is  $n$ , which ranges from 0 to 4. The second column gives the range of domain wall height where, as a function of  $n$ , the homogeneous solution (3.9) is normalizable. In particular, for  $n = 0$  this range is  $0 < M < 2$ . The next column gives the number of corners, hence the number of (pairs of) linearly independent zero modes with the given value of  $n$ . The last column gives the *physical* chirality of the zero modes. Notice that while Eq. (3.9) has a fixed chiral projector  $P_R$ , the physical chirality alternates between RH and LH, depending on whether  $n$  is even or odd. In brief, the reason is that the way to determine the continuum-limit properties of the massless fermion near a given corner  $p_0$  is to first apply a discrete transformation that brings  $p_0$  to the origin of the Brillouin zone. These discrete transformation are constructed from the Dirac matrices, and act on the wave function of the fermions as well. Hence, the chirality of the transformed wave function can be flipped. For a detailed explanation see Refs. [1, 10].

---

<sup>6</sup>It is easy to verify that there are no LH homogeneous solutions at any corner of the Brillouin zone. Consider the equation  $P_L \sum_{s'} D_{DW}(s, s') \chi_L(s') = 0$ . For  $s = 1$  the only solution is  $\chi_L(1) = 0$ . Using this, we next find  $\chi_L(2) = 0$ , and so on.

Before we continue, we digress to compare the situation on the lattice with the continuum zero mode of Eq. (2.3). Instead of a semi-infinite fifth direction, we momentarily consider an infinite fifth direction, with domain-wall height  $M$  for  $s \geq 1$  as before, and a different domain-wall height  $-M'$  for  $s \leq 0$ , with  $M' > 0$ . Omitting the spinor indices, the RH homogeneous solutions at the corners of the Brillouin zone are now<sup>7</sup>

$$\chi_R(s) = \begin{cases} (1 + 2n + M')^{s-1} & s \leq 0, \\ (1 + 2n - M)^{s-1} & s \geq 1. \end{cases} \quad (3.10)$$

Since  $M' > 0$ , the wave function for negative  $s$  is always normalizable. As for the wave function for positive  $s$ , it will be normalizable under the same condition as before, namely, if and only if  $|1 + 2n - M| < 1$ . Adding the negative- $s$  region has thus not changed the fact that the zero modes spectrum of Table 1 is controlled by the positive- $s$  region only. The negative- $s$  half-space carries no benefit with it, and we will thus avoid it.

Returning to the semi-infinite fifth direction with  $s \geq 1$ , in lattice QCD with domain wall fermions one always dials the domain wall height to have a single zero mode at the origin of the Brillouin zone, the case  $n = 0$  in Table 1. Disregarding the overall normalization, the zero mode wave function is then  $\chi_R(s) = P_R(1 - M)^s$ . While as already noted, this solution is normalizable for  $0 < M < 2$ , the region  $1 < M < 2$  gives rise to an oscillatory behavior as a function of  $s$ , which we would like to avoid. Hence we will further restrict  $0 < M \leq 1$ . The special case  $M = 1$  is peculiar: the wave function becomes completely localized on the boundary layer,  $\chi_R(s) = \delta_{s,1}$ . This ideally localized wave function is only possible in the free theory. In Sec. 5 we will see how the wave function gets modified in the interacting theory, as well as how this affects the optimal choice of the domain wall height  $M$ .

We next show that the pair of zero modes attached to the boundary that we have at  $p = 0$  when  $0 < M \leq 1$  correspond to a four-dimensional Weyl fermion. One way to demonstrate this is to consider momentarily the domain wall hamiltonian

$$H_{DW}(\vec{p}) = \gamma_4 D_{DW}(\vec{p}; p_4 = 0). \quad (3.11)$$

We seek the bound states of  $H_{DW}$  localized near the boundary. We parametrize an eigenstate as

$$\Psi(\vec{p}, s) = P_R \chi_R(s; \vec{p}) \phi(\vec{p}), \quad (3.12)$$

where  $\phi(\vec{p})$  is a two-component spinor.<sup>8</sup> We now take  $\chi_R(s; \vec{p}) = b^s(\vec{p})$ , requiring that this wave function is normalizable. In this introduction we use the chiral representation of the Dirac matrices (in  $2 \times 2$  block notation)

$$\gamma_k = \begin{pmatrix} 0 & i\sigma_k \\ -i\sigma_k & 0 \end{pmatrix}, \quad \gamma_4 = \begin{pmatrix} 0 & 1 \\ 1 & 0 \end{pmatrix}, \quad \gamma_5 = \begin{pmatrix} 1 & 0 \\ 0 & -1 \end{pmatrix}, \quad (3.13)$$

<sup>7</sup>For  $n = 0$ , the continuum wave function (2.3) can be reproduced by reintroducing the lattice spacing in the fifth direction  $a_5$  and taking the limit  $a_5 \rightarrow 0$ . We leave this exercise to the reader.

<sup>8</sup>Strictly speaking,  $\phi(\vec{p})$  is the RH part of a four-component spinor whose LH part vanishes identically.

with  $\sigma_k$  the Pauli matrices. In particular,

$$\gamma_4 D_K(\vec{p}; p_4 = 0) = i \sum_{k=1}^3 \gamma_4 \gamma_k \bar{p}_k , \quad (3.14)$$

where

$$i\gamma_4 \gamma_k \bar{p}_k = \begin{pmatrix} \sigma_k \bar{p}_k & 0 \\ 0 & -\sigma_k \bar{p}_k \end{pmatrix} = \gamma_5 \begin{pmatrix} \sigma_k \bar{p}_k & 0 \\ 0 & \sigma_k \bar{p}_k \end{pmatrix} , \quad (3.15)$$

exhibiting the familiar connection between chirality and helicity eigenstates. The part of  $H_{DW}(\vec{p})$  that anti-commutes with  $\gamma_5$  annihilates  $\chi_R(s; \vec{p})$ , hence also  $\Psi(\vec{p}, s)$ , and it follows that the three-dimensional wave function is a RH helicity eigenstate,

$$\sum_{k=1}^3 \sigma_k \bar{p}_k \phi(\vec{p}) = E(\vec{p}) \phi(\vec{p}) . \quad (3.16)$$

This interpretation is valid for  $p_k \ll 1$  in lattice units, which allows us to approximate  $\bar{p}_k = p_k$ .

The chiral bound states localized near the boundary exist for a range of lattice momenta which is constrained by  $|b(\vec{p})| < 1$ . As long as we take  $M = O(1)$ , this condition defines an open subset of the Brillouin zone which includes the origin, and which is also  $O(1)$  in lattice units; thus it becomes an infinite range in the continuum limit.

For any  $\vec{p}$ , in addition to the single bound state, the hamiltonian  $H_{DW}(\vec{p})$  has a continuous spectrum as well. Because of complete reflection at the boundary of the semi-infinite fifth dimension, the continuum eigenstates are standing waves. When  $|b(\vec{p})| = 1$ , the wave function  $\chi(s; \vec{p})$  of the bound state becomes delocalized, and its energy reaches the threshold of the continuous spectrum.

Returning to euclidean space, we can alternatively establish the existence of the massless RH Weyl fermion near the four-dimensional boundary by examining the singularity structure of the domain wall propagator. We start with the five-dimensional Wilson operator on an infinite fifth direction,

$$D_5 = P_R \delta_{s+1, s'} + P_L \delta_{s-1, s'} + (-b(p) + i\vec{p}) \delta_{s, s'} . \quad (3.17)$$

As before, we work in momentum space for the four physical dimensions. As an operator acting on the fifth coordinate, the inverse of  $D_5$  can be expressed as  $D_5^\dagger G_5$ , where  $G_5$  is the inverse of the (discretized) second-order operator

$$\Omega_5 \equiv D_5 D_5^\dagger = -b(p)(\delta_{s+1, s'} + \delta_{s-1, s'}) + (b^2(p) + \vec{p}^2 + 1) \delta_{s, s'} , \quad (3.18)$$

Explicitly

$$\begin{aligned} G_5 &= \mathcal{N} e^{-\alpha(p)|s-s'|} , \\ \mathcal{N}^{-1} &= 2b(p) \sinh \alpha(p) , \end{aligned} \quad (3.19)$$

where  $\alpha(p)$  is the positive solution of

$$2 \cosh \alpha(p) = \frac{1 + b^2(p) + \bar{p}^2}{b(p)} . \quad (3.20)$$

Notice that  $e^{\pm\alpha(p)s}$  are the homogeneous solutions of the equation  $D_5 D_5^\dagger \chi = 0$ , while  $G_5$  is the Green function that satisfies physical boundary conditions: it vanishes when the separation  $|s - s'|$  tends to infinity. We have required  $0 < M \leq 1$ , hence  $b(p) \geq 0$ . For  $p \rightarrow 0$ , both  $b(p)$  and  $e^{-\alpha(p)}$  tend to  $1 - M$ . Below, we will need the  $O(p^2)$  corrections,

$$b(p) = 1 - M + \frac{p^2}{2} + \dots , \quad (3.21a)$$

$$e^{-\alpha(p)} = 1 - M - \frac{M^2 - 4M + 2}{2M(2 - M)} p^2 + \dots . \quad (3.21b)$$

Expanding  $b(p)$  is trivial. For  $e^{-\alpha(p)}$ , we write  $x \equiv e^{-\alpha} = 1 - M + cp^2$ , and solve Eq. (3.20) to  $O(p^2)$  for  $c$ , noting that the left-hand side is  $x + x^{-1}$ .

We now turn to the domain wall propagator  $G_{DW}$ . As before, it can be expressed as  $G_{DW} = D_{DW}^\dagger G$ , where now  $G$  is the inverse of

$$\Omega_{DW} \equiv D_{DW} D_{DW}^\dagger = P_R \Omega_+ + P_L \Omega_- . \quad (3.22)$$

The explicit form of the operator  $\Omega_{DW}$  on a finite lattice is given in Eq. (3.32) below. The operators  $\Omega_\pm$  carry no Dirac indices, and so  $G$  admits a similar decomposition

$$G = P_R G_+ + P_L G_- . \quad (3.23)$$

Several considerations help us in constructing  $G_\pm$ . First, in the absence of a boundary we already know the inverse of the second-order operator  $\Omega_5$ , it is  $G_5$ . Hence we expect  $G_\pm = G_5 + \dots$ , where the ellipsis stands for an additional term that corrects for the existence of the boundary. Now, for  $s$  away from the boundary we have

$$\sum_{s''} \Omega_{DW}(s, s'') G_5(s'', s') = \sum_{s''} \Omega_5(s, s'') G_5(s'', s') = \delta_{s, s'} . \quad (3.24)$$

This relation is true except when  $s$  is right on the boundary, namely except for  $s = 1$ . The reason is that both  $D_{DW}$  and  $\Omega_{DW} = D_{DW} D_{DW}^\dagger$  contain only nearest-neighbor couplings. In order not to spoil the already correct behavior, the new term must somehow be formed from the homogeneous solutions of the translationally covariant second-order operator  $\Omega_5 = D_5 D_5^\dagger$ . Next, as follows from Eqs. (3.22) and (3.32), the operators  $\Omega_\pm = (\Omega_\pm)_{ss'}$  are symmetric in the indices  $s$  and  $s'$ , hence the same must be true for the new term. Last, this term must exhibit sensible physical behavior when the fifth coordinate tends to infinity. Suppressing the  $p$  dependence, this implies<sup>9</sup>

$$G_\pm(s, s') = G_5(s, s') + A_\pm e^{-\alpha(s+s'-2)} , \quad s, s' \geq 1 . \quad (3.25)$$

<sup>9</sup>The slight difference between Eq. (3.25) and the corresponding equation in Ref. [17] is because here we assume  $s = 1, 2, \dots$ , while Ref. [17] assumes  $s = 0, 1, \dots$ .

where the above considerations determine the form of the new term up to the proportionality constants  $A_{\pm}$ .

It remains to determine the amplitude  $A_{\pm}$  by requiring that  $G_{\pm}$  is the inverse of  $\Omega_{\pm}$ , including in particular at the boundary. The result is

$$A_+ = -\mathcal{N} e^{-2\alpha}, \quad (3.26)$$

$$A_- = \mathcal{N} e^{-2\alpha} \frac{e^{\alpha} - b}{b - e^{-\alpha}}. \quad (3.27)$$

The amplitudes  $\mathcal{N}$  (Eq. (3.19)) and  $A_+$  are regular for all values of  $p$ , but  $A_-$  has a pole. Using Eq. (3.21) we find

$$A_-(p) = \frac{M(2-M)}{p^2} + \dots, \quad p \rightarrow 0. \quad (3.28)$$

The Ellipsis stands for regular terms. This leads to a pole in the domain wall propagator as well,

$$\begin{aligned} G_{DW} &= D_{DW}^{\dagger} G = D_{DW}^{\dagger} P_L G_- + \dots \\ &= -i P_R \frac{\not{p}}{p^2} M(2-M)(1-M)^{s+s'-2} + \dots \end{aligned} \quad (3.29)$$

Note that  $(M(2-M))^{1/2}(1-M)^{s-1}$  is the normalized zero mode for  $p \rightarrow 0$ . The singularity of the domain wall propagator clearly exhibits the presence of a massless RH chiral fermion near the boundary, a result which is valid for the semi-infinite fifth direction. In the next subsection, we will see how this result changes when the fifth direction is finite.

## 3.2 Finite fifth direction

We next consider a finite fifth direction,  $s = 1, 2, \dots, N_5$ , always assuming that  $N_5$  is even. The domain-wall fermion matrix is

$$D_{DW} = \begin{pmatrix} D-1 & P_R & 0 & 0 & \dots & 0 & 0 & 0 & -mP_L \\ P_L & D-1 & P_R & 0 & \dots & 0 & 0 & 0 & 0 \\ 0 & P_L & D-1 & P_R & \dots & 0 & 0 & 0 & 0 \\ \vdots & \vdots & \ddots & \ddots & \ddots & \vdots & \vdots & \vdots & \vdots \\ 0 & 0 & 0 & 0 & \dots & P_L & D-1 & P_R & 0 \\ 0 & 0 & 0 & 0 & \dots & 0 & P_L & D-1 & P_R \\ -mP_R & 0 & 0 & 0 & \dots & 0 & 0 & P_L & D-1 \end{pmatrix} \quad (3.30)$$

The Wilson operator satisfies  $\gamma_5$ -hermiticity, namely,  $\gamma_5 D \gamma_5 = D^{\dagger}$ , and thus  $\gamma_5 D$  is hermitian. Related, a hermitian version of the domain-wall fermion operator is  $\mathcal{H}_{DW} = \mathcal{R} \gamma_5 D_{DW}$ , where  $\mathcal{R}$  is the reflection on the 5th coordinate:  $\mathcal{R}(s) = N_5 + 1 - s$ . Equivalently,  $D_{DW}^{\dagger} = \mathcal{R} \gamma_5 D_{DW} \mathcal{R} \gamma_5$ . It follows that  $\det(D_{DW})$  is real.

In addition to the RH zero mode  $\chi_R(s) \propto P_R(1 - M)^s$  localized near the  $s = 1$  boundary, now there is also a LH zero mode  $\chi_L(s) \propto P_L(1 - M)^{N_5 - s}$  localized near the  $s = N_5$  boundary. Neither of these modes are exact: the boundary at  $s = N_5$  somewhat disrupts the RH zero mode, and vice versa. But the effect is exponentially small, proportional to  $(1 - M)^{N_5}$ , and vanishes for  $N_5 \rightarrow \infty$ . This can be established via a variational argument. One uses  $\chi_R(s)$  and  $\chi_L(s)$  as trial wave functions for the second-order operator  $\mathcal{H}_{DW}^2$ . Introducing  $|\xi\rangle = \mathcal{H}_{DW} |\chi_R\rangle$ , one has  $\xi(s) = 0$  for  $1 \leq s < N_5$ . The reason is that the domain wall operator contains only nearest-neighbor couplings, and so for this range of the fifth coordinate the action of  $\mathcal{H}_{DW}$  on  $\chi_R$  coincides with that of the domain wall operator on a semi-infinite lattice. In other words,  $\mathcal{H}_{DW} |\chi_R\rangle$  does not vanish only because of the new boundary at  $s = N_5$ , hence  $\langle \chi_R | \mathcal{H}_{DW}^2 | \chi_R \rangle \sim (1 - M)^{2N_5}$ , with a similar result for  $\chi_L$ . Since  $\mathcal{H}_{DW}^2$  is a positive operator, it must therefore have two eigenvectors with a common eigenvalue  $E^2$  where  $E \sim (1 - M)^{N_5}$ . This, in turn, implies that  $\mathcal{H}_{DW}$  has two eigenvectors with eigenvalues  $E_{\pm} = \pm E$ , where both eigenvectors are, approximately, linear superpositions of  $\chi_R(s)$  and  $\chi_L(s)$ . For now we will neglect such exponentially small effects, but we will return to the question of their role at the end of this section.

In the case of a semi-infinite fifth direction (Sec. 3.1), the RH zero mode signals the presence of a RH chiral field. Similarly, we now have both RH and LH chiral fields, localized on opposite boundaries. Together, they form a very light Dirac fermion (if the exponentially small mixing between the two boundaries is not neglected), which becomes massless for  $N_5 \rightarrow \infty$ . We may introduce an effective four-dimensional “domain wall quark” field for the light Dirac fermion, simply by picking the appropriate components of the five-dimensional domain-wall field  $\psi(x, s)$ . The domain wall quark field is defined as

$$\begin{aligned} q(x) &= P_R \psi(x, 1) + P_L \psi(x, N_5) , \\ \bar{q}(x) &= \bar{\psi}(x, 1) P_L + \bar{\psi}(x, N_5) P_R . \end{aligned} \tag{3.31}$$

This four-dimensional effective field will turn out to be very useful.

Notice the off-diagonal terms proportional to  $m$  in Eq. (3.30). These terms couple the opposite-chirality zero modes, and thus play the role of a mass term for the domain wall quark, as we will soon confirm explicitly. This allows the mass of the domain wall quark to be controlled independently of the extent of the fifth direction. In later sections, we will see that in the interacting theory there are additional, quantum effects that contribute to the mass of the domain wall quark.

The mass term was first introduced in Ref. [17], but with a sign convention opposite to what we are using here. The present convention follows Ref. [20]. As was shown in that paper, when  $m > 0$  in Eq. (3.30), one has  $\det(D_{DW}) > 0$  for arbitrary four-dimensional gauge fields (see Sec. 4 below).

Our next task is to obtain the domain wall propagator for a finite fifth direction, and from it, the propagator of the effective domain wall quark field. The (free) second

order operator  $\Omega = D_{DW}D_{DW}^\dagger$  in momentum space is now (compare Eq. (3.18))

$$\Omega = \begin{pmatrix} X_{++} & -b & 0 & 0 & \dots & 0 & 0 & 0 & X_{-+} \\ -b & Y & -b & 0 & \dots & 0 & 0 & 0 & 0 \\ 0 & -b & Y & -b & \dots & 0 & 0 & 0 & 0 \\ \vdots & \vdots & \ddots & \ddots & \ddots & \vdots & \vdots & \vdots & \vdots \\ 0 & 0 & 0 & 0 & \dots & -b & Y & -b & 0 \\ 0 & 0 & 0 & 0 & \dots & 0 & -b & Y & -b \\ X_{+-} & 0 & 0 & 0 & \dots & 0 & 0 & -b & X_{--} \end{pmatrix}, \quad (3.32)$$

where<sup>10</sup>

$$Y = b^2(p) + \bar{p}^2 + 1, \quad (3.33a)$$

$$X_{++} = Y + P_L(m^2 - 1) \quad (3.33b)$$

$$X_{--} = Y + P_R(m^2 - 1) \quad (3.33c)$$

$$X_{+-} = X_{-+} = mb(p). \quad (3.33d)$$

The second-order operator is real symmetric, and writing

$$\Omega = P_R\Omega_+ + P_L\Omega_-, \quad (3.34)$$

it follows that  $\Omega_+ = \mathcal{R}\Omega_-\mathcal{R}$  or, explicitly,

$$\Omega_+(s, s') = \Omega_-(N_5 + 1 - s, N_5 + 1 - s'). \quad (3.35)$$

As before, the domain wall propagator can be expressed as  $G_{DW} = D_{DW}^\dagger G$ , where  $G$  is the inverse of  $\Omega$ . By Eq. (3.34),  $G$  admits a similar decomposition in terms of  $G_\pm$ , and since  $G_+ = \mathcal{R}G_-\mathcal{R}$ , it is enough to construct  $G_-$ .

Noting that  $\Omega$  is symmetric,  $G_-$  must have the form

$$G_-(s, s') = G_5(s, s') + A_- e^{-\alpha(s+s'-2)} + A_+ e^{-\alpha(2N_5-s-s')} + A_m(e^{-\alpha(N_5-1+s-s')} + e^{-\alpha(N_5-1+s'-s)}). \quad (3.36)$$

Notice that now all four combinations of the homogeneous solutions  $e^{\alpha(\pm s \pm s')}$  are present. As the inverse of  $\Omega_-$ , the relation defining  $G_-$  is

$$\sum_{s''} \Omega_-(s, s'')G_-(s'', s') - \delta_{s,s'} = 0. \quad (3.37)$$

For  $2 \leq s \leq N_5 - 1$ , this equation is satisfied for arbitrary values of the amplitudes  $A_-, A_+, A_m$ . Only for  $s = 1$  or  $s = N_5$  is the left-hand side of Eq. (3.37) different from zero for general  $A_-, A_+, A_m$ , which in turn allows us to determine these amplitudes by imposing Eq. (3.37). There are two matrix equations relating these amplitudes,

<sup>10</sup>The construction of the domain wall propagator is generalized to the interacting theory in Sec. 4.2, following Ref. [21].

since the dependence of the left-hand side on  $s'$  can be  $e^{\pm\alpha s'}$ . Since the left-hand side does not vanish for both  $s = 1$  and  $s = N_5$ , we obtain two 2-by-2 matrix equations

$$\mathcal{C} \begin{pmatrix} A_- \\ A_m \end{pmatrix} = \mathcal{N} \begin{pmatrix} 1 - b e^{-\alpha} - m^2 \\ -mb \end{pmatrix}, \quad (3.38)$$

$$\mathcal{C} \begin{pmatrix} A_m \\ A_+ \end{pmatrix} = \mathcal{N} \begin{pmatrix} -mb \\ -b e^{-\alpha} \end{pmatrix}, \quad (3.39)$$

where

$$\mathcal{C} = \begin{pmatrix} b e^\alpha + m^2 - 1 & mb \\ mb & b e^\alpha \end{pmatrix}. \quad (3.40)$$

In the expression for  $\mathcal{C}$  we neglected exponentially small corrections of order  $e^{-N_5\alpha}$ . Notice that  $A_m$  is over-constrained. Nonetheless, these equations have a consistent solution<sup>11</sup>

$$A_- = \Delta^{-1} \mathcal{N} (1 - m^2) (e^\alpha - b), \quad (3.41)$$

$$A_+ = \Delta^{-1} \mathcal{N} (1 - m^2) (e^{-\alpha} - b), \quad (3.42)$$

$$A_m = -2\Delta^{-1} \mathcal{N} b m \sinh \alpha, \quad (3.43)$$

where

$$\Delta = b^{-1} \det \mathcal{C} = e^\alpha (b e^\alpha - 1) + m^2 (e^\alpha - b). \quad (3.44)$$

In order to expose the light Dirac fermion we keep only the leading behavior for  $p^2, m^2 \ll 1$ , obtaining

$$\Delta^{-1} = \frac{M(2-M)(1-M)}{p^2 + M^2(2-M)^2 m^2} = M(2-M)(1-M) \mathcal{D}^{-1}, \quad (3.45)$$

where  $\mathcal{D} = p^2 + M^2(2-M)^2 m^2$ , and

$$A_- = M(2-M) \mathcal{D}^{-1}, \quad (3.46)$$

$$A_+ = -\frac{(1-M)^2}{M(2-M)} p^2 \mathcal{D}^{-1}, \quad (3.47)$$

$$A_m = -M(2-M)(1-M) m \mathcal{D}^{-1}. \quad (3.48)$$

We may now obtain the propagator of the domain-wall quark field introduced in Eq. (3.31). Once again neglecting exponentially small corrections, we find<sup>12</sup>

$$\langle q \bar{q} \rangle = -M(2-M) \frac{i \not{p} + m_q}{p^2 + m_q^2}, \quad (3.49)$$

showing the presence of a Dirac fermion with mass

$$m_q = M(2-M)m. \quad (3.50)$$

<sup>11</sup>Equation (3.43) corrects a mistake in Eq. (37) of Ref. [17].

<sup>12</sup>Since  $\bar{q}_L(x) = \bar{\psi}(x, 1) P_L$ , and the domain wall propagator is  $G_{DW} = D_{DW}^\dagger G$ , it follows that the contribution of  $A_+$  to  $\langle q \bar{q} \rangle$  is always exponentially small, and the right-hand side of Eq. (3.49) receives contributions from  $A_-$  and  $A_m$  only.

Remember that the normalized wave function of the RH zero mode near the  $s = 1$  boundary is  $\chi(s) = (M(2 - M))^{1/2}(1 - M)^{1-s}$ , hence  $|\chi(1)|^2 = M(2 - M)$ . Similar statements apply to the LH zero mode localized near the  $s = N_5$  boundary. Thus, the factors of  $M(2 - M)$  are seen to originate from the support of the wave functions of the zero modes on their respective boundary layers.

Our construction of the domain wall quarks could be generalized in two related ways. Instead of Eq. (3.31), which defines the effective quark fields  $q(x), \bar{q}(x)$  in terms of the five-dimensional fields on the boundary layers only, we could define the effective quark fields as some weighted average of the five-dimensional fields  $\psi(x, s), \bar{\psi}(x, s)$  on near-boundary layers. Similarly, we could consider mass terms that couple near-boundary layers on the two sides, and not just the two boundary layers themselves, as we have done in Eq. (3.30). Such generalizations are less economic, and do not provide any advantage. Hence we will always use the simplest domain wall quark field and mass term introduced above.

The mass of the free domain wall quark is  $m_q$  in the limit  $N_5 \rightarrow \infty$ . If we moreover set  $m = 0$ , the RH and LH components of the domain wall quark completely decouple, and behave as if they each live on their own semi-infinite fifth direction. This then reproduces the idealization discussed in Sec. 3.1.

While Eqs. (3.49) and (3.50) are important for the physical interpretation of domain wall fermions, the concrete relation in Eq. (3.50) between the parameter  $m$  that couples the two boundary layers and the mass  $m_q$  of the domain wall quark is largely inconsequential, because it will be modified in the interacting theory. Similarly, the factor of  $M(2 - M)$  in Eq. (3.49) will undergo renormalization in the interacting theory.

In any numerical lattice calculation using domain wall fermions,  $N_5$  is necessarily finite. This raises the following question. In this subsection we have dealt with two qualitatively different types of parametrically small quantities. One is  $(1 - M)^{N_5}$  or, more generally,  $e^{-\alpha(p)N_5}$ , which results from the finiteness of  $N_5$ . The other small parameters are  $p^2$  and  $m^2$ , which will ultimately be associated with some physical scale (expressed in lattice units) of the interacting theory. The question we should be asking ourselves is what if these two sets of parametrically small quantities are comparable in size, or more generally, what if finite- $N_5$  effects<sup>13</sup> are not negligible compared with the effect of an explicit domain wall quark mass term? As we will see, this situation is in fact common in numerical lattice calculations. The strategies developed to trace and control such effects will play a central role in subsequent sections. But first we have to introduce the interacting theory.

## 4 Interacting domain wall fermions

In this section we discuss interacting domain wall fermions as introduced in Ref. [20]. As usual, the gauge field degrees of freedom live on the four-dimensional links. The

---

<sup>13</sup>For the exponentially small terms relevant for the construction of the domain wall propagator, see appendix A of Ref. [21].

hopping terms in the Wilson kernel (3.2) become

$$D_K(x, y) = \frac{1}{2} \sum_{\mu} [\delta_{x+\hat{\mu}, y} U_{\mu}(x) - \delta_{x-\hat{\mu}, y} U_{\mu}^{\dagger}(y)] \gamma_{\mu} , \quad (4.1)$$

$$W(x, y) = \frac{1}{2} \sum_{\mu} [2\delta_{xy} - \delta_{x+\hat{\mu}, y} U_{\mu}(x) - \delta_{x-\hat{\mu}, y} U_{\mu}^{\dagger}(y)] . \quad (4.2)$$

The link variables  $U_{\mu}(x)$  take values in a Lie group  $G$ , which is usually assumed to be compact. For QCD the group is  $G = \text{SU}(3)$ . So far, this is standard. What is special about domain wall fermions is that the fermion field lives on a five-dimensional lattice. Noting how the domain-wall fermion operator (3.30) depends on the Wilson kernel, we immediately see that the coupling of the fermion degrees of freedom to the four-dimensional gauge field is independent of the fifth coordinate. The continuum limit will therefore be a four-dimensional gauge theory. We will keep choosing the domain wall height  $M$  such that each (five-dimensional) domain-wall fermion field gives rise to a single light (four-dimensional) quark field. As discussed in Sec. 3.1, for the free theory we take  $0 < M \leq 1$ . We will discuss how the appropriate range of  $M$  is modified in the interacting theory in Sec. 5.1 and Sec. 6.2.

Considering for simplicity a lattice gauge theory with a single domain wall fermion, the partition function is

$$Z = \prod_{x\mu} dU_{\mu}(x) e^{-S_g/g_0^2} \det(D_{DW}(m)) \det^{-1}(D_{DW}(1)) , \quad (4.3)$$

where  $dU_{\mu}(x)$  is an invariant group measure (for  $\text{SU}(N)$ , the Haar measure).  $S_g$  is the gauge field action, a lattice discretization of the continuum action, and  $g_0$  is the bare coupling. The fermion determinant can be represented in the usual way as a Grassmann path integral,

$$\det(D_{DW}(m)) = \prod_{x,s} d\psi(x, s) d\bar{\psi}(x, s) e^{-S_F} , \quad (4.4)$$

where as before,  $\psi(x, s), \bar{\psi}(x, s)$  are the five-dimensional fermion fields. The fermion action is  $S_F = \bar{\psi} D_{DW}(m) \psi$ , where we have suppressed the summations over all coordinates and indices of the fermion field.  $D_{DW}(m)$  is the domain wall fermion operator of Eq. (3.30), where we have indicated explicitly its dependence on the parameter  $m$  occurring in the upper-right and lower-left entries that couple the two boundaries.

Apart from its anticipated dependence on the gauge and fermion fields, the partition function (4.3) includes an additional factor,  $\det^{-1}(D_{DW}(1))$ , usually called the ‘‘Pauli-Villars determinant.’’ Its role will be explained in Sec. 4.4 below. For now, we only note that it does not introduce any new light degrees of freedom, because for  $m = 1$  the operator (3.30) implements anti-periodic boundary conditions in the fifth direction, and thus it describes a five-dimensional fermion field whose mass is  $O(1)$  in lattice units.

## 4.1 Flavor symmetries and currents

We next turn to the flavor symmetries of a lattice gauge theory coupled to several domain wall fermions. We will assume that there are  $N_f$  domain-wall fermion fields, all belonging to the same representation of the gauge group (the fundamental representation of  $SU(3)$ , for QCD). We will also assume for simplicity that the mass parameter  $m$  in the domain-wall fermion operator (3.30) is the same for all fermion species, which implies that all the domain wall quarks are degenerate. The results can be generalized straightforwardly to the case of non-degenerate masses.

The five-dimensional fermion action is invariant under global  $U(N_f) = SU(N_f) \otimes U(1)$  symmetry. The conserved five-dimensional currents have the following structure. For  $\mu = 1, \dots, 4$ , and all  $1 \leq s \leq N_5$ ,

$$j_\mu^a(x, s) = \frac{1}{2} (\bar{\psi}(x, s)(1 + \gamma_\mu)U_\mu(x)\lambda^a\psi(x + \hat{\mu}, s) - \bar{\psi}(x + \hat{\mu}, s)(1 - \gamma_\mu)U_\mu^\dagger(x)\lambda^a\psi(x, s)). \quad (4.5)$$

The hermitian matrix  $\lambda^a$  is one of the  $U(N_f)$  generators. For the  $U(1)$  group, which is the fermion number symmetry,  $\lambda^a$  is the identity matrix. For  $SU(N_f)$ , the generators  $\lambda^a$  are hermitian and traceless. Apart from the additional dependence on the fifth coordinate  $s$ , Eq. (4.5) is recognized as the familiar vector current of Wilson fermions. For the fifth component we define

$$j_5^a(x, s) = \begin{cases} \bar{\psi}(x, s)P_R\lambda^a\psi(x, s+1) - \bar{\psi}(x, s+1)P_L\lambda^a\psi(x, s), & 1 \leq s < N_5, \\ -m\bar{\psi}(x, N_5)P_R\lambda^a\psi(x, 1) + m\bar{\psi}(x, 1)P_L\lambda^a\psi(x, N_5), & s = N_5. \end{cases} \quad (4.6)$$

Using the Noether procedure, the five-dimensional continuity equation is

$$\sum_\mu \Delta_\mu j_\mu^a(x, s) = -\Delta_5 j_5^a(x, s). \quad (4.7)$$

Here  $\Delta_\mu$  and  $\Delta_5$  are the backward difference operators

$$\Delta_\mu f(x, s) = f(x, s) - f(x - \hat{\mu}, s), \quad (4.8)$$

and

$$\Delta_5 f(x, s) = \begin{cases} f(x, s) - f(x, s-1), & 1 < s \leq N_5, \\ f(x, 1) - f(x, N_5), & s = 1. \end{cases} \quad (4.9)$$

This is the usual form of the backward difference operator for periodic boundary conditions. The special boundary conditions in the fifth direction are taken care of by the dependence of  $j_5^a(x, N_5)$  on  $m$ . In particular,  $j_5^a(x, N_5)$  vanishes for  $m = 0$ . The above expressions for  $j_5^a(x, N_5)$  and for  $\Delta_5$  are somewhat different from Ref. [20], but the expression for  $\Delta_5 j_5^a(x, s)$  remains the same for all  $s$ . When carried out on the lattice, the Noether procedure has a certain degree of freedom, and as a result, relegating the  $m$  dependence to  $j_5^a$  (as we did here) or to  $\Delta_5$  (as was done in Ref. [20]) are both valid options.<sup>14</sup>

<sup>14</sup>See Sec. 7.1.3 for a related discussion.

We will now use the five-dimensional conserved currents as the building blocks for four-dimensional vector and axial currents. There is a unique set of conserved vector currents, obtained by summing the conserved five-dimensional current over all  $s$  values,

$$\mathcal{V}_\mu^a(x) = \sum_{s=1}^{N_5} j_\mu^a(x, s). \quad (4.10)$$

Conservation of these vector currents,  $\sum_\mu \Delta_\mu \mathcal{V}_\mu^a = 0$ , follows from the five-dimensional continuity equation (4.7).

Unlike the vector currents, it is not possible to define exactly conserved axial currents. In order to define partially conserved axial currents, we take advantage of the global separation of the RH and LH components of the effective quark field (3.31), which are supported on opposite boundaries of the five-dimensional lattice. We will define the axial transformations to act *vectorially* on each four-dimensional layer, but we assign opposite charges to fermion degrees of freedom in the two half-spaces

$$\begin{aligned} \delta_A^a \psi(x, s) &= +i\epsilon(s)\lambda^a \psi(x, s), \\ \delta_A^a \bar{\psi}(x, s) &= -i\epsilon(s)\bar{\psi}(x, s)\lambda^a, \end{aligned} \quad (4.11)$$

where<sup>15</sup>

$$\epsilon(s) = \begin{cases} 1, & 1 \leq s \leq N_5/2, \\ -1, & N_5/2 < s \leq N_5. \end{cases} \quad (4.12)$$

For the effective domain wall quark fields defined in Eq. (3.31), the transformations (4.11) take the form

$$\begin{aligned} \delta_A^a q(x) &= i\gamma_5 \lambda^a q(x), \\ \delta_A^a \bar{q}(x) &= i\bar{q}(x)\lambda^a \gamma_5, \end{aligned} \quad (4.13)$$

which are recognized as axial transformations.

The virtue of this construction is that, just like the vector currents, the partially-conserved axial currents take the form of suitable sums over the five-dimensional conserved currents. Explicitly,

$$\mathcal{A}_\mu^a(x) = - \sum_{s=1}^{N_5} \epsilon(s) j_\mu^a(x, s). \quad (4.14)$$

For  $m = 0$  (see Eq. (3.30)), the non-invariance of the action under the transformations (4.11) comes solely from the coupling between the four-dimensional layers  $s = N_5/2$  and  $s = N_5/2 + 1$ . For  $m \neq 0$ , there is an additional contribution coming from the direct coupling between the boundary layers  $s = 1$  and  $s = N_5$ . As a result, the axial currents satisfy the partial conservation equation<sup>16</sup>

$$\sum_\mu \Delta_\mu \mathcal{A}_\mu^a(x) = 2m J_5^a(x) + 2J_{5q}^a(x), \quad (4.15)$$

<sup>15</sup>Recall we always take  $N_5$  even.

<sup>16</sup>If we restore the lattice spacing, the coefficient of  $J_{5q}^a(x)$  in Eq. (4.15) becomes  $2/a$ .

where

$$-mJ_5^a(x) = j_5^a(x, N_5) , \quad (4.16)$$

$$J_{5q}^a(x) = j_5^a(x, N_5/2) . \quad (4.17)$$

The operator  $j_5^a(x, N_5)$  can be expressed in terms of the effective quark fields of Eq. (3.31). Having factored out the  $m$  dependence on the left-hand side of Eq. (4.16),  $J_5^a$  takes the form of the familiar pseudoscalar density

$$J_5^a(x) = \bar{q}(x)\gamma_5\lambda^a q(x) . \quad (4.18)$$

We see that, were it not for the extra term  $J_{5q}^a(x)$  on its right-hand side, Eq. (4.15) would express the familiar partial conservation of the axial current (PCAC).

For later use, the associated Ward-Takahashi identities (WTIs) are

$$\begin{aligned} \sum_{\mu} \Delta_{\mu} \langle \mathcal{A}_{\mu}^a(x) O(y_1, y_2, \dots) \rangle &= 2m \langle J_5^a(x) O(y_1, y_2, \dots) \rangle \\ &+ 2 \langle J_{5q}^a(x) O(y_1, y_2, \dots) \rangle \\ &+ i \langle \delta_A^a(x) O(y_1, y_2, \dots) \rangle . \end{aligned} \quad (4.19)$$

The multi-local operator  $O(y_1, y_2, \dots)$  will be assumed to be a product of the domain-wall quark fields  $q(y)$  and  $\bar{q}(y)$ , on which the local variation acts as  $\delta_A^a(x)q(y) = i\delta_{x,y}^4\gamma_5\lambda^a q(y)$  and  $\delta_A^a(x)\bar{q}(y) = i\delta_{x,y}^4\bar{q}(y)\lambda^a\gamma_5$ .

## 4.2 Chiral symmetry restoration for $N_5 \rightarrow \infty$

In the rest of this section we distinguish between the singlet and non-singlet currents by omitting the upper index  $a$  for the singlet currents. Postponing the discussion of the singlet axial current  $\mathcal{A}_{\mu}(x)$  to the next subsection, in this subsection we discuss the non-singlet axial currents  $\mathcal{A}_{\mu}^a(x)$ . We will show that, in an appropriate sense, the operator  $J_{5q}^a$  on the right-hand side of Eq. (4.15) vanishes for  $N_5 \rightarrow \infty$ . This is a result of the following theorem.

*Theorem: chiral symmetry restoration.* Consider the correlation function of  $J_{5q}^a$  with an arbitrary set of domain-wall quark fields,

$$\langle J_{5q}^a(x) q(y_1)q(y_2) \cdots \bar{q}(z_1)\bar{q}(z_2) \cdots \rangle . \quad (4.20)$$

Then, for  $N_5 \rightarrow \infty$ , this correlation function vanishes.

Less formally, thought of as an operator that acts on states created by the boundary fields  $q$  and  $\bar{q}$  only, the theorem states that  $J_{5q}^a$  vanishes for  $N_5 \rightarrow \infty$ . Assuming that the axial currents  $\mathcal{A}_{\mu}^a(x)$  act on the same set of states, it follows immediately that the PCAC relation is reproduced,

$$\sum_{\mu} \Delta_{\mu} \mathcal{A}_{\mu}^a(x) = 2mJ_5^a(x) , \quad N_5 \rightarrow \infty . \quad (4.21)$$

A proof of chiral symmetry restoration for  $N_5 \rightarrow \infty$  was first given in Ref. [20] using a second-quantized transfer matrix formalism. Usually, the transfer matrix describes propagation in euclidean space along the time direction [22], but here it was adapted to describe propagation along the fifth direction [23, 24, 20].

The proof rests on three essential physical ingredients. The first ingredient is that the gauge field is independent of the fifth coordinate. As a result, propagation along the fifth direction is controlled by a second-quantized transfer matrix  $\hat{\mathcal{T}} = \hat{T}(\mathcal{U})$ , which is also independent of the fifth coordinate. Here  $\mathcal{U}$  denotes the four-dimensional gauge field. We may write  $\hat{\mathcal{T}} = \exp(-\hat{\mathcal{H}})$ , regarding  $\hat{\mathcal{H}}$  as a ‘‘hamiltonian’’ in  $4 + 1$  dimensions. Consider now momentarily an infinite fifth direction where  $-\infty < s < \infty$ . Let us excite an eigenstate of  $\hat{\mathcal{H}}$  with energy  $E > 0$  above the second-quantized vacuum on a four-dimensional layer with fifth coordinate  $s$ , and propagate it to another layer  $s'$ . This yields a suppression factor  $\exp(-E|s - s'|)$ , exhibiting translation invariance in the fifth direction. The transfer matrix formalism can be generalized to the case of domain wall fermions where  $1 \leq s \leq N_5$ , and translation invariance in the fifth direction is explicitly broken by the boundaries. Using this formalism one derives expressions for  $\det(D_{DW}(m))$ , as well as for the correlation functions of domain wall fermions [20].

The second ingredient is that, as we shall see, any violation of the conservation of a non-singlet axial current in a correlation function of the domain-wall quark fields, Eq. (4.20), requires fermion propagation across the entire fifth dimension, hence a factor of  $\sim \exp(-N_5 \hat{\mathcal{H}})$ .

In order to understand the last crucial ingredient let us momentarily assume that for a given background gauge field the ground state of  $\hat{\mathcal{H}}$  is separated from the first excited state by a gap  $\Delta > 0$ . In this case the correlation function (4.20) is bounded by  $\exp(-N_5 \Delta)$  and vanishes for  $N_5 \rightarrow \infty$ . In reality, there are special gauge-field configurations for which  $\Delta = 0$ , equivalently, the transfer matrix has an eigenvalue equal to one, and the argument will have to be suitably refined.

In the rest of this subsection we will discuss the proof more fully but still omit various technicalities. The full details may be found in Refs. [20, 21]. The proof we will describe here makes use of the physical ingredients explained above, but avoids the technically elaborate second-quantized transfer matrix formalism of Ref. [20]. The discussion is based on Ref. [21], which uses a ‘‘first quantized’’ transfer matrix formalism instead.<sup>17</sup>

In the standard treatment of a Grassmann path integral, the contraction of two fermion fields gives rise to a propagator which is the inverse of the Dirac operator occurring in the (bilinear) fermion action. In the free theory, we constructed the domain wall propagator in Sec. 3.2. In brief, the propagator can be constructed in a standard manner in terms of the inverse of the second-order domain wall operator  $\Omega$  (Eq. (3.32)), which in turn can be decomposed into its chirality components (Eq. (3.34)), and the inverse  $G_-$  of  $\Omega_-$  was given explicitly in Eq. (3.36).

Because the gauge field is the same on all four-dimensional slices (and it has no fifth component) the solution of Sec. 3.2 can be generalized to the interacting case.

---

<sup>17</sup>For the relation between the first-quantized and second-quantized transfer matrices see Ref. [20].

We begin by writing the Wilson kernel in  $2 \times 2$  block form as

$$D = D(M; \mathcal{U}) = \begin{pmatrix} 1 - B & C \\ -C^\dagger & 1 - B \end{pmatrix}, \quad (4.22)$$

where

$$B = 1 + W - M. \quad (4.23)$$

Both  $B$  and  $C$  carry a  $2 \times 2$  spinor index, and  $B$  is proportional to the identity matrix in spinor space. The explicit form of  $C$  can be inferred from Eqs. (3.2), (3.13) and (4.1). In the presence of a gauge field the second-order operator  $\Omega = D_{DW} D_{DW}^\dagger$  is still given by Eq. (3.32),<sup>18</sup> while Eq. (3.33) has a suitable generalization. In particular, in the interacting case  $Y$  is given explicitly by

$$Y = 2B + DD^\dagger. \quad (4.24)$$

Next, introducing

$$K = \begin{pmatrix} B^{-1/2} & 0 \\ C^\dagger B^{-1/2} & B^{1/2} \end{pmatrix}, \quad K^\dagger = \begin{pmatrix} B^{-1/2} & B^{-1/2} C \\ 0 & B^{1/2} \end{pmatrix}, \quad (4.25)$$

we construct two transfer matrices sharing the same eigenvalue spectrum,

$$T = KK^\dagger = \begin{pmatrix} B^{-1} & B^{-1} C \\ C^\dagger B^{-1} & B + C^\dagger B^{-1} C \end{pmatrix}, \quad (4.26)$$

$$\tilde{T} = K^\dagger K = \begin{pmatrix} B^{-1} + B^{-1/2} C C^\dagger B^{-1/2} & B^{-1/2} C B^{1/2} \\ B^{1/2} C^\dagger B^{-1/2} & B \end{pmatrix}. \quad (4.27)$$

We will encounter the transfer matrix  $T$  in Sec. 4.5 and Sec. 7.1. Here we will make use of the alternative version  $\tilde{T}$ . A key result is

$$\gamma_5 B^{-1/2} Y \gamma_5 B^{-1/2} = \tilde{T} + \tilde{T}^{-1}. \quad (4.28)$$

In this subsection we restrict the domain wall height to  $0 < M < 1$ . As a result,  $B$  is a positive operator, and the same is true for the transfer matrices. We will consider the full range  $0 < M < 2$  in Sec. 7.2.1.

We next introduce the spectral decomposition

$$\tilde{T} = \sum_i |v_i\rangle \lambda_i \langle v_i|, \quad (4.29)$$

where  $|v_i\rangle$  are the eigenvectors. Note that the eigenvalues  $\lambda_i$  are all positive. From the same ingredients we construct a third transfer matrix

$$Q = \sum_i |v_i\rangle \eta_i \langle v_i|, \quad (4.30)$$

---

<sup>18</sup>Notice that the definition of  $\Omega$  in Eq. (3.2) of Ref. [21] is slightly different.

where  $\eta_i = \min\{\lambda_i, \lambda_i^{-1}\}$ . An immediate consequence is that the norm of  $Q$  is bounded by one. Equivalently, denoting the maximal eigenvalue of  $Q$  by  $\eta_{\max}$ , it follows that  $\eta_{\max} \leq 1$ . The virtue of  $Q$  is that it satisfies physical boundary conditions. Namely,  $Q^{|s-s'|}$  vanishes when the separation  $|s-s'|$  tends to infinity. This is true provided that no eigenvalue is exactly equal to 1, and thus  $\eta_{\max} < 1$ . This feature, alongside with Eq. (4.28) which exhibits the algebraically equivalent roles of an eigenvalue  $\lambda_i$  and its inverse, allows us to construct the inverse of  $\Omega$  as  $\gamma_5 B^{-1/2} \tilde{G} \gamma_5 B^{-1/2}$  where<sup>19</sup>

$$\tilde{G}(s, s') = \tilde{G}_5(s, s') + H_{+,+}(s, s') + H_{-,-}(s, s') + H_{+,-}(s, s') + H_{-,+}(s, s') . \quad (4.31)$$

The translationally invariant part (compare Eq. (3.19)) is now given by

$$\tilde{G}_5(s, s') = Q^{|s-s'|} f(Q) , \quad (4.32)$$

where  $f^{-1}(Q) = Q^{-1} - Q$ . Each of the four translationally non-invariant terms has the general form

$$H_{\pm,\pm}(s, s') = Q^{d(s)} A_{\pm,\pm} Q^{d(s')} , \quad (4.33)$$

where  $d(s)$  is equal to  $s$  or to  $N_5 + 1 - s$ , in other words,  $d(s)$  is the distance to one of the boundaries. The matrix amplitudes  $A_{\pm,\pm}$  provide a suitable generalization of the amplitudes  $A_+$ ,  $A_-$  and  $A_m$  of Eq. (3.36) to the interacting theory. We note also that Eq. (4.28) is the generalization of Eq. (3.20) to the interacting theory. Correspondingly, the eigenvalues  $\eta_i$  of the matrix  $Q$  generalize the factors of  $e^{-\alpha(p)}$  encountered in Sec. 3. In the absence of a gauge field  $Q$  is diagonal in momentum space, and its eigenvalues reduce to  $e^{-\alpha(p)}$ .

Having constructed the domain wall propagator in the interacting theory we now make the following crucial observation. Because of the traceless flavor matrix  $\lambda^a$  contained in the definition of  $J_{5q}^a$ , the contraction of the  $\psi$  and  $\bar{\psi}$  fields in  $J_{5q}^a$  with each other always vanishes identically. Hence, for the correlation function (4.20) to be nonzero, the field  $\psi$  in  $J_{5q}^a$  must be contracted with a boundary field  $\bar{q}$ . A similar statement applies to the  $\bar{\psi}$  field. Since  $J_{5q}^a$  lives in the middle of the fifth direction, we are looking at two factors of  $\sim Q^{N_5/2}$ , one from each fermion propagator. Because the exponent is proportional to  $N_5$ , propagation in the fifth direction will be dominated by those eigenvalues of  $Q$  which are very close to its maximal eigenvalue  $\eta_{\max}$ . Up to subleading power corrections, in a given background gauge field all the correlation functions in Eq. (4.20) are thus bounded by  $c \eta_{\max}^{N_5}$ , where the exponential factor  $\eta_{\max}^{N_5}$  is universal, and only the prefactor  $c$  depends on the specifics of the correlation function.

We now come to the last step. First, we momentarily assume that  $\eta_{\max} = \eta_{\max}(\mathcal{U})$  admits a non-trivial global bound<sup>20</sup> for all gauge fields  $\mathcal{U}$ . Namely,  $\eta_{\max}(\mathcal{U}) \leq \Lambda_0$  for some  $\Lambda_0 < 1$ . In that case, the ensemble average of any of the correlators (4.20) would be bounded by  $\Lambda_0^{N_5}$ , and would thus vanish for  $N_5 \rightarrow \infty$ .

<sup>19</sup>For the full details, see Ref. [21].

<sup>20</sup>This is attainable by imposing a constraint on the gauge field configuration space that does not alter the continuum limit [25, 26].

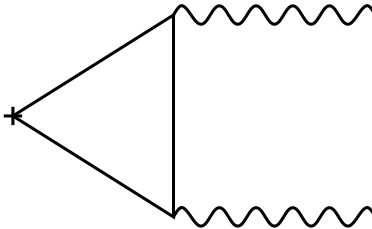


Figure 1: The triangle anomaly. The vertex on the left represents the divergence of the singlet axial current in the regularized theory. For domain wall fermions, it is  $J_{5q}$ .

If no constraint is imposed on the gauge field configuration space, there exist special configurations for which  $\eta_{\max}(\mathcal{U}) = 1$ , in other words, the transfer matrix has an eigenvalue equal to one. Let us show that this implies the existence of a zero mode of the Wilson kernel  $D = D(M; \mathcal{U})$  of Eq. (4.22) [20]. Using Eqs. (4.24) and (4.28), as well as  $\gamma_5$ -hermiticity of the Wilson kernel, it follows that if  $\tilde{T}|v\rangle = |v\rangle$  then  $\langle v|B^{-1/2}D^\dagger DB^{-1/2}|v\rangle = 0$ . Since  $B$  is bounded,  $B^{-1/2}$  cannot have a zero mode, and therefore  $B^{-1/2}|v\rangle$  is a zero mode of the Wilson kernel. We will discuss the physical significance of the kernel’s zero modes in Sec. 6. Here we will only note that  $D(M)$  does not have any zero mode in the free theory for  $0 < M < 2$ , and that configurations for which  $D(M; \mathcal{U})$  has a zero mode are expected to be rare when the continuum limit is approached.

Mathematically, having a zero mode means that  $\det(D(M; \mathcal{U})) = 0$ , a constraint which is satisfied on a measure zero subset of the gauge-field configuration space. We will use this observation to refine the proof of chiral symmetry restoration. Choosing some  $0 < \epsilon \ll 1$  we divide this space into a “large” and a “small” part. The large part consists of the configurations for which  $\eta_{\max}(\mathcal{U}) \leq 1 - \epsilon$ . The small part, which is the rest, consists of configurations for which  $1 - \epsilon < \eta_{\max}(\mathcal{U}) \leq 1$ . Consider now the contributions of these two parts to some correlation function in Eq. (4.20). For  $N_5 \gg 1$  the contribution of the large part is dominated by the eigenvalues close to  $1 - \epsilon$ , and thus it scales as  $O((1 - \epsilon)^{N_5})$ . The contribution of the small part is  $O(\epsilon)$  of course. The contribution of the large part vanishes for  $N_5 \rightarrow \infty$ , leaving us in this limit with the contribution of the small part only, which in turn implies an estimate of  $O(\epsilon)$  for any correlation function in Eq. (4.20). Finally, since we can repeat the same argument for arbitrarily small  $\epsilon$ , it follows again that all the correlation functions in Eq. (4.20) must vanish for  $N_5 \rightarrow \infty$ . This completes the proof of chiral symmetry restoration, and thus that the non-singlet axial currents satisfy the PCAC relation (4.21).

We will expand the scope of the proof of chiral symmetry restoration in Sec. 7.2.1.

### 4.3 The axial anomaly

Unlike the flavor non-singlet axial currents considered in the previous subsection, whose conservation for  $m \rightarrow 0$  is recovered in the  $N_5 \rightarrow \infty$  limit, the singlet axial

current is not conserved when the same limits are taken. This is as it must be, since in the target continuum theory the singlet axial current is anomalous (Fig. 1).

At the technical level (see Eq. (4.15)), the difference is that in the case of the singlet current, the expectation value  $\langle J_{5q} \rangle$  remains nonzero in the presence of a background gauge field, even in the limit  $N_5 \rightarrow \infty$ . A one-loop calculation in lattice perturbation theory, whose details we will not repeat here, finds that when the limit  $N_5 \rightarrow \infty$  is taken, and up to corrections that vanish in the continuum limit, the divergence of the singlet axial current is [27, 28]

$$\sum_{\mu} \Delta_{\mu} \mathcal{A}_{\mu}(x) = 2mJ_5(x) + \frac{ig^2 N_F}{4\pi^2} \sum_{\mu\nu\lambda\rho} \epsilon_{\mu\nu\lambda\rho} \partial_{\mu} A_{\nu}(x) \partial_{\lambda} A_{\rho}(x). \quad (4.34)$$

Here  $g$  is the (bare) gauge coupling. For simplicity, we have assumed that  $A_{\mu}$  is the vector potential of an abelian background field. (The relation between the link variable and the vector potential is  $U_{\mu}(x) = e^{igaA_{\mu}(x)}$  where we have re-introduced the lattice spacing  $a$ . See for example Ref. [10].) This result is valid for  $N_F$  domain wall fermions in the fundamental representation. The last term on the right-hand side of Eq. (4.34) is recognized as the axial anomaly, a result which is in agreement with continuum calculations of the anomaly for  $N_F$  Dirac fermions.

In Ref. [27], which considered a geometrical limit equivalent to the formal limit of a semi-infinite fifth direction, it was moreover shown that as the domain-wall height  $M$  is varied, the coefficient of the anomaly matches the number and chirality of the Weyl fermions in Table 1.

As originally observed by Kaplan [9, 13] the anomaly emerges via the *Callan-Harvey mechanism* [29]. Consider for simplicity a single domain wall fermion. We sum the four-dimensional components of the five-dimensional conserved current over a limited range of the fifth coordinate,  $\sum_{s=1}^{s_0} j_{\mu}(x, s)$ . We assume that both  $s_0$  and  $N_5 - s_0$  are large, and set  $m = 0$ . The only light degrees of freedom that contribute to  $j_{\mu}(x, s)$  in this sum are those coming from the RH Weyl field localized near the  $s = 1$  boundary. But when the global U(1) transformation associated with the five-dimensional conserved current is applied to this RH Weyl field only, it becomes anomalous. The anomaly must therefore be reproduced by the four-divergence  $\Delta_{\mu} \sum_{s=1}^{s_0} j_{\mu}(x, s)$ . At the same time, since the five-dimensional current is conserved (Eq. (4.7)), we have  $\Delta_{\mu} \sum_{s=1}^{s_0} j_{\mu}(x, s) = -j_5(x, s_0)$ , which means that the anomaly is reproduced again by  $-j_5(x, s_0)$ , also called the Chern-Simons current in this context [9, 27, 13].

We may also consider the complement five-dimensional sum,  $\sum_{s=s_0+1}^{N_5} j_{\mu}(x, s)$ , whose four-divergence is equal to  $+j_5(x, s_0)$ . This now correctly accounts for the anomaly arising from the LH chiral mode near the  $s = N_5$  boundary, including its opposite sign. The remarkable effect is that  $j_5(x, s_0)$  “knows” about the light degrees of freedom near the boundaries, even though it is located far from both of them, deep inside the five-dimensional bulk which in itself supports only massive degrees of freedom. Moreover, as we have seen,  $\pm j_5(x, s_0)$  correctly accounts for the anomaly due to the chiral field near each boundary.

When we sum  $j_\mu(x, s)$  over the entire range of the fifth coordinate the two anomalous contributions cancel each other, and we recover the conserved four-dimensional fermion-number current (Eq. (4.10) for the U(1) case). If instead we consider the difference of the two sums taking  $s_0 = N_5/2$  for definiteness, we recover the U(1) axial current (Eq. (4.14) for the U(1) case), where the anomalous contributions of the RH and LH fields add up, yielding the axial anomaly of a Dirac fermion in Eq. (4.34).

Additional differences of a more technical nature exist between the singlet and non-singlet axial currents. These will be discussed in Sec. 5.2.

## 4.4 The Pauli-Villars determinant

In this subsection we complete the description of the domain-wall fermion partition function (4.3), by explaining the role of the Pauli-Villars (PV) determinant. Thought of as a set of  $N_5$  four-dimensional fields, a domain wall fermion field describes one light Dirac field and  $N_5 - 1$  heavy Dirac fields whose masses are  $O(1)$  in lattice units.<sup>21</sup> Integrating out all the  $N_5 - 1$  heavy four-dimensional fields, but not the light four-dimensional field, would generate a *local* effective action for the lattice gauge field. By this we mean that we expect the couplings between remote sites (or links) in this effective action to decay exponentially, with a decay rate that is  $O(1)$  in lattice units. The total action for the gauge field (before including the contribution of the PV determinant) can thus be expressed as

$$S_{\text{tot}} \approx \frac{1}{g_0^2} S_g + (N_5 - 1) S_{\text{eff}} + S'_{\text{eff}} . \quad (4.35)$$

Here  $S_g/g_0^2$  is the lattice discretization of the continuum gauge field action introduced in Eq. (4.3). The contribution of the heavy fermion degrees of freedom that we have integrated out splits into two terms. The dominant term is  $N_5 S_{\text{eff}}$ , where  $S_{\text{eff}}$  is the effective action arising from integrating out a single four-dimensional layer deep inside the five-dimensional bulk, and the factor of  $N_5$  arises from the approximate translation invariance in the fifth direction away from the boundaries. The rest of the effective action,  $S'_{\text{eff}} - S_{\text{eff}}$ , is a correction that accounts for the influence of the boundaries on the heavy degrees of freedom.

We immediately see the problem with Eq. (4.35). A fixed, finite value for  $N_5$  would induce some finite renormalization of the bare coupling. But since we are interested in the limit  $N_5 \rightarrow \infty$ , this would entail a diverging contribution to the effective action of the gauge-field.

The PV determinant remedies this problem. The PV field is a five-dimensional field with  $m = 1$  in Eq. (3.30). As noted already, this implements anti-periodic boundary conditions in the fifth direction. Hence, the PV field represents  $N_5$  four-dimensional fields, all massive, with opposite statistics to the domain-wall fermion field. We thus expect that the PV contribution to the total gauge field effective action will be

$$-N_5 S_{\text{eff}} . \quad (4.36)$$

---

<sup>21</sup>For the actual masses of the heavy fields, see [30].

In the sum of Eqs. (4.35) and (4.36) the large contribution proportional to  $N_5$  drops out. One is left with some  $N_5$ -independent contribution, which is equivalent to a finite renormalization of the bare coupling.

The tight relation between the domain wall fermion and PV operators has many useful consequences. One such implication will be discussed in the next subsection. In modern numerical QCD calculations using domain wall fermions, the intimate relation between the domain wall and PV operators is taken one step further. One writes

$$\det(D_{DW}(m)) \det^{-1}(D_{DW}(1)) = \det(D_{DW}^{-1}(1)D_{DW}(m)) , \quad (4.37)$$

and treats  $D_{DW}^{-1}(1)D_{DW}(m)$  as a new domain-wall fermion operator. This will be further discussed in the next subsection, as well as in Sec. 7.1. Considered as the domain-wall fermion operator,  $D_{DW}^{-1}(1)D_{DW}(m)$  couples lattice sites with arbitrarily large separation, because the same is true for  $D_{DW}^{-1}(1)$ . Nevertheless, the Dirac operator  $D_{DW}^{-1}(1)D_{DW}(m)$  is local in a similar sense to what we have discussed above. Because the operator  $D_{DW}^{-1}(1)$  has only lattice-scale excitations, one expects that the coupling of remote sites via  $D_{DW}^{-1}(1)$  will decay exponentially with a lattice-scale rate.<sup>22</sup>

## 4.5 The effective Dirac operator for the light fermion

When we integrate out the five-dimensional heavy fermion degrees of freedom, this not only generates an effective action for the gauge field, but also induces an effective Dirac operator for the light four-dimensional fermion field. In this subsection we examine this effective Dirac operator in more detail, both for finite  $N_5$  and in the limit  $N_5 \rightarrow \infty$ . We will consider a single domain wall field, and for simplicity we will first set  $m = 0$ . We will show how, with the help of the PV determinant, one obtains an effective Dirac operator for the light four-dimensional field that satisfies the Ginsparg-Wilson (GW) relation [16] in the limit  $N_5 \rightarrow \infty$ .

We start by examining the global WTI for the domain-wall quark propagator in a fixed gauge field background  $\mathcal{U}$  (the dependence on  $\mathcal{U}$  will usually be omitted). To this end we choose a bi-local operator  $O(y_1, y_2) = q(y_1)\bar{q}(y_2)$  in Eq. (4.19), considering the singlet axial current. Upon summing over the four-dimensional coordinates the left-hand side of Eq. (4.19) vanishes, and for  $m = 0$  we obtain

$$2 \sum_x \left\langle J_{5q}(x) q(y_1)\bar{q}(y_2) \right\rangle = \{ \gamma_5, G_q(y_1, y_2) \} , \quad (4.38)$$

$$G_q(y_1, y_2) = \left\langle q(y_1)\bar{q}(y_2) \right\rangle . \quad (4.39)$$

In the free theory, the expectation value  $\langle J_{5q} \rangle$  vanishes for  $N_5 \rightarrow \infty$  (for relevant technicalities see, *e.g.*, Ref. [28]). This implies that the left-hand side of Eq. (4.38) does not have a disconnected contribution. As for the connected contribution, the domain wall fields from which the ‘‘midpoint’’ pseudoscalar density  $J_{5q}$  is built are

---

<sup>22</sup>For a discussion of the closely related issue of locality of exact or approximate GW operators, see Sec. 6.6.

contracted with the boundary fields  $q$  and  $\bar{q}$ . Much like the non-singlet case (Sec. 4.2), this contribution vanishes for  $N_5 \rightarrow \infty$  as well. Thus, the left-hand side of Eq. (4.38) as a whole vanishes in this limit. We comment in passing that the same conclusion applies in the background of perturbative gauge fields. The physical reason is that the anomaly (Eq. (4.34)) can be expressed as the divergence of a gauge non-invariant current whose integral is the topological charge, which is zero in perturbation theory. Hence  $\sum_x \langle J_{5q}(x) \rangle$  again vanishes. (This is true up to the usual discretization effects associated with the definition of the topological charge on the lattice.)

The conclusion is that for  $N_5 \rightarrow \infty$ , the domain wall quark propagator  $\langle q \bar{q} \rangle$  anti-commutes with  $\gamma_5$  for  $m = 0$ . This result can be confirmed in the free theory using the explicit form of the propagator derived in Sec. 3.2, as well as in the presence of a perturbative background field using the more general result derived in Ref. [21]. In all cases, the conclusion simply follows from the fact that, for  $m = 0$ , the mixed-chirality components  $\langle q_R \bar{q}_L \rangle$  and  $\langle q_L \bar{q}_R \rangle$  require coupling between the two boundaries, and thus vanish exponentially for  $N_5 \rightarrow \infty$ .<sup>23</sup>

The anti-commutativity of the domain-wall quark propagator  $\langle q \bar{q} \rangle$  with  $\gamma_5$  is an expression of the restoration of chiral symmetry at  $m = 0$  for  $N_5 \rightarrow \infty$ . Naively, it suggests that in this limit we may define an effective domain-wall quark operator as

$$D_{\text{eff}}^{-1} = \langle q \bar{q} \rangle . \quad (4.40)$$

Being the inverse of the domain-wall quark propagator,  $D_{\text{eff}}$  anti-commutes with  $\gamma_5$  as well. However, this leads to a highly undesirable consequence! According to the no-go theorems about fermion doubling [1, 2, 3, 4, 5], a free lattice Dirac operator that anti-commutes with  $\gamma_5$  cannot describe a single massless Dirac fermion if the dispersion relation is smooth. In order to figure out what is going on, let us reexamine the free propagator  $\langle q \bar{q} \rangle$  for  $m_q = 0$ , in the limit  $N_5 \rightarrow \infty$ . In Sec. 3.2 we have calculated this propagator for  $p \ll 1$  and general  $m$ , finding that for  $m = 0$  it has a pole at  $p = 0$  that represents one massless Dirac fermion (Eq. (3.49)). Returning to general  $p$  (keeping  $m = 0$ ), the relevant term in the free propagator takes the form of  $\not{p} A_-(p^2)$  up to a proportionality constant. The amplitude  $A_-(p^2)$  has a  $1/p^2$  pole for  $p \rightarrow 0$ , whereas everywhere else in the Brillouin zone it is regular. It follows that  $\langle q \bar{q} \rangle$  has a massless pole,  $\not{p}/p^2$ , at  $p = 0$ , but at the other 15 corners of the Brillouin zone it has *zero* eigenvalues. Using Eq. (4.40), the effective Dirac operator  $D_{\text{eff}}$  thus has *poles* at all the corners of the Brillouin zone except for the origin. While the presence of poles in  $D_{\text{eff}}$  means that it is not subject to the no-go theorems, this is clearly an undesirable situation that limits the ability to interpret  $D_{\text{eff}}$  as an effective low-energy operator. For relevant discussion in the context of the no-go theorems, see Refs. [4, 5, 31, 32].

It should be clear that the issue we encounter here is not a fundamental flaw of domain wall fermions. Indeed we already know that the domain wall operator describes one light four-dimensional field alongside with  $N_5 - 1$  heavy fields with cutoff scale masses that decouple in the continuum limit. Rather, the presence of poles in  $D_{\text{eff}}$  is an artifact of our attempt to use the inverse of  $\langle q \bar{q} \rangle$  as the effective

---

<sup>23</sup>For perturbative gauge fields the transfer matrix (Sec. 4.2) cannot have any eigenvalue equal to one.

Dirac operator for the light field. As it turns out, in order to remedy this problem it is enough to modify the definition of the effective Dirac operator by postulating that its inverse is equal to the right-hand side of Eq. (4.40) up to a contact term. For any  $x \neq y$  the new free propagator will still be equal to  $\langle q(x) \bar{q}(y) \rangle$ , and will thus anti-commute with  $\gamma_5$ . But this will no longer be true at coinciding points. As we will see, the new Dirac operator satisfies the GW relation.

The construction works as follows [30, 33]. Starting from the representation of the product

$$Z_{DW} = \det(D_{DW}(m=0)) \det^{-1}(D_{DW}(m=1)) , \quad (4.41)$$

as a path integral over five-dimensional fermion and PV fields, we first integrate out most of the fermion and PV degrees of freedom, obtaining (we suppress the dependence on  $N_5$ )

$$Z_{DW} = \int dq d\bar{q} dQ dQ^\dagger \exp(-\bar{q} D_{\text{eff}} q - Q^\dagger (D_{\text{eff}} + 1) Q) , \quad (4.42)$$

where  $D_{\text{eff}}$  is defined in Eq. (4.40). The domain wall fermion degrees of freedom that we have integrated out include the four-dimensional layers  $s = 2, 3, \dots, N_5 - 1$ , as well as half of the degrees of freedom on the two boundary layers, those that are *not* used in the construction of the domain-wall quark field (3.31). We treat the PV fields similarly, with the remaining  $Q(x)$  and  $Q^\dagger(x)$  four-dimensional PV fields constructed similarly to Eq. (3.31). Notice that for the degrees of freedom that have been integrated out, the domain-wall fermion and PV operators are identical, as none of these degrees of freedom couple to the  $m$ -dependent terms in Eq. (3.30). Hence, the determinants resulting from this integration cancel each other.

The remaining degrees of freedom that occur on the right-hand side of Eq. (4.42) are those that compose the domain-wall quark field, as well as the corresponding PV degrees of freedom. The difference between the two effective operators is simply because the PV operator has the mass terms with  $m = 1$  coupling the two boundaries in Eq. (3.30), whereas for the domain-wall fermions we set  $m = 0$ . We now make a change of variables

$$\bar{\Psi} = \bar{q} , \quad \Psi = (D_{\text{eff}} + 1)q . \quad (4.43)$$

Expressing the partition function in terms of the new variables gives

$$Z_{DW} = \int d\Psi d\bar{\Psi} \exp(-\bar{\Psi} D_{GW} \Psi) , \quad (4.44)$$

where

$$D_{GW} = \frac{D_{\text{eff}}}{1 + D_{\text{eff}}} , \quad (4.45)$$

and the change of variables (4.43) has absorbed the determinant resulting from the integration over the remaining PV fields. This result is valid for any  $N_5$ .

A first encouraging observation is that the fifteen poles that  $D_{\text{eff}}$  admits for  $N_5 \rightarrow \infty$  cancel out between the numerator and the denominator in Eq. (4.45),

without affecting the existence of the relativistic massless state at  $p = 0$ . Further understanding of the physical nature of the new Dirac operator comes from considering the new propagator. From Eq. (4.45),

$$D_{GW}^{-1} = D_{\text{eff}}^{-1} + 1 , \quad (4.46)$$

a result which is again valid for any  $N_5$ . We have seen that for  $N_5 \rightarrow \infty$ , the propagator  $D_{\text{eff}}^{-1}$  anti-commutes with  $\gamma_5$ . Hence in this limit

$$\{D_{GW}^{-1}, \gamma_5\} = \{D_{\text{eff}}^{-1}, \gamma_5\} + 2\gamma_5 = 2\gamma_5 . \quad (4.47)$$

As promised, in this limit the new propagator  $D_{GW}^{-1}$  still anti-commutes with  $\gamma_5$ , *except* at coinciding points. In fact, what we have found is that for  $N_5 \rightarrow \infty$ , the effective Dirac operator  $D_{GW}$  satisfies the GW relation,

$$\{D_{GW}, \gamma_5\} = 2D_{GW}\gamma_5D_{GW} . \quad (4.48)$$

So far we have only used the general structure of the domain wall operator (3.30) and the restoration of chiral symmetry for  $N_5 \rightarrow \infty$ . A lengthy derivation [30, 33] yields an explicit expression for the approximate GW operator at finite  $N_5$ ,

$$D_{GW}(N_5) = \frac{1}{2} \left( 1 + \gamma_5 \tanh \left( (N_5/2) H_T \right) \right) \quad (4.49a)$$

$$= \frac{1}{2} \left( 1 + \gamma_5 \frac{1 - T^{N_5}}{1 + T^{N_5}} \right) , \quad (4.49b)$$

where the transfer matrix  $T$  is given in Eq. (4.26), and

$$H_T = -\frac{1}{2} \log T^2 . \quad (4.50)$$

This definition ensures that  $H_T$  is well defined in the presence of both positive and negative eigenvalues of the transfer matrix  $T$ .<sup>24</sup> In the limit  $N_5 \rightarrow \infty$  we recover the familiar expression for the GW operator,

$$D_{GW} = \frac{1}{2} \left( 1 + \gamma_5 \epsilon(H) \right) , \quad (4.51)$$

where  $\epsilon(x)$  is the sign function,  $\epsilon(x) = +1$  for  $x > 0$  and  $\epsilon(x) = -1$  for  $x < 0$ , and  $H = H_T$ . The difference between this GW operator and the standard overlap operator [18] is in the choice of  $H$ . While here  $H_T$  is defined in terms of the transfer matrix via Eq. (4.50), in the case of the standard overlap operator  $H$  is chosen to be the hermitian version of the Wilson kernel,  $H_W = \gamma_5 D$  (see Eq. (3.2)). We will further examine the relation between these two GW operators in Sec. 6, where we also discuss the special case of zero eigenvalues of  $H$ .

---

<sup>24</sup>Negative eigenvalues of the transfer matrix are discussed in Sec. 7.2.1. Since we always take  $N_5$  even, we are allowed to replace  $T$  by the positive square root of  $T^2$  in Eq. (4.49b).

The generalization to a nonzero mass for the domain wall fermion is obtained by simply replacing  $\bar{q} D_{\text{eff}} q$  by  $\bar{q}(D_{\text{eff}} + m)q$  in Eq. (4.42) and repeating the subsequent steps. Equation (4.45) can be inverted to give

$$D_{\text{eff}} = \frac{D_{GW}}{1 - D_{GW}} , \quad (4.52)$$

and for  $N_5 \rightarrow \infty$  we find

$$D_{GW}(m) = \frac{1+m}{2} + \frac{1-m}{2} \gamma_5 \epsilon(H) = D_{GW}(0) + m(1 - D_{GW}(0)) , \quad (4.53)$$

where the massless GW operator  $D_{GW} = D_{GW}(0)$  is given in Eq. (4.51). For more details, see for example Refs. [30, 34].

In summary, our starting point was the four-dimensional operator  $D_{\text{eff}}$  defined by Eq. (4.40), which anti-commutes with  $\gamma_5$ , hence it is invariant under ordinary chiral transformations. But  $D_{\text{eff}}$  also has some undesirable properties, which are necessary in order to reconcile its chiral invariance with the no-go theorems. Instead, we have reached a closely related operator that satisfies the GW relation. Any GW operator enjoys a modified form of chiral symmetry [35]. Here we will only note that the chiral anomaly is correctly reproduced by the variation of the lattice fermion measure under this modified chiral transformation. For a detailed discussion of the GW relation, including its modified chiral symmetry, we refer to the companion chapter of the *LQCD@50* book by DeGrand [15].

We conclude with a technical comment. The PV fields are bosonic variables, and so in order to make the integration over them rigorously well defined an analytic continuation is needed. With  $D_{PV} = D_{DW}(m=1)$ , and denoting the PV fields as  $\Phi$  and  $\Phi^\dagger$ , we have

$$\det^{-1}(D_{PV}) = \lim_{\epsilon \rightarrow 0} \int d\Phi d\Phi^\dagger \exp(\Phi^\dagger (i\gamma_5 \mathcal{R} D_{PV} - \epsilon) \Phi) . \quad (4.54)$$

Thanks to the  $\gamma_5$ -hermiticity properties discussed below Eq. (3.30), the eigenvalues of  $i\gamma_5 \mathcal{R} D_{PV}$  are pure imaginary, and the added factor of  $\epsilon$  ensures convergence of the integral.<sup>25</sup> All the results we have obtained above remain valid with this more careful procedure.

## 5 Residual breaking of chiral symmetry

So far, the quantitative information we have on domain wall fermions was mostly restricted to the free theory (Sec. 3). Beyond that, the discussion of chiral symmetry restoration in Sec. 4 gave us a glimpse into the dynamics of the interacting theory. In particular, we observed that the transfer matrix can have eigenvalues equal to unity. Hence, the probability to encounter near-unity eigenvalues of the transfer matrix in

---

<sup>25</sup>For a similar analytic continuation, see Ref. [36].

an ensemble of configurations is going to affect the rate at which chiral symmetry is restored for  $N_5 \rightarrow \infty$ .

In the rest of this introduction we will delve deeper into the physics of domain wall fermions. The main issue is the rate of restoration of chiral symmetry with increasing  $N_5$ , and the quality of chiral symmetry which is achievable in practice in numerical simulations. In this section we will introduce the notion of the residual mass, which is a quantitative measure of the imperfect chiral symmetry at finite  $N_5$ . We will study the restoration of chiral symmetry for  $N_5 \rightarrow \infty$ , equivalently the vanishing of the residual mass, within lattice perturbation theory. Later, in Sec. 6.7, we will extend the discussion to non-perturbative effects (this will include the role of the near-unity eigenvalues of the transfer matrix).

We begin in Sec. 5.1 with a calculation of the dependence of the wave function of a domain-wall quark on the fifth coordinate. In the free theory, the wave function is just  $(1 - M)^s$ . In particular we noted that by setting the domain wall height to  $M = 1$ , this wave function is entirely supported on the relevant boundary layer when  $m = 0$ . We cannot expect this ideal situation to survive when the gauge interactions are turned on, which leads us to study the wave function in (tadpole improved) one-loop perturbation theory as the next step.

In Sec. 5.2 we turn to the most important physical effect that depends on the “tail” of the wave function. Much like (four-dimensional) Wilson fermions, this is an additive correction to the mass of the domain-wall quark, which is not proportional to the parameter  $m$  introduced into the domain-wall fermion operator (3.30). While the additive correction is guaranteed to vanish for  $N_5 \rightarrow \infty$  (Sec. 4.2), where chiral symmetry is restored, in order to design numerical calculations using domain wall fermions we need a pretty good idea what to expect for finite  $N_5$ .

Wilson fermions completely lack chiral symmetry at finite lattice spacing. This implies that the bare Wilson mass is not renormalized multiplicatively. In numerical lattice calculations the additive correction to the bare Wilson mass is typically  $O(1)$  in lattice units. Large additive corrections similarly afflict other chirally sensitive observables calculated using Wilson fermions. By contrast, for domain wall fermions it is common to achieve an additive mass correction smaller by several orders of magnitude. Hence the name residual mass [37, 38]. This is a dramatic improvement over Wilson fermions, that extends to other chirally sensitive observables as well. Unlike staggered fermions, at the same time the (vector) flavor symmetry is fully preserved.

## 5.1 Wave function of domain wall fermions

In Sec. 5.1.1 we discuss tadpole improvement of the domain-wall quark wave function, and in Sec. 5.1.2 the genuine one-loop correction.

### 5.1.1 Tadpole improvement

We start with the tadpole correction [39, 40, 41]. In the limit  $N_5 \rightarrow \infty$ , hence in the absence of any mixing between the RH and LH zero modes, the tadpole improved

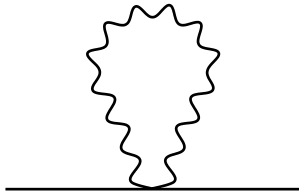


Figure 2: Tadpole correction in one-loop lattice perturbation theory.

tree-level wave function of the RH zero mode is (as in Eq. (3.10) we omit spinor indices and disregard an overall normalization factor)

$$\chi_R(s) = (1 + \delta M - M)^s = (1 - \overline{M})^s, \quad (5.1)$$

where  $\overline{M} = M - \delta M$ . Diagrammatically, the leading tadpole correction arises from the one-loop diagram shown in Fig. 2. As such, the tadpole correction  $\delta M$  is formally an  $O(g_0^2)$  effect. We can expand the tadpole improved wave function around the tree level one,

$$(1 + \delta M - M)^s = (1 - M)^s \left( 1 + s R_M + \frac{s(s-1)}{2} R_M^2 + \dots \right), \quad (5.2)$$

where  $R_M = \delta M / (1 - M)$ . Naively, it appears that  $R_M$  is also an  $O(g_0^2)$  quantity, and in view of the usual rules of a perturbative expansion we ought to truncate the expansion (5.2) at linear order in  $R_M$ . In fact, this truncation must *not* be done, as we will now explain.

The first argument invokes the order of limits adequate for domain wall fermions. Since the fifth coordinate  $s$  ranges from 1 to  $N_5$ , the expansion parameter of Eq. (5.2) is effectively  $g_0^2 N_5$ . If the chiral limit  $N_5 \rightarrow \infty$  is taken first, then  $g_0^2 N_5$  diverges. If the continuum limit  $g_0^2 \rightarrow 0$  is taken first,  $g_0^2 N_5$  vanishes. However, it is the chiral limit that we want to take first, in order to restore chiral symmetry of the effective four-dimensional theory already at finite lattice spacing (Sec. 4.2 and Sec. 4.5). Hence  $g_0^2 N_5 \gg 1$ , and we must always resum the expansion in (5.2). This, of course, recovers the tadpole-improved tree level wave function in Eq. (5.1).

A comparison of Eqs. (4.23) and (5.1) suggests that the physical origin of the tadpole correction  $\delta M$  is the expectation value of the (positive) Wilson term  $W$  on the dominant eigenmodes of the transfer matrix  $Q$ : the eigenmodes whose eigenvalues are closest to unity (Sec. 4.2). Equivalently, these are the near-zero eigenmodes of the transfer matrix hamiltonian  $H_T$ , Eq. (4.50). Let us look for numerical evidence that the additive mass renormalization  $m_c$  of Wilson fermions represents essentially the same physical effect as the additive correction to the optimal domain wall height. Why this is the case will be made clearer in Sec. 6.

When using Wilson fermions, in order to recover a massless quark in the continuum limit we must tune the bare mass  $m_0$  non-perturbatively such that  $m_0 + m_c = 0$ . Hence  $m_0 = -m_c$ , where the value of the critical mass  $m_c$  is usually in the range of

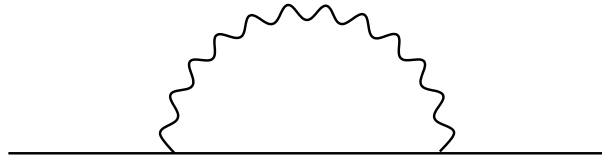


Figure 3: Setting sun diagram, the dominant contribution to the quantum wave function of the domain wall quark.

0.7 – 1.0 for typical values of the bare coupling in simulations [42]. As for domain wall fermions, the values of the domain wall height  $M$  that yield the best damping of the domain wall quark wave function are usually found to be in the range of 1.7 – 1.8. As a heuristic way to determine the tadpole correction  $\delta M$  let us assume that this optimal domain wall height corresponds to the most localized tree-level improved wave function, for which  $\overline{M} = 1$  in Eq. (5.1). Equivalently, this implies  $\delta M = M - 1$  after optimizing the value of  $M$ . With the above range for the optimal  $M$ , we obtain that  $\delta M$  is 0.7 – 0.8, nicely consistent with the range of the critical Wilson mass  $m_c$ .

Back to Eq. (5.2), the above procedure for estimating  $\delta M$  amounts to tuning the domain wall height  $M$  such that  $\delta M + 1 - M = 0$ , hence  $R_M = -1$ . While it is formally true that  $\delta M = O(g_0^2)$ , we see that  $1 - M$  is tuned to be of exactly the same size. This leads to a stronger conclusion: as long as we apply this procedure, it does not matter which limit will be taken first, the chiral limit  $N_5 \rightarrow \infty$  or the continuum limit  $g_0^2 \rightarrow 0$ . Either way, the expansion in Eq. (5.2) is not controlled by a small parameter, and thus it must always be resummed to yield the tadpole improved wave function (5.1).

With  $M$  in the range 1.7 – 1.8, which means  $1 < M < 2$ , the operator  $B$  will have negative eigenvalues, and the same is true for the transfer matrix.<sup>26</sup> In practice, negative eigenvalues of  $B$  are rarely encountered, suggesting that on a realistic ensemble of gauge field configurations the expectation value of the Wilson term that we have loosely described above is fairly stable, and bounded below by  $M - 1$ . We will return to the connection between the critical Wilson mass and the optimal domain wall height in Sec. 6.2.

### 5.1.2 One loop wave function

We now turn to the genuine one-loop correction to the domain wall quark wave function which results from the “setting sun” diagram in Fig. 3. We will first present the final result, and then explain the main steps of the calculation.<sup>27</sup> Following Ref. [41], in this subsection we set  $m = 0$ .

We define an effective wave function  $\chi_{\text{eff}}(s)$  for the domain wall quark by looking at the singular part of the dressed domain wall propagator  $G_{s,s'}(p)$  arising from the RH massless field near the  $s = 0$  boundary, the part proportional to  $P_R \not{p}^{-1}$  (compare

<sup>26</sup>For example, in the free theory for  $p = 0$ .

<sup>27</sup>For some discussion of two loop and higher corrections see Ref. [41].

Eq. (3.29)). Taking the limit  $N_5 \rightarrow \infty$ , we may calculate the perturbative corrections to the effective wave function using the semi-infinite setting of Sec. 3.1. The factor multiplying  $P_R \not{p}^{-1}$  is then expected to be the product of the (index-less) effective wave functions at  $s$  and  $s'$ . We thus make the *ansatz*

$$G_{s,s'}(p) = \chi_{\text{eff}}(s) P_R \frac{1}{i\not{p}(1 + g_0^2 \Sigma_K)} \chi_{\text{eff}}(s') + \dots, \quad (5.3)$$

neglecting terms whose  $p$  dependence is regular. Here  $\Sigma_K$  is a standard logarithmic correction that leads to a wave-function renormalization of the domain wall quark field [39]. As a further simplification, we will calculate  $\chi_{\text{eff}}(s)$  for  $s, s' \gg 1$ . Within tadpole-improved one loop perturbation theory one finds<sup>28</sup>

$$\chi_{\text{eff}}(s) = (\overline{M} (2 - \overline{M}))^{1/2} (1 - \overline{M})^s + \chi_1(s) = \delta_{s,0} + \chi_1(s), \quad (5.4)$$

where the second equality is valid in the limit  $\overline{M} \rightarrow 1$ , equivalently, after tuning  $M$  to its optimal value  $1 + \delta M$ . The genuine one-loop wave function is then

$$\chi_1(s) = -c g_0^2 \frac{1}{s^2 2^s}, \quad (5.5)$$

where  $c \approx 0.8$ .

This result is obtained as follows. Tuning  $M$  to its optimal value in the tadpole improved wave function  $(1 + \delta M - M)^s$  is effectively the same as taking the limit  $M \rightarrow 1$  in the tree level wave function  $(1 - M)^s$ . We similarly take the limit  $M \rightarrow 1$  in the expressions for the tree level propagator obtained in Sec. 3.1. On the external legs of the self-energy diagram in Fig. 3 we thus have both  $M \rightarrow 1$  and  $p \rightarrow 0$ . As is easily inferred from the derivation in Sec. 3.1, in this special limit the domain wall propagator can connect a given four-dimensional layer only to itself or to one of its neighboring layers.

By contrast, the domain wall propagator inside the loop can carry any momentum, and can therefore connect any two four-dimensional layers. When one of these layers is the  $s = 0$  boundary or very close to it, the amplitude is  $\sim e^{-\alpha(p)s}$ . Moreover, the gauge field couples equally to all the four-dimensional layers, and provides no extra suppression as the separation in the fifth direction grows. The outcome is that for large separations in the fifth direction, the self-energy diagram behaves like  $\sim \eta_{\text{max}}^s$ , where  $\eta_{\text{max}}$  is the maximum of  $e^{-\alpha(p)}$  over the whole Brillouin zone. For  $M \rightarrow 1$  the maximum is  $\eta_{\text{max}} = 1/2$ , and it is obtained at the four corners of the Brillouin zone where one momentum component is equal to  $\pi$ , while the rest are zero. The exponential dependence of the self-energy on  $s$  thus goes like  $1/2^s$ . The  $1/s^2$  power correction in Eq. (5.5) arises from the four-dimensional phase space of a saddle-point integral around any one of the four degenerate maxima of  $e^{-\alpha(p)}$  [41].

The lesson from this calculation is the following. Both the purely tree-level and the tadpole improved wave functions can be tuned to be entirely localized on the boundary. But this is no longer possible for the genuinely quantum part of the wave

<sup>28</sup>In this subsection we assume that the fifth coordinate takes values  $s = 0, 1, 2, \dots$

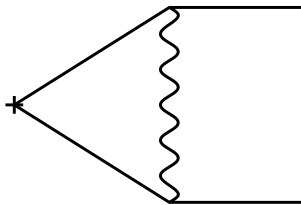


Figure 4: Mixing of  $J_{5q}^a$  with  $J_5^a$ , or  $J_{5q}$  with  $J_5$ .

function. The quantum broadening of the wave function occurs because the virtual fermion propagating inside the diagram can have arbitrary momentum (with a matching momentum carried by the gauge field). Hence, the least damped propagation in the fifth direction is always controlled by the maximum of  $e^{-\alpha(p)}$  over the Brillouin zone. More generally, in an arbitrary gauge field background the least damped propagation will originate from the largest eigenvalues of the transfer matrix  $Q$  (Eq. (4.30)), as we will discuss in Sec. 6.7.

## 5.2 The residual mass

There is no consistent regularization method that fully preserves chiral symmetry. The reason is that any consistent regularization must reproduce the chiral anomaly.<sup>29</sup> For example, in the continuum, and for a vanishing fermion mass, the classical continuity equation of a flavor non-singlet axial current is

$$\partial_\mu J_{5\mu}^a = 0 . \quad (5.6)$$

When dimensional regularization is used, the continuity equation develops a nonzero right-hand side

$$\partial_\mu J_{5\mu}^a = \Delta^a , \quad d \neq 4 . \quad (5.7)$$

Here  $\Delta^a$  is an *evanescent* operator: an operator that formally vanishes for  $d \rightarrow 4$ . Thanks to the cancellation between a factor of  $d - 4$ , arising from the evanescent operator, and a factor of  $1/(d - 4)$ , arising from the loop integral, for  $d \rightarrow 4$  one obtains

$$\Delta^a = (1 - Z_5) \partial_\mu J_{5\mu}^a , \quad (5.8)$$

with finite  $Z_5$ . This result implies that the renormalized current (defined by generating canonically normalized contact terms in WTIs) is  $Z_5 J_{5\mu}^a$ . In this case one can further show that in fact  $Z_5 = 1$ , namely, the non-singlet axial currents are unrenormalized, at least at one loop [43]. However, this depends on further specific properties of dimensional regularization that need not apply to other consistent regularization schemes.

In the case of domain wall fermions, the counterpart of Eq. (5.7) is Eq. (4.15), in which the quantum breaking of the conservation of a non-singlet axial current  $\mathcal{A}_\mu^a$

<sup>29</sup>For the way the chiral anomaly arises for GW fermions, see, *e.g.*, Refs. [10, 14].

is represented by the mid-point pseudoscalar density  $J_{5q}^a$ . Re-introducing the lattice spacing  $a$  and generalizing Eq. (5.8) to  $a > 0$  we may write

$$(1/a)J_{5q}^a(x) = m_{\text{res}}J_5^a(x) + \frac{1 - Z_{\mathcal{A}}}{2} \sum_{\mu} \Delta_{\mu} \mathcal{A}_{\mu}^a(x) + O(a) . \quad (5.9)$$

This equation expresses the action of the operator  $J_{5q}^a$  on states created from the domain-wall quark fields  $q$  and  $\bar{q}$  (see the discussion around Eq. (4.20)). The expansion on the right-hand side involves operators with the same quantum numbers as  $J_{5q}^a$  under the exact lattice symmetries. In addition to the dimension-three operator  $J_5^a$  and the dimension-four operator  $\sum_{\mu} \Delta_{\mu} \mathcal{A}_{\mu}^a$ , there are corrections that involve operators of dimension five and higher which are made out of the quark fields  $q$  and  $\bar{q}$ , and are multiplied by positive powers of the lattice spacing. This equation defines the residual mass  $m_{\text{res}}$  as the coefficient of  $J_5^a$  on the right-hand side.  $m_{\text{res}}$  is thus a function of the bare coupling only. We recall that  $J_5^a$  is the standard pseudoscalar density constructed from the quark fields on the four-dimensional boundaries. Similarly,  $(1 - Z_{\mathcal{A}})/2$  is the coefficient of  $\sum_{\mu} \Delta_{\mu} \mathcal{A}_{\mu}^a$  itself. Equation (5.9) applies within the Symanzik effective theory, which is an expansion in powers of the lattice spacing. The terms shown explicitly in Eq. (5.9) are the ones that survive in the continuum limit. Substituting this expansion back into Eq. (4.15), it becomes<sup>30</sup>

$$Z_{\mathcal{A}} \sum_{\mu} \Delta_{\mu} \mathcal{A}_{\mu}^a(x) = 2(m + m_{\text{res}})J_5^a(x) + O(a) . \quad (5.10)$$

This result applies when considering any correlation function involving only the boundary quark fields, as per Eq. (4.20). The WTIs that follow from this partial conservation equation will have canonically normalized contact terms, as in Eq. (4.19).

We would like to draw attention to a somewhat unusual feature of Eq. (5.9). Suppose that our goal was to expand the mid-point operator  $J_{5q}^a$ , which lives inside the five-dimensional bulk, in terms of operators made out solely of the  $q$  and  $\bar{q}$  fields, from which the effective four-dimensional theory is built. In this case we should not make use of the partially-conserved current  $\mathcal{A}_{\mu}^a$  in the expansion, because this current is not built solely from the  $q$  and  $\bar{q}$  fields. However, our ultimate goal is to reach the expansion (5.10) for the partially-conserved axial current itself, hence the presence of the  $\sum_{\mu} \Delta_{\mu} \mathcal{A}_{\mu}^a$  term on the right-hand side of Eq. (5.9). Our final result, Eq. (5.10), indeed meets the expectation that all the operators occurring on its right-hand side are built from the  $q$  and  $\bar{q}$  fields only.

In Sec. 5.1 we have seen that the quantum wave function of the domain-wall quarks decays exponentially as we move in the  $s$  direction away from the boundaries. When the domain wall height is tuned to its optimal value, the actual falloff rate is  $\eta_{\text{max}}^s$ . Since  $J_{5q}^a$  must connect to quark and anti-quark operators on the boundaries, this will always come with a factor of  $\eta_{\text{max}}^{2(N_5/2)} = \eta_{\text{max}}^{N_5}$ . In the rest of this subsection we will elaborate on this observation.

<sup>30</sup>In this subsection we are not concerned with multiplicative mass renormalization, and the associated renormalization of scalar and pseudoscalar densities, hence  $m$ ,  $m_{\text{res}}$  and  $J_5^a$  are all bare quantities.

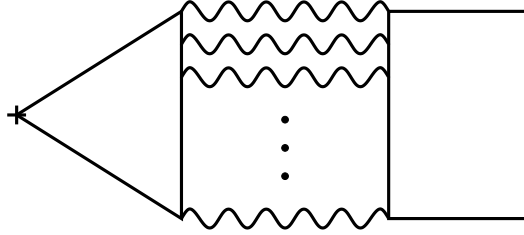


Figure 5: Mixing of  $J_{5q}$  with  $J_5$  only.

Consider first the mixing of  $J_{5q}^a$  with  $J_5^a$  for finite  $N_5$ . As we will shortly see, this mixing arises at the one loop level from the diagram shown in Fig. 4. Before we discuss this one-loop diagram, however, let us consider the corresponding tree diagram obtained by omitting the gauge field propagator in Fig. 4. In this tree diagram,  $J_{5q}^a$  will be connected to the quark fields at the boundaries by two tree-level propagators in which we must take the limits  $M \rightarrow 1$  and  $p \rightarrow 0$ . But, as we have seen in Sec. 5.1, the tree-level propagator vanishes for this kinematics.

The first diagram that may contribute to the mixing of  $J_{5q}^a$  with  $J_5^a$  is thus the one-loop diagram of Fig. 4. This works in essentially the same way as in Sec. 5.1. While the external propagators are constrained by both  $M \rightarrow 1$  and  $p \rightarrow 0$ , the internal fermion propagators can carry any momentum. Once again, this implies that the loop integral will be dominated by those virtual momenta for which  $e^{-\alpha(p)}$  is close to its maximal value  $\eta_{\max}$ . The resulting exponential suppression factor will be  $\sim g_0^2 \eta_{\max}^{N_5}$  (this is true up to subleading power-law corrections, compare Eq. (5.5)). We thus expect  $m_{\text{res}}$  in Eq. (5.10) to be parametrically of this size, as far as perturbative corrections are concerned. The same estimate applies to the magnitude of  $Z_{\mathcal{A}} - 1$ , when all quantities are evaluated in lattice units:

$$am_{\text{res}}, Z_{\mathcal{A}} - 1 \sim g_0^2 \eta_{\max}^{N_5}. \quad (5.11)$$

Turning to the singlet axial current, we follow the same reasoning while taking into account the axial anomaly (Eq. (4.34)). This leads to

$$\begin{aligned} Z_{\mathcal{A}}^s \sum_{\mu} \Delta_{\mu} \mathcal{A}_{\mu}(x) &= 2(m + m_{\text{res}}^s) J_5(x) \\ &+ \frac{ig_0^2 N_F}{4\pi^2} \sum_{\mu\nu\lambda\rho} \epsilon_{\mu\nu\lambda\rho} \partial_{\mu} A_{\nu}(x) \partial_{\lambda} A_{\rho}(x) + O(a), \end{aligned} \quad (5.12)$$

where the superscript  $s$  indicates quantities pertaining to the singlet axial current. The question arises whether or not the parameter  $m_{\text{res}}^s$  associated with the singlet axial current is equal to the residual mass parameter  $m_{\text{res}}$  of the non-singlet currents. The answer is that they are different. A class of diagrams that contribute to  $m_{\text{res}}^s$  but not to  $m_{\text{res}}$  is shown in Fig. 5. Similarly,  $Z_{\mathcal{A}}^s$  and  $Z_{\mathcal{A}}$  are not equal.

An alternative notion of the residual mass<sup>31</sup> may be introduced by directly com-

<sup>31</sup>Historically, the residual mass was defined by Eq. (5.13) when it was first introduced [37].

paring a physical matrix element of  $J_{5q}^a$  with the corresponding matrix element of  $J_5^a$  [38, 44],

$$m'_{\text{res}} = \frac{1}{a} \frac{\langle 0 | J_{5q}^a | \pi^a \rangle}{\langle 0 | J_5^a | \pi^a \rangle}. \quad (5.13)$$

The pion state is taken at  $\vec{p} = 0$ . Unlike  $m_{\text{res}}$  of Eq. (5.9), which is by definition independent of the input quark mass  $m$ , Eq. (5.13) allows  $m'_{\text{res}}$  to depend on  $m$ . One can determine  $m_{\text{res}}$  at one particular value of the bare coupling by first obtaining  $m'_{\text{res}}$  for several values of  $m$ , and then extrapolating  $m'_{\text{res}}$  to the limit of a vanishing input mass,  $m \rightarrow 0$ . In practice, the differences between  $m'_{\text{res}}$  and  $m_{\text{res}}$  turn out to be at the few percents level (see, for example, Fig. 7 of Ref. [45]). Hence, both  $m_{\text{res}}$  and  $m'_{\text{res}}$  qualify as a qualitative measure of the goodness of chiral symmetry at finite  $N_5$ .

Expressions such as Eq. (5.10), and their generalizations to higher powers of lattice spacing  $a$  within the Symanzik effective theory, provide a crucial intermediate step in the application of chiral perturbation theory for domain wall fermions. For details, we refer to the original literature [46, 45, 47, 34].

## 6 The Wilson kernel

The goal of this section is to explore non-perturbative effects associated with the Wilson kernel. These effects influence the rate of restoration of chiral symmetry with increasing  $N_5$ , as well as the locality properties of the effective four-dimensional operator for the domain wall quarks. As it turns out, some ground work has to be done first.

We start in Sec. 6.1 with a seemingly unrelated topic: the phase diagram of QCD with two flavors of dynamical Wilson fermions. Three different types of phases are identified. This includes the Aoki phase in which isospin, the vector SU(2) symmetry, is spontaneously broken to U(1) by a pion condensate; parity is spontaneously broken as well.

The next task is to understand the relevance of this phase diagram for dynamical domain wall fermions. Crucially, from the perspective of the Wilson operator, or Wilson kernel, this means that we are dealing with a quenched phase diagram. What we mean by this is the following. All expectation values will be defined by the partition function of dynamical domain wall fermions. For each quark flavor the Boltzmann weight contains the determinant of the domain wall operator,  $\det(D_{DW}(m))$ , with an appropriate value of  $m$ , times the PV determinant  $\det^{-1}(D_{DW}(1))$  (see Eq. (4.3)); the Boltzmann weight does not depend directly on the determinant of the Wilson kernel. We will refer to this setup as *Wilson-quenched*, to distinguish it from the fully quenched case, in which no fermion determinant at all is included in the Boltzmann weight. The conceptually more involved Wilson-quenched phase diagram is discussed in Sec. 6.2. We identify the phase in which domain wall (or overlap) fermions are to be defined. We also further clarify the connection, already discussed in Sec. 5.1.1, between the optimal domain wall height  $M$  and the critical Wilson-fermion mass  $m_c$ .

In Sec. 6.3 we discuss the key role of the Wilson kernel's zero modes in defining

topological sectors. In Sec. 6.4 we extend the discussion to the kernel's low lying spectrum. It is convenient to work with the hermitian version of the Wilson operator

$$H_W = \gamma_5 D , \tag{6.1}$$

where  $D$  is defined in Eq. (3.2). We present evidence that the spectrum of  $H_W$  has no gap everywhere in the super-critical region. In terms of its spectral density  $\rho(\lambda)$ , this means that  $\rho(\lambda) \neq 0$  for small  $\lambda$ , except possibly for  $\lambda = 0$ . For the theory with dynamical Wilson fermions,  $\rho(\lambda) \rightarrow 0$  for  $\lambda \rightarrow 0$  in the super-critical region, except inside the Aoki phase where  $\rho(0) > 0$ . By contrast, in the Wilson-quenched phase diagram we argue that  $\rho(0) > 0$  throughout the entire super-critical region. This conclusion appears to challenge the standard physical picture of spontaneous symmetry breaking: the connection between the spectral density  $\rho(0)$ , the condensate, and the Goldstone theorem.

The resolution of this paradox is presented in Sec. 6.5. It is based on concepts familiar in condensed matter physics. A key notion is the mobility edge  $\lambda_c \geq 0$ , which distinguishes between *extended* eigenmodes of  $H_W$  for  $|\lambda| > \lambda_c$  and exponentially *localized* eigenmodes for  $|\lambda| < \lambda_c$ . We will see how the mobility edge helps us identify the various phases, and explain how the Goldstone theorem is avoided in a Wilson-quenched phase when the eigenmodes with  $\lambda \sim 0$  are localized. The related important issue of locality of the effective four-dimensional operator (4.49), as well as of the overlap operator, is addressed in Sec. 6.6.

In Sec. 6.7 we turn to the implications for the residual mass. The near-zero modes of the Wilson kernel give rise to a power-law component of the wave function of the domain wall quarks. The corresponding contribution to the residual mass generically decays only like  $1/N_5$ . While this decay rate is very slow, the magnitude of this component can still be small provided that the spectral density of near-zero modes is small.

In Sec. 6.8 we discuss methods for decreasing the slow  $1/N_5$  component of the residual mass by reducing the density of the Wilson kernel's near-zero modes. We conclude with the emerging general strategy for cost-optimal numerical calculations with domain wall fermions. Finally Sec. 6.9 contains a brief summary comparing domain wall fermions to GW fermions on the one hand and to ordinary Wilson fermions on the other hand. Methods for further reducing the residual breaking of chiral symmetry that involve changing the domain-wall operator itself will be discussed in Sec. 7.

## 6.1 Aoki phase

In this subsection we review the phase diagram of QCD with two flavors of dynamical Wilson fermions. The following heuristic argument suggests the existence of a phase with a pionic condensate [48, 49]. Consider the effective potential for pions, and let  $m_\pi^2$  be the curvature of this potential at the origin. According to continuum chiral perturbation theory,  $m_\pi^2 \propto m$ , where  $m \geq 0$  is the quark mass (in the following we assume that proportionality constants are positive). By contrast, for Wilson fermions there is an additive correction to the bare mass  $m_0$ , and the continuum relation gets

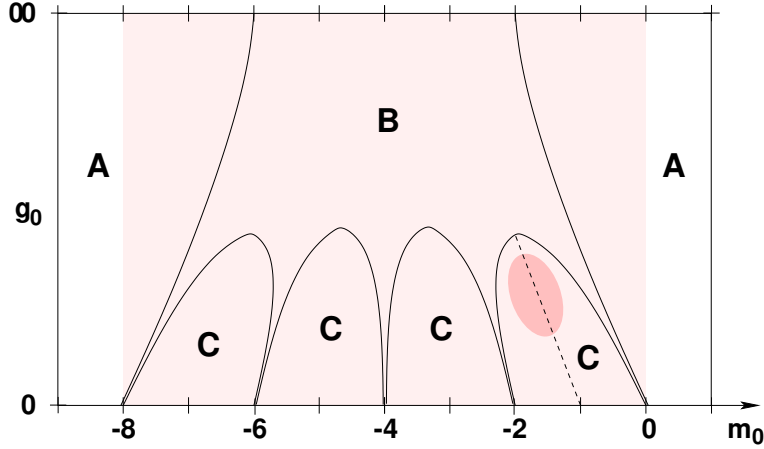


Figure 6: Schematic phase diagram of lattice QCD with two dynamical Wilson fermions. The (linear) horizontal axis is the bare mass  $m_0$ . The vertical axis is the bare coupling  $g_0$ , with values extending from zero to infinity. The phase diagram is symmetric under reflection with respect to the  $m_0 = -4$  line. See text for further explanation.

replaced by

$$m_\pi^2 \propto m_0 + m_c(g_0) , \quad (6.2)$$

with a critical mass  $m_c(g_0) > 0$  which is a function of the bare coupling. As long as  $m_0 + m_c(g_0) > 0$  the curvature,  $m_\pi^2$ , is positive, and the pions are massive. When  $m_0$  is tuned to  $-m_c(g_0)$  the curvature vanishes, and accordingly the pions become massless. If we further decrease  $m_0$ , we expect that the curvature  $m_\pi^2$  at the origin will become negative, hence, the pion field will condense.

The phase diagram is depicted schematically in Fig. 6. Before we describe the various phases we note the following general features. First, the phase diagram is symmetric under reflection with respect to the  $m_0 = -4$  line. The reason is that the effect of the transformation  $\Psi(x) \rightarrow \epsilon(x)\Psi(x)$  and  $\bar{\Psi}(x) \rightarrow -\epsilon(x)\bar{\Psi}(x)$ , where  $\Psi(x), \bar{\Psi}(x)$  are the four-dimensional Wilson fermion fields and  $\epsilon(x) = (-1)^{x_1+x_2+x_3+x_4}$ , can be undone by the replacement  $m_0 \rightarrow -8 - m_0$ .

The second observation concerns the super-critical region  $-8 < m_0 < 0$ , the lightly shaded region in the figure. Let us show that only in this region can the Wilson operator have zero modes. To this end, it is convenient to use the complex Wilson operator  $D$  of Eq. (3.2). Consider the eigenvalue equation  $D\Psi = \lambda\Psi$  where  $\Psi$  is a normalized eigenfunction and in general the eigenvalue  $\lambda$  is complex. Writing  $D = A + iB$  with hermitian  $A$  and  $B$ , it follows that

$$2\text{Re } \lambda = \langle \Psi | D^\dagger + D | \Psi \rangle = 2 \langle \Psi | A | \Psi \rangle . \quad (6.3)$$

If  $\Psi$  is a zero mode of  $D$  (or of  $H_W$ ), then we must have  $\langle \Psi | A | \Psi \rangle = 0$ . Recalling that  $M = -m_0$ , we have  $A = -(W + m_0)$ . Since the spectrum of the Wilson term is

bounded both above and below,  $0 \leq W \leq 8$ , it follows that for  $m_0 > 0$  or  $m_0 < -8$  the expectation value  $\langle \Psi | A | \Psi \rangle$  cannot vanish, and thus  $D$  (or  $H_W$ ) cannot have a zero eigenvalue.

We now turn to a description of the phase diagram. The existence of a phase with a pion condensate, the Aoki phase, was first proposed in Refs. [48, 49], based on strong coupling arguments. This is phase B in the figure. The A and C phases are massive. Notice that the C phases are fully contained within the super-critical region. As we will see this plays a crucial role for both domain wall and overlap fermions. The borderlines of the super-critical region,  $m_0 = 0$  and  $m_0 = -8$ , each belong to a different A phase, but nothing special happens in the A phase when this line is crossed, except of course in the continuum limit  $g_0 \rightarrow 0$ .

Starting from some large positive  $m_0$  in the A phase in the right part of Fig. 6, as we move horizontally to the left at some generic value of  $g_0$ , the mass of the three pions will be (roughly) described by Eq. (6.2). The A phase is isospin symmetric, and all three pions have the same mass. When we reach  $m_0 = -m_c(g_0)$ , which is the phase transition line separating the A and B phases, the pions become massless. Upon entering the Aoki phase (B), one of the pions condense, while the other two pions become massless Nambu-Goldstone bosons (NGBs) associated with the spontaneous breaking of the (vectorial) SU(2) isospin symmetry down to U(1). It is conventional to take the condensate pointing in the third isospin direction by adding a so-called twisted mass term (see Sec. 6.5). The pion associated with the direction of the condensate is not an NGB, and it becomes massive again inside the Aoki phase.

The boundaries of the Aoki phase in the strong coupling limit were first determined prior to the understanding of the Aoki phase itself in Ref. [50]. They are located at  $m_0 = -2, -6$ , as shown in Fig. 6. As for the weak coupling limit, the Aoki phase has the characteristic “fingers,” reaching the critical points at  $m_0 = 0, -2, -4, -6, -8$  on the  $g_0 = 0$  axis, where the free four-dimensional Wilson operator admits massless states. The basic features of the fingers were described analytically using Wilson chiral perturbation theory (WChPT) in Ref. [51]. Writing down the WChPT lagrangian appropriate for the rightmost finger, which touches the  $m_0 = 0$  point on the  $g_0 = 0$  axis, two possible scenarios were identified depending on the sign of a particular low-energy constant. (By symmetry, the same WChPT lagrangian accounts for the finger that touches the point  $m_0 = -8$  as well.) According to the first scenario, the width  $\Delta m_0$  of the finger scales like  $a\Delta m_0 \sim (a\Lambda)^3$ , where  $\Lambda$  is a physical QCD scale. According to the other scenario, the Aoki phase doesn’t reach the  $g_0 = 0$  line. Instead, the finger ends at some  $g_0 > 0$ , beyond which the A phase on the right and the C phase on the left are separated by a first-order transition line. While both phases are isospin symmetric, along their borderline the derivative of the pion mass with respect to  $m_0$  is discontinuous.

Before moving on, we comment in passing that a different WChPT description is required for the fingers associated with the  $m_0 = -2$  and  $m_0 = -6$  critical points on the  $g_0 = 0$  line, and a yet another WChPT description is required for the central critical point on the symmetry axis  $m_0 = -4$ . The reason is the different numbers of continuum-limit quark species, and hence pions, associated with these critical points.

It is thus possible in principle that, for some specific choice of the complete lattice action, the  $m_0 = 0$  and  $m_0 = -8$  fingers will follow the first scenario, while the  $m_0 = -2$  and  $m_0 = -6$  fingers will follow the second scenario, *etc.*.

## 6.2 Wilson-quenched Phase diagram

Returning to domain wall fermions, when we study the Wilson kernel we are in principle interested in a three-dimensional phase diagram spanned by the parameters  $(g_0, M, m_0)$ . As before  $g_0$  is the bare coupling while  $M$  is the domain wall height. But we now consider the bare mass  $m_0$  of the Wilson kernel as an independent parameter. This is equivalent to a *mixed-action* theory with dynamical (or sea) domain wall fermion and valence Wilson fermions. The actual Wilson kernel used by the domain wall fermions is recovered by restricting to the plane defined by  $m_0 = -M$ .

As might be expected, the symmetry structure of this three-dimensional phase diagram is more complicated than that of the pure Wilson fermions of Fig. 6. First, as a generalization of the symmetry discussed in Sec. 6.1, in  $d$  dimensions the phase diagram of pure Wilson fermions is symmetric around the  $m_0 = -d$  line. Indeed, by itself the phase diagram of domain wall fermions inherits the symmetry of five-dimensional Wilson fermions around the  $M = 5$  axis, as reflected by Table 1. But since the  $(g_0, M, m_0)$  phase diagram treats independently the five-dimensional domain wall fermions and the four-dimensional Wilson kernel, in contrast with Fig. 6 the “physical plane” defined by  $(g_0, m_0 = -M)$  might not have any obvious symmetry structure. Still, we will only be interested in the C phase between the two rightmost fingers in Fig. 6. Its boundary on the  $g_0 = 0$  axis is given by  $-2 < m_0 < 0$ , and so this phase defines the region where a domain wall field gives rise to a single light quark in the continuum limit. For this C phase, it is reasonable to expect that the geometry of the corresponding portion of the  $(g_0, m_0 = -M)$  plane of the Wilson-quenched phase diagram will be qualitatively similar to the way this phase has been depicted in Fig. 6.

We already discussed in Sec. 5.1.1 the plausible connection  $\delta M \sim m_c(g_0)$  between the tadpole correction  $\delta M$  for the domain wall height and the critical Wilson mass  $m_c(g_0)$ . With the phase diagram in Fig. 6 in mind we now propose a broader view of this connection. To this end, first, we will ignore the small width of the fingers, identifying the whole rightmost finger with the critical line  $m_0 = -m_c(g_0)$ . In order to reach a simple physical picture we will further assume that the next finger is roughly parallel, and thus, when approximated by a line, is given by  $m_0 = -2 - m_c(g_0)$ . As we increase  $g_0$ , the appropriate range of domain wall height is given by the corresponding section of the rightmost C phase in Fig. 6. Moreover, under the simplifying assumptions we have made, as long as  $g_0$  is not too large this section is given by (now making the usual identification  $M = -m_0$ )

$$m_c(g_0) \lesssim M \lesssim 2 + m_c(g_0) , \quad (6.4)$$

for which the tadpole improved wave function

$$(1 + m_c(g_0) - M)^s , \quad (6.5)$$

is a bound state. The dashed line in Fig. 6 corresponds to the optimal choice  $M = 1 + m_c(g_0)$ . To complete the picture, the darker blob is meant to represent the parameter range actually used in numerical calculations with domain wall fermion.

The standard overlap operator [18, 14] is defined by Eq. (4.51) taking  $H = H_W$  to be the usual Wilson kernel. Similarly to domain wall fermions, in virtually all numerical work with overlap fermions one requires that the overlap operator will describe a single quark field in the continuum limit. This implies that the bare mass of the Wilson kernel must be chosen so as to place it inside the rightmost C phase in Fig. 6, precisely the same region that we have just identified as suitable for domain wall fermions.

We will discuss the phase diagram of domain wall fermions in more detail in Sec. 7.2.2.

### 6.3 Topological sectors

A characteristic feature of massless continuum fermions is the existence of exact zero modes in topologically non-trivial backgrounds. According to the index theorem the net chiral charge of the zero modes is proportional to the net topological charge of the background field. The group theoretical proportionality constant is a positive integer, conventionally equal to one for the fundamental representation of  $SU(N_c)$ . By contrast, on the lattice the gauge field configuration space does not have any intrinsic topological structure, as any configuration is continuously connected to the trivial configuration  $U_\mu(x) = I$ . Various lattice discretizations of the continuum topological charge have been used to estimate the topological charge of lattice configurations, but obviously any such expression suffers from discretization errors (compare Eq. (4.34)).

Nonetheless, overlap fermions support stable, exact zero modes [18]. More generally, this is true for any GW fermion defined by Eq. (4.51) with some reasonable  $H$ . In the free-field case, the Wilson kernel  $H_W$  has an equal number of positive and negative eigenvalues, and thus the sign function  $\epsilon(H_W)$  has equal numbers, both even, of  $+1$  and  $-1$  eigenvalues. If a single eigenvalue of  $H_W$  crosses zero and changes sign, making the total number of negative eigenvalues odd, this leads to the existence of a stable zero modes of the overlap operator. The stable zero modes all share the same chirality, and their number times their  $\pm$  chirality can be used to define the topological charge of the background field [18, 14].

There are plenty of reasonable choices for the hermitian kernel used to the define the GW operator in Eq. (4.51). The relation between the Wilson kernel  $H_W$  of the standard overlap operator, and the hamiltonian  $H_T$  derived from the transfer matrix of domain wall fermions, is particularly tight. As already mentioned in Sec. 4.2,  $H_W$  and  $H_T$  share the same zero eigenmodes [20]. Hence, the standard overlap operator, and the GW operator defined by the  $N_5 \rightarrow \infty$  limit of domain wall fermions, always share the same (chirality and) number of stable zero modes.

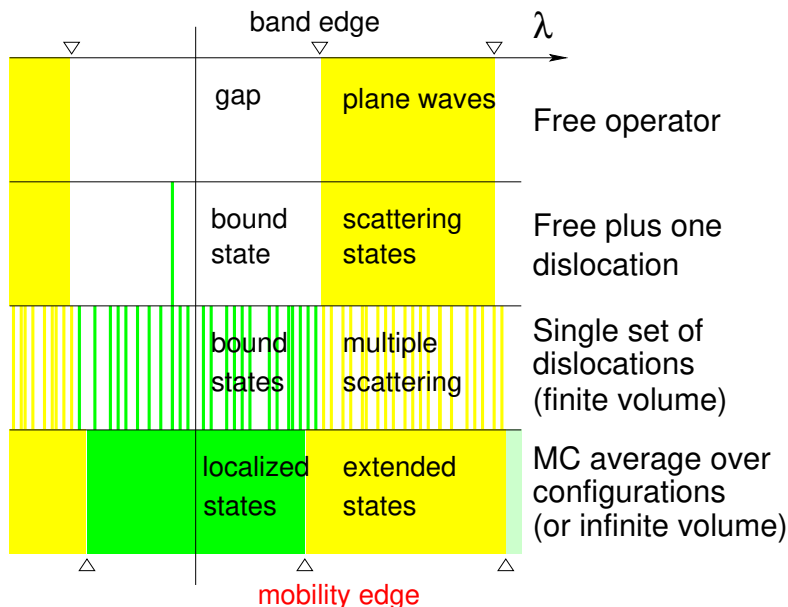


Figure 7: How the spectrum of  $H_W$  changes as one adds to the gauge field (top to bottom) one dislocation, many dislocations, and a random ensemble of dislocations.

## 6.4 Low-lying eigenstates and their spectral density

By now we have encountered several important features of domain wall fermions as well as overlap fermions which, one way or another, are controlled by the low-lying spectrum of the Wilson kernel  $H_W$  or of the closely related transfer matrix hamiltonian  $H_T$ . In this subsection and the next one we will focus on the simpler Wilson kernel  $H_W$ , assuming that the behavior of the transfer matrix hamiltonian  $H_T$  is qualitatively similar. We start by organizing the available information about the low-lying spectrum. This will lead to a certain puzzle, whose resolution will be the subject of the next subsection.

The free Wilson operator  $H_W^0$ , in which all links are set to  $U_\mu(x) = I$ , has a gap for all values of  $m_0$  except at the five critical points on the  $g_0 = 0$  axis,  $m_0 = \{0, -2, -4, -6, -8\}$ . The gap  $\mathcal{E}$  is given by the distance from  $m_0$  to the closest critical point (see, for example, Ref. [52]). The five critical points are visible in Fig. 6, while the gap for some value of  $m_0$  (including super-critical values) is depicted in the top segment of Fig. 7. That said, we have noted in Sec. 6.1 that the bounds on the Wilson term allow in principle for the existence of zero modes in the entire super-critical region  $-8 < m_0 < 0$ . Furthermore, as we have just seen in the previous subsection, the (simultaneous) zero modes of  $H_W$  and  $H_T$  can be used to define the boundaries of topological sectors of the lattice gauge field configuration space. If we are to reproduce topological sectors in the continuum limit, then evidently these zero modes should exist on a subspace of the gauge field configuration space of codimension

one. In addition, in Sec. 4 and Sec. 5 we found out that the rate of restoration of chiral symmetry for  $N_5 \rightarrow \infty$  is controlled by the smallest eigenvalues of  $H_T$ . And, as we will see later on in this section, the low-lying eigenmodes of  $H_W$  or  $H_T$  are also important for the locality properties of the overlap operator or the effective four-dimensional operator for domain wall quarks (4.49).

The accumulation of these observations, which were mostly known by the late 1990s, prompted a more detailed research of the low-lying spectrum of  $H_W$ . Following up on earlier numerical work [53], interesting progress was made in Ref. [54]. The question raised in this paper was whether super-critically, namely having  $-8 < m_0 < 0$ , is not just a necessary condition, but also a sufficient condition for the existence of gauge field configurations which support a zero mode of  $H_W$ . The main result of Ref. [54] was the following. Consider a gauge field configuration equal to the classical vacuum  $U_\mu(x) = I$  almost everywhere, except inside a single hypercube of size  $\ell^4$ , whose link variables can take any value in the gauge group. We will refer to such configurations as having a single *dislocation*. Ref.[54] considered in particular dislocations contained in a unit hypercube (*i.e.*,  $\ell = a$ ) for the SU(2) gauge group. Using a combination of analytic considerations and numerical minimization methods, it was found that the gauge links of the dislocation can be dialed so as to produce a bound state whose eigenvalue  $\lambda_1$  lies inside the gap of the free Wilson operator,  $-\mathcal{E} < \lambda_1 < \mathcal{E}$  (see the second segment of Fig. 7). Moreover, it is possible to tune the dislocation to support a zero mode,  $\lambda_1 = 0$ , for roughly  $-7 \lesssim m_0 \lesssim -1$ . In view of this result it is plausible that, by allowing the dislocation to gradually occupy a larger and larger hypercube, eventually single-dislocation configurations will be found that support a zero mode of  $H_W$  throughout the entire super-critical region. Henceforth, we will assume that this is indeed the case.

The next logical step is to consider a large volume with  $n$  dislocations placed far apart from each other. Intuitively, we expect each dislocation to support essentially the same bound state(s) as before; the presence of other, remote, dislocations should have a negligible effect (third segment of Fig. 7). As for the continuous spectrum of the free operator, in the presence of a single dislocation the plane waves turn into scattering states, while in the presence of more than one dislocation we have multiple scattering.

Taking the infinite volume limit we arrive at the following conclusion. Based on the above evidence, we assume the existence of a bound state spectrum of  $H_W$  for any  $\lambda$  inside the gap  $\mathcal{E}$  of the free operator for appropriately chosen gauge field configurations, everywhere inside the super-critical region. It follows that the spectral density  $\rho(\lambda)$  of  $H_W$  is nonzero for any  $-\mathcal{E} \leq \lambda \leq \mathcal{E}$  in the super-critical region of the Wilson-quenched phase diagram. Of course, the spectral density is nonzero for  $|\lambda| > \mathcal{E}$  as well (bottom segment of Fig. 7).<sup>32</sup> It is important to note that the same conclusion might or might not apply to  $\rho(0)$  in the case of (two) dynamical Wilson fermions (Sec. 6.1). The Boltzmann weight then contains a factor of  $\det^2(H_W)$ , that

---

<sup>32</sup>The Wilson operator  $H_W$  is a bounded operator, hence its entire spectrum is contained in some interval  $-\lambda_{\max} \leq \lambda \leq \lambda_{\max}$ , with  $\lambda_{\max} = \lambda_{\max}(m_0)$ . Here we will not be concerned with the upper limit.

acts to suppress gauge field configurations with near-zero eigenvalues. But no such suppression factor is present in the case of the Wilson-quenched phase diagram, hence it will have a nonzero  $\rho(0)$  throughout the entire super-critical region. We will further discuss the differences between the dynamical Wilson and quenched Wilson cases in the next subsection.

We have now arrived at the following puzzle. Consider the Wilson-quenched phase diagram for two valence Wilson fermions, which possess an isospin symmetry. The Banks-Casher relation asserts that the pion condensate is equal to  $2\pi\rho(0)$ , hence the condensate is nonzero whenever  $\rho(0)$  is. A nonzero pion condensate implies the spontaneous breaking of the (valence) isospin symmetry. Moreover, according to the usual picture of spontaneous symmetry breaking, the pion condensate ought to be accompanied by two massless NGBs, which are the other two pions. Finally, all this is supposed to happen *everywhere* inside the super-critical region, since we have argued that  $\rho(0)$  is nonzero in the entire super-critical region of the Wilson-quenched phase diagram. As we will see in the next subsection, some of these conclusions are in fact incorrect: for the Wilson quenched case there is a way out that evades the Goldstone theorem.

## 6.5 Localization and mobility edge

The key element missing from the discussion of the previous subsection is the need to distinguish between *extended* and (exponentially) *localized* eigenstates of  $H_W$ . Understanding the different roles of the extended and the localized spectra is the subject of this subsection. To avoid inessential technicalities, we will assume an infinite volume unless otherwise stated.

Let us revisit Fig. 7, whose second segment describes the spectrum for a single dislocation, the case considered in Ref. [54]. We can write

$$H_W = H_W^0 + V , \quad (6.6)$$

where the potential  $V$  is confined to the hypercube containing the dislocation. Everywhere else,  $H_W$  is equal to the free operator  $H_W^0$ . Consider an eigenstates with an eigenvalue  $\lambda$ . If  $|\lambda|$  is smaller than the gap  $\mathcal{E}$  of the free operator, this is a bound state that decays exponentially away from the dislocation. In the third segment of Fig. 7 we have bound states attached to several dislocations which are far from each other. Due to the exponential decay of all bound states, remote dislocations will indeed cause an (exponentially) small disruption, a feature we have already invoked in the previous subsection. The bound states of both the single dislocation and the several (but far apart) dislocations are examples of localized eigenstates.

For an ensemble of configurations that belong to some point of the Wilson-quenched phase diagram the situation is the following. Up to short-distance random fluctuations, the mode density of an exponentially localized eigenstate  $\Psi(x)$  is expected to behave like

$$|\Psi(x)|^2 \sim \ell^{-4} \exp\left(-\frac{|x-x_0|}{\ell}\right) , \quad |x-x_0| \gg 1 . \quad (6.7)$$

Here  $x_0$  is some “center,” while  $\ell$  is the localization length. As the eigenvalue  $\lambda$  of a localized eigenstate grows starting from  $\lambda = 0$ , we expect the localization length to be a monotonically increasing function of  $\lambda$ . Eventually, we will reach a critical value  $\lambda_c$ , called the mobility edge, where the localization length diverges, and the eigenstate becomes an extended state.<sup>33</sup> As long as  $H_W$  can be expressed by Eq. (6.6) with a potential  $V$  that is confined to a compact region of the total (infinite) volume, the mobility edge  $\lambda_c$  will be equal to the gap  $\mathcal{E}$  of the free operator. This is the situation depicted in the second and third segments of Fig. 7. But for a realistic ensemble,  $\lambda_c$  will in general be different from  $\mathcal{E}$ .

Focusing our attention on the mobility edge, let us increase  $g_0$  at some fixed super-critical  $m_0$ , moving vertically inside the rightmost C phase in Fig. 6. As the bare coupling  $g_0$  is increased, the randomness of typical gauge field configurations in an ensemble will increase. As a result, we expect the mobility edge  $\lambda_c$  to go down, eventually reaching zero. We can define the Aoki phase as the region where  $\lambda_c = 0$ , and the spectral density  $\rho(0)$  comes from extended states. This definition applies to both the dynamical Wilson and quenched Wilson cases. In the A and C phases of the Wilson-quenched case  $\rho(0)$  remains nonzero,<sup>34</sup> but it comes from localized states. In the dynamical-Wilson case, the factor of  $\det^2(H_W)$  in the Boltzmann weight is sufficiently effective to yield  $\rho(0) = 0$  outside of the Aoki phase, in other words, whenever  $\lambda_c > 0$ .

Let us summarize the emerging understanding of the super-critical region. We will consider infinite volume ensembles defined by the partition function of (two) dynamical Wilson fermions, or by the partition function of (one or more) dynamical domain wall fermions—the Wilson-quenched case. We start with the common features:

1. There is no spectral gap throughout the entire super-critical region of the phase diagram,  $-8 < m_0 < 0$ . At a generic point in the super-critical region the spectrum of  $H_W$  consists of localized states below the mobility edge,  $|\lambda| < \lambda_c$ , and extended states<sup>35</sup> above it,  $|\lambda| \geq \lambda_c$ .
2. The Aoki phase can always be defined by the vanishing of the mobility edge,  $\lambda_c = 0$ . In the A and C phases,  $\lambda_c > 0$ . The Aoki phase is thus characterized by nonzero  $\rho(0)$  coming from extended states.
3. The main difference between the dynamical-Wilson and Wilson-quenched cases is the following. In the dynamical Wilson case,  $\rho(0) = 0$  in the A and C phases, whereas in the Wilson-quenched case  $\rho(0) \neq 0$  in the entire super-critical region. In the A and C phases  $\rho(0)$  comes from localized states.

---

<sup>33</sup> The situation is similar for negative  $\lambda$ . We expect the mobility edges at positive and negative  $\lambda$  to have the same absolute value. Also note that, because of boundedness of  $H_W$  (see the previous footnote), a second pair of mobility edges may exist at a larger  $|\lambda|$ , where the spectrum turns back from extended to localized eigenstates. This situation is depicted in the bottom segment of Fig. 7. We will not be concerned with these additional mobility edges.

<sup>34</sup>For the A phase this is true in the super-critical region.

<sup>35</sup>See, however, footnote 33.

The Wilson-quenched phase diagram was studied using effective field theory (EFT) methods in Ref. [36] (see also Ref. [55]). As explained there, the low-energy EFT is only sensitive to the long-range degrees of freedom, and thus it predicts the existence of a pionic condensate only when it arises from extended states. This is consistent with the definition of the Aoki phase in point (2) above. The main conclusion of Ref. [36] is that, for small enough lattice spacing where the EFT applies, the phase structure of the Wilson-quenched case is qualitatively similar to the unquenched case, including the feasibility of the two scenarios discussed in Sec. 6.1.

It remains to resolve the puzzle associated with the Goldstone theorem [52, 56]. We will show that in the Wilson-quenched case, if the pion condensate  $2\pi\rho(0)$  comes from localized states, it is possible to have no massless NGBs and indeed no long-range correlations at all in the valence sector, as first shown in Ref. [57].

To this end we introduce a small twisted mass term that will control any infrared divergences and provide the seed for the pion condensate and hence for the orientation of isospin symmetry breaking,

$$D \Rightarrow D - i\mu\gamma_5\tau_3 = \gamma_5(H_W - i\mu\tau_3) . \quad (6.8)$$

Here  $\tau_i$  are the Pauli matrices acting on the isospin index of the Wilson fermions. Let us consider the momentum space WTI

$$\sum_{\mu} p_{\mu}\tilde{\Gamma}_{\mu}(p) + 2\mu\tilde{\Gamma}(p) = \langle\pi_3\rangle , \quad (6.9)$$

which is true on the lattice up to  $O((ap)^2)$  corrections. The correlators  $\tilde{\Gamma}(p)$  and  $\tilde{\Gamma}_{\mu}(p)$  are the Fourier transforms of  $\langle\pi_+(x)\pi_-(y)\rangle$  and  $\langle J_{\mu}^+(x)\pi_-(y)\rangle$  respectively.  $J_{\mu}^+(x)$  is a conserved isospin current, and the  $\pm$  refer to operators involving the Pauli matrices  $\tau_{\pm}$  that raise or lower isospin by one unit.

For  $\mu > 0$  isospin symmetry is explicitly broken, and there are no massless states. This applies to hadrons made of both sea and valence Wilson fermions, including any (would-be) NGBs. We can therefore set  $p = 0$  Eq. (6.9). The  $\tilde{\Gamma}_{\mu}(p)$  term drops out, and we arrive at

$$\tilde{\Gamma}(0) = \frac{\langle\pi_3\rangle}{2\mu} , \quad \mu > 0 . \quad (6.10)$$

This result is valid for both sea and valence Wilson fermions in finite volume, as well as in the infinite volume limit. However, the physical implications of Eq. (6.10) are qualitatively different in the two cases.

We first consider valence Wilson fermions. We will assume, as discussed above, that the spectral density  $\rho(0)$  is nonzero, and that it comes from localized states, in other words, the mobility edge is  $\lambda_c > 0$ . According to the Banks-Casher relation the pion condensate is  $\langle\pi_3\rangle = 2\pi\rho(0) \neq 0$ , hence the valence isospin symmetry is broken spontaneously already in finite volume. In fact it is natural that the same behavior will be found in both finite and infinite volume, because localized states are insensitive to the volume (as soon as the linear size of the system is large compared to their localization length). According to Eq. (6.10),  $\langle\pi_3\rangle \neq 0$  implies that  $\tilde{\Gamma}(0)$

diverges like  $1/\mu$ . Moreover, since by assumption the mobility edge is  $\lambda_c > 0$ , for small enough  $p$  one can further show that [52, 56]

$$\tilde{\Gamma}(p) = \frac{\langle \pi_3 \rangle}{2\mu} \left( 1 + O\left(p^2 \ell_0^2\right) \right) , \quad (6.11)$$

where  $\ell_0$  is an average localization length that characterizes the near-zero modes. Hence, the  $1/\mu$  divergence of  $\tilde{\Gamma}(p)$  extends to a range of  $p \neq 0$  as well. This evades the Goldstone theorem: Because  $\lambda_c > 0$  there are no long-range correlations for any  $\mu$ , including for  $\mu \rightarrow 0$ .  $\tilde{\Gamma}_\mu(p)$  is regular, and  $p_\mu \tilde{\Gamma}_\mu(p)$  vanishes for  $p \rightarrow 0$ . Finally, for  $\langle \pi_3 \rangle \neq 0$  the left-hand side of the WTI (6.9) is dominated by  $2\mu \tilde{\Gamma}(p)$ , which stays finite when  $p$  and/or  $\mu$  tends to zero thanks to the  $\mu \rightarrow 0$  divergence of  $\tilde{\Gamma}(p)$ .

In order to complete the physical picture we revisit the proof of the Goldstone theorem for the case of two dynamical Wilson fermions. We begin by proving the absence of any  $1/\mu$  divergence in finite volume. In the case at hand the rules of Grassmann integration imply, first, that any *unnormalized* fermion correlation function is a holomorphic function of the parameters of the fermion action. We note that the same is *not* true in the Wilson-quenched case. The formal reason is that while the valence Wilson fermions contribute to the Boltzmann weight a factor of  $\det^2(H_W)$ , there is a matching contribution of  $\det^{-2}(H_W)$  coming from the ghost quarks, and these two contributions cancel each other by construction.

In addition, the Boltzmann weight  $\det^2(H_W)$  of the dynamical Wilson fermions is always real and non-negative. Moreover, in finite volume  $H_W$  can have any exact zero modes only on a measure zero subset of the gauge field configuration space.<sup>36</sup> On the complementary subset we have  $\det^2(H_W) > 0$ . As a result, the partition function is always strictly positive, and bounded below by some  $z_0 > 0$  for a range of values of  $\mu$  that includes  $\mu = 0$  for any bare mass. It follows that normalized fermion correlation functions are holomorphic functions of  $\mu$  as well. This rules out a  $1/\mu$  divergence in  $\tilde{\Gamma}(p)$ . By Eq. (6.10), the fermion condensate must therefore vanish (at least) linearly with  $\mu$  in finite volume. This recovers the familiar result that spontaneous symmetry breaking cannot occur in finite volume.

In the thermodynamical limit (first taking the infinite volume limit and then sending  $\mu \rightarrow 0$ ) we arrive at

$$\sum_\mu p_\mu \tilde{\Gamma}_\mu(p) = \langle \pi_3 \rangle . \quad (6.12)$$

This is the Goldstone theorem: if  $\langle \pi_3 \rangle \neq 0$  then  $\tilde{\Gamma}_\mu(p)$  must have a  $p_\mu/p^2$  pole. In the dynamical-Wilson theory a fermion condensate can only arise from extended states, and only in the infinite volume limit. As we have just explained, any nonzero  $\rho(0)$  coming from localized states in the infinite volume limit would have existed already in finite volume. But this would entail a  $1/\mu$  divergence in  $\tilde{\Gamma}(p)$ , which is impossible in the dynamical-Wilson case. Thus, a nonzero  $\rho(0)$  necessarily comes from extended

---

<sup>36</sup>This property was already used in the proof of chiral symmetry restoration in Sec. 4.2, and it is true for any value of the Wilson mass parameter.

states, consistent with the fact that NGBs describe long-range fluctuations of the order parameter. This is the situation realized in the Aoki phase of the dynamical-Wilson theory.

In order to avoid any confusion, we note that all the “sicknesses” discussed above of the Wilson-quenched phase diagram have to do with the correlation functions of *valence* Wilson fermions in a lattice theory with dynamical domain wall fermions. No similar issues arise in a unitary theory. In particular, the Goldstone theorem applies to every theory of dynamical domain wall fermions, just as to every theory of dynamical Wilson fermions, and spontaneous symmetry breaking can occur only in the thermodynamical limit.

The localization properties of the low lying spectrum of  $H_W$  and the mobility edge were studied numerically in Refs. [58, 59, 60]. Strictly speaking, the distinction between localized and extended states can be made precise only in infinite volume. Nevertheless, there exist good estimators for the localization length, and, as a result, for the mobility edge, which can be applied in numerical simulations. A notable numerical result is that, below the mobility edge, the spectral density of the localized states drops rapidly with decreasing  $\lambda$ , but remains non-zero. The rapid drop is good news for residual chiral symmetry breaking effects, as we will discuss in Sec. 6.7 below.

## 6.6 Locality of Ginsparg-Wilson operators

Any GW operator cannot be ultra-local: its coordinate representation  $D_{GW}(x, y)$  does not vanish for arbitrarily large separation  $|x - y|$  [61]. GW operators can be local, however, in the following sense. Consider the standard overlap operator  $D_{ov}$  with the free Wilson kernel  $H_W^0$ , where  $-2 < m_0 < 0$ . If both  $|m_0|$  and  $|2 + m_0|$  are  $O(1)$ , we expect  $D_{ov}(x, y)$  to decay exponentially with the separation,<sup>37</sup>

$$\|D_{ov}(x, y)\| \sim \exp(-M_{ov}|x - y|), \quad |x - y| \gg 1, \quad (6.13)$$

with a decay rate  $M_{ov} = O(1)$  in lattice units. A similar behavior is expected for relatively smooth gauge fields. This was proved rigorously in Ref. [25], which showed that a bound of the form of Eq. (6.13) holds provided that the (lattice) field strength is everywhere constrained to be smaller than some constant. A similar rigorous result was proved in Ref. [26] for the effective four-dimensional operator for domain wall quarks, the approximate GW operator (4.49). For the overlap operator, Ref. [25] further showed that a similar bound holds also if the spectrum of  $H_W$  contains a single exponentially localized eigenstate inside an otherwise empty spectral gap. These situations correspond to the upper two segments of Fig. 7, except that the gap will in general be slightly different from the gap of the free operator.

Constraints on the lattice field strength of the kind invoked in Refs. [25, 26] do not alter the continuum limit, because any field strength of the order of some physical scale becomes vanishingly small in lattice units in the continuum limit. But it is

---

<sup>37</sup>The distance  $|x - y|$  can be for example the usual euclidean norm or alternatively the “taxi driver’s distance.”

unrealistic to impose similar constraints for ensemble generation using Monte-Carlo methods. For realistic ensembles, information about the range of the overlap operator or of the effective domain-wall quarks operator must rely on numerical results. One option is to measure the range of these operators directly. Alternatively, one can combine analytic considerations with numerical data about the localized and extended spectrum of the kernel and the mobility edge [58, 59, 60].

Understanding the effects that control the range of (exact or approximate) GW operators requires slightly more refined acquaintance with the localized spectrum. As we increase  $\lambda$ , starting from  $\lambda = 0$  and moving towards the mobility edge, several effects take place. First, the spectral density  $\rho(\lambda)$  of the localized eigenmodes, which is very small for  $\lambda \sim 0$ , grows rapidly. Second, the localization length  $\ell(\lambda)$  increases, ultimately diverging at the mobility edge. Third, the eigenmodes that we encounter for small  $\lambda$  typically have a single center around which the mode density is localized. But as we increase  $\lambda$  past some  $\bar{\lambda}$  where  $0 < \bar{\lambda} < \lambda_c$ , the localized modes start becoming multi-centered. We should consider separately the contribution of different spectral ranges. For definiteness we will discuss the overlap operator, but essentially the same considerations apply also to the effective four-dimensional operator for domain wall quarks [58, 59, 60, 46].

The lowest range is  $0 \leq |\lambda| \leq \bar{\lambda}$ . The modes in this range are exponentially localized and single-centered. Using Eq. (6.7) and the triangle inequality their contribution is easily estimated as

$$\begin{aligned} \langle |D_{ov}(x, y)| \rangle_{|\lambda| \leq \bar{\lambda}} &\lesssim \int_{-\bar{\lambda}}^{\bar{\lambda}} d\lambda \rho(\lambda) \exp\left(-\frac{|x-y|}{2\ell(\lambda)}\right) \\ &\lesssim \bar{\lambda} \rho(\bar{\lambda}) \exp\left(-\frac{|x-y|}{2\ell(\bar{\lambda})}\right). \end{aligned} \quad (6.14)$$

The second estimate holds because both  $\rho(\lambda)$  and  $\ell(\lambda)$  are monotonically increasing, hence the integral is dominated by its lower and upper bounds.

The second and third ranges have in common that the modes are either localized but multi-centered ( $\bar{\lambda} \leq |\lambda| \leq \lambda_c$ ) or extended ( $|\lambda| \geq \lambda_c$ ). For these ranges of eigenmodes, which are all separated from zero by a minimal gap  $\bar{\lambda}$ , one could envisage the application of some generalization of the techniques of Refs. [25, 26]. In practice, the growth of the spectral density towards the mobility edge and beyond is so rapid that one expects the contribution of the extended modes to dominate, with the mobility edge effectively playing the role of a gap in the spectrum. This contribution should be qualitatively similar to the effect of integrating out a massive field whose mass is  $\lambda_c$ . It is thus estimated as

$$\langle |D_{ov}(x, y)| \rangle_{|\lambda| \geq \lambda_c} \approx \mathcal{C} \exp(-\lambda_c |x-y|), \quad (6.15)$$

where  $\mathcal{C} = O(1)$ . Numerical evidence [59] suggests that the contribution of the extended modes, Eq. (6.15), indeed dominates over the entire contribution of the localized spectrum, including both the single-centered and multi-centered modes.

These considerations also clarify what goes wrong when we enter the Aoki phase. With the vanishing of the mobility edge  $\lambda_c$ , the (exact or approximate) GW operators

we have considered become non-local. As long as we are careful to stay inside the C phase, these operators are local, nevertheless one should pay attention to their actual range, as illustrated by the following examples. Working with (fully) quenched ensembles generated using different gauge actions, Ref. [59] found for several ensembles with a cutoff of  $\sim 2$  GeV that the estimated range of the overlap operator corresponded to a mass scale of  $\sim 800$  MeV. Depending on the QCD observable of interest, this scale might or might not be high enough to be considered as part of the discretization effects. For a lattice cutoff of  $\sim 1$  GeV, depending on the gauge action, the estimated range of the overlap operator corresponded to a mass scale of  $250 - 320$  MeV, clearly way too low. Of course, by today's standards, a lattice cutoff of 1 GeV would usually be considered much too low anyway.

## 6.7 The residual mass revisited

We are finally in a position to identify the non-perturbative effects that contribute to the residual mass, in addition to the perturbative effects discussed in Sec. 5. The residual mass is defined by the mixing of the operator  $J_{5q}^a$  with  $J_5^a$ , a local effect (see Eq. (5.9)). Considerations similar to the ones of the previous subsection lead to the phenomenological estimate [41, 55, 60]

$$m_{\text{res}} \approx \int d\lambda \rho(\lambda) e^{-N_5|\lambda|}, \quad (6.16)$$

where we now refer to the spectrum of the transfer matrix hamiltonian  $H_T$ . For a mode with eigenvalue  $\lambda$ , the factor  $e^{-N_5|\lambda|}$  accounts for the dependence on  $N_5$ , the length of the fifth direction. The occurrence of  $|\lambda|$  in the exponential echoes the replacement of the transfer matrix  $T$  by its bounded version  $Q$ , discussed in Sec. 4.2.

The combined effect of the suppression factor  $e^{-N_5|\lambda|}$  and the rapid damping of the spectral density below the mobility edge is that the contribution of the spectral range  $|\lambda| \gtrsim \lambda_c$  to Eq. (6.16) is peaked near  $|\lambda| = \lambda_c$ . A saddle-point integration yields the contribution  $\rho(\lambda_c)e^{-N_5\lambda_c}/N_5$ . In addition, as  $N_5$  gets larger and larger, the contribution of the (localized) near-zero modes will eventually dominate since it effectively lacks the exponential suppression with  $N_5$ . This yields a second contribution

$$\int_{-1/N_5}^{1/N_5} d\lambda \rho(\lambda) e^{-N_5|\lambda|} \approx \int_{-1/N_5}^{1/N_5} d\lambda \rho(\lambda) \approx \frac{\rho(1/N_5)}{N_5}. \quad (6.17)$$

As in Eq. (6.14),  $\rho(1/N_5)$  provides a better estimate than  $\rho(0)$ , because the spectral density of the localized modes increases rapidly with  $\lambda$ . Putting the two contributions together we arrive at

$$m_{\text{res}} \approx \frac{\rho(\lambda_c) e^{-N_5\lambda_c}}{N_5} + \frac{\rho(1/N_5)}{N_5}. \quad (6.18)$$

For a slightly more refined estimate, see Ref. [60].

The exponentially suppressed term in Eq. (6.18) in effect replaces the perturbative estimate of Eq. (5.5). Notice that (setting  $s = N_5$ ) the power law correction in Eq. (5.5) is  $1/N_5^2$ , while here it is  $1/N_5$ . The reason is that in Eq. (5.5) the power

law correction arises from the phase space around the maximum of  $e^{-\alpha(p)}$  for the free theory. By contrast, here the power correction reflects the nonzero spectral density for  $\lambda \approx \lambda_c$ . For a related discussion see Appendix C of Ref. [41].

As for the last term on the right-hand side of Eq. (6.18), apart from the slow  $1/N_5$  power law, some further damping with  $N_5$  may be provided by  $\rho(1/N_5)$ , because below the mobility edge the spectral density  $\rho(\lambda)$  is always found to be a monotonically increasing function of  $\lambda$ . Since we are targeting the rightmost C phase of Fig. 6, it being part of the super-critical region of the Wilson-quenched phase diagram means that in all cases  $\rho(0)$  is nonzero. But its variation among different ensembles can be very large [59].

In conclusion, the main difference between the perturbative and non-perturbative estimates of  $m_{\text{res}}$  originates from the kernel’s near-zero modes, whose contribution to  $m_{\text{res}}$  is not suppressed exponentially. We first encountered this effect in Sec. 4.2, and now we have arrived at a semi-quantitative expression for this contribution. Luckily, it is possible to achieve a sufficiently small spectral density for the kernel’s near-zero modes that the slow  $\rho(1/N_5)/N_5$  tail will not lead to an uncomfortably large  $m_{\text{res}}$ .

## 6.8 Remedies

Now that we understand the physical mechanisms that control the residual breaking of chiral symmetry, and  $m_{\text{res}}$  in particular, the natural next step is to look for “knobs” that will allow us to reduce  $m_{\text{res}}$  at fixed values of the fifth direction  $N_5$  and of the lattice spacing  $a$  (in physical units). In this subsection we consider methods that involve changing of the Boltzmann weight without changing the domain wall fermion operator itself. In Sec. 7 we will discuss methods based on changing the domain wall fermion operator.

Perhaps the simplest and most obvious modification to try out is to use different gauge actions. There is extensive literature on this topic, see in particular Refs. [44, 62, 63, 64] Gauge actions that have received special attention include the standard Wilson plaquette action; the Iwasaki action [65], which typically yields a smaller  $m_{\text{res}}$ ; and the DBW2 action [66], which yields a yet smaller  $m_{\text{res}}$ , all for the same  $N_5$  and lattice spacing. The intuitive explanation for this behavior is that dislocations that can support near-zero modes of the Wilson kernel are suppressed by the Iwasaki action, and even more so by the DBW2 action.

Another idea is to mimic the way small eigenvalues are suppressed in a theory of dynamical Wilson fermions, by adding to the Boltzmann weight a factor of  $\det(f(H_W))$  for a suitable function  $f(H_W)$  of the Wilson kernel [67, 68, 69]. When the continuum limit  $g_0 \rightarrow 0$  is approached, we should let the domain wall height  $M = -m_0$  move along the dashed line in Fig. 6. Hence  $m_0$  is always far from both critical points  $m_0 = 0$  and  $m_0 = -2$  that mark the boundary of the rightmost C phase on the  $g_0 = 0$  axis, where the Wilson kernel will support massless fermions in the continuum limit. Any near-zero modes of the Wilson kernel  $H_W$  are thus lattice artifacts; they are localized states lying well below the mobility edge. Hence, adding a factor of  $\det(f(H_W))$  to the Boltzmann weight does not modify the continuum limit.

This method goes under name of *dislocation suppressing determinant ratio* (DSDR), and the function of choice is usually taken to be

$$f(H_W) = \frac{H_W^2 + \epsilon_f^2}{H_W^2 + \epsilon_b^2}, \quad (6.19)$$

where one takes  $\epsilon_f \ll 1$  and  $\epsilon_b \lesssim 1$ . A naive choice that achieves the suppression of near-zero modes would be simply  $f(H_W) = H_W^2$ . The reason for the added  $\epsilon_f^2$  in the numerator is not to overly suppress the near-zero modes and along with them the transitions between topological sectors (we return to this point shortly). The introduction of the denominator, with  $\epsilon_b \lesssim 1$ , is aimed to limit the effect of the DSDR factor to the smaller kernel eigenvalues, while avoiding a lot of “noise” from the majority of the eigenvalues which are  $O(1)$ , and thus anyway irrelevant for the goal of the DSDR factor.

Large scale domain-wall fermion simulations nowadays usually employ the following strategy. The complete lattice action and (if present) DSDR factor are designed such that, at most, roughly one half of the bare mass of the light quarks comes from  $m_{\text{res}}$ . With the current lattice cutoffs of order few GeVs, this implies that  $m_{\text{res}}$  has to be on the order of  $10^{-3}$  or smaller. The total bare mass is<sup>38</sup>

$$\tilde{m}_\ell = m_\ell + m_{\text{res}}. \quad (6.20)$$

The tunable mass parameter  $m = m_\ell$  in the domain wall fermion operator (3.30) then provides the rest of the desired  $\tilde{m}_\ell$ , which in turn is multiplicatively renormalizable. Since  $m_{\text{res}} < \tilde{m}_\ell$  by design, we need  $m_\ell > 0$ . This is important, because it implies that the determinant of the domain wall operator is always positive (Sec. 3.2), which in turn stabilizes the fermion inversions.

This strategy optimizes the cost of simulations, and works well for most observables. An exception is observables that suffer from a power divergence, such as notably the fermion condensate. For such observables, suitable subtractions or indirect methods may be necessary (see, *e.g.*, Ref. [46]). Cases include weak decays [70, 71, 72] and the attendant non-perturbative renormalization of four-quark operators or when the decay as computed on the lattice is slightly off-shell [71].

The kernel’s (near-)zero modes have a welcome feature: they are responsible for the transitions between topological sectors; they also have an undesirable feature: their slowly decaying contribution to  $m_{\text{res}}$  and other residual chiral symmetry breaking effects. The two facets of the near-zero modes need to be balanced. We expect the spectral density of the kernel’s near-zero modes to decrease rapidly when the bare coupling  $g_0$  is decreased towards to the continuum limit,  $g_0 \rightarrow 0$ . This can be understood by noting that a near-zero mode is expected to be attached to a dislocation in the lattice gauge field, a situation idealized by the second segment of Fig. 7. A dislocation is a small region of the lattice where many gauge links are far from the identity element. Hence, the contribution of a dislocation to the lattice action of the gauge field  $S_g$  is given by some  $C > 0$  where  $C = O(1)$ . This amounts

---

<sup>38</sup>For simplicity we consider the isospin limit  $m_d = m_u = m_\ell$ .

to a multiplicative factor in the Boltzmann weight (see Eq. (4.3)) with the form of  $\exp(-C/g_0^2)$ . The dependence on  $g_0$  explains why dislocations are strongly suppressed as we get closer to the continuum limit.

For a low lattice cutoff, or equivalently larger  $g_0$ , the spectral density of near-zero modes will be relatively large, implying that there is a lot of topological activity, but maybe also an uncomfortably large  $m_{\text{res}}$ . Under these circumstances, adding the DSDR factor may help reducing  $m_{\text{res}}$  to smaller values, while still leaving enough topological activity.

By contrast, many of today's numerical simulations have such a high cutoff (equivalently, small  $g_0$ ) that topological transitions may be suppressed too much. In the case of domain wall fermions we expect that  $m_{\text{res}}$  will then be so tiny that one could tolerate larger values. Under these circumstances, it has been proposed to introduce a dislocation *enhancing* determinant ratio, which is basically just the inverse of the DSDR factor [73]. This would increase the near-zero modes density, and thus also the topological activity. While  $m_{\text{res}}$  would grow, presumably it could still be kept small enough. Investigations for  $a^{-1} \approx 3$  GeV appear promising [73], but a comprehensive study has yet to be done.

## 6.9 Conclusion

If perfect chiral symmetry was our deciding consideration, we would always take the chiral limit  $N_5 \rightarrow \infty$  of domain wall fermions analytically, which amounts to utilizing the associated four-dimensional GW operator. In this limit the residual mass vanishes, and the existence of the massless four-dimensional quark field is topologically stable in the sense that we can choose the bare coupling  $g_0$  together with the domain wall height  $M = -m_0$  anywhere inside the rightmost C phase of Fig. 6.

Let us consider a different question that we have not raised till now: how do domain wall fermions behave when  $N_5$  is very small? The smallest  $N_5$  for which the five-dimensional space has two separate boundaries is  $N_5 = 2$ . The one-loop wave function of the effective four-dimensional quark field was calculated in Sec. 5.1.2, and, for  $N_5, s \gg 1$ , it is given by Eq. (5.5). For  $N_5 = s = 2$  the approximations used in the derivation do not apply, but what we can say without a detailed calculation is that the wave function will be given by  $c_2 g_0^2$  for some  $c_2 = O(1)$  number. Reinstating the lattice spacing this result is  $O(g_0^2/a)$ , and the same estimate applies to the residual mass as well.

For  $N_5 = 2$  we thus have  $m_{\text{res}} = O(g_0^2/a)$ , with no further suppression factors; this is the same parametric behavior as the additive renormalization of the mass of ordinary Wilson fermions. Hence, for very small  $N_5$  domain wall fermions are qualitatively the same as ordinary Wilson fermions.

The practical success of domain wall fermions thus depends on the remarkably fast falloff of the wave function of the effective four-dimensional quark field with the fifth coordinate, so that already for modest values of  $N_5$  (say in the range of 10 to 30 as a figure of merit) the wave function has dropped by several orders of magnitude and, with it,  $m_{\text{res}}$ . Perturbatively, the exponential falloff is described by Eq. (5.5).

Non-perturbatively, a phenomenological description for the behavior of  $m_{\text{res}}$  is given in Eq. (6.18), which includes the slow “tail” originating from the near zero modes of the Wilson kernel. While the spectrum of localized modes goes down all the way to  $\lambda = 0$ , luckily the spectral density of the near-zero modes is very small. The end result is that values of  $am_{\text{res}}$  on the order of  $10^{-3}$  are common in numerical simulations. As we have explained in the previous subsection, this is what one needs in order that  $m_{\text{res}}$  will be smaller than the (bare) mass or the light quarks.

## 7 Improved domain wall fermions

The improvement program aims to reduce discretization effects in lattice calculations, and achieve faster convergence to the continuum limit. The discretization effects are responsible in particular for breaking the continuum symmetry group to a much smaller lattice symmetry group. As a result, reducing the discretization effects typically also gives rise to faster restoration of the continuum symmetries.

For fermions, the continuum symmetries which are broken explicitly on the lattice include the axial (non-singlet) flavor symmetries.<sup>39</sup> The basic version of domain wall fermions, introduced in sections 3 and 4, already has much improved chiral symmetry in comparison with Wilson fermions. The main goal of the improvement program in the context of domain wall fermions is to achieve the same quality of chiral symmetry (as measured, *e.g.*, by the residual mass) for smaller extent of the fifth coordinate, thereby reducing the cost of numerical calculations with domain wall fermions.

In Sec. 7.1 we discuss Möbius fermions, which have become the method of choice for large-scale numerical calculations using domain wall fermions. In Sec. 7.2 we revisit two topics already discussed in earlier parts using results from Sec. 7.1. We resume the discussion of improvements in Sec. 7.3, where we discuss a version of domain wall fermions with couplings that depend on the fifth coordinate, aimed to minimize the residual mass for any given  $N_5$ . Sec. 7.4 is devoted to attempts to obtain faster reduction of chiral symmetry violations by using different four-dimensional kernels. Finally Sec. 7.5 presents a method to reduce the residual chiral symmetry violations via deflation.

### 7.1 Möbius fermions

In this subsection we discuss Möbius fermions [74]. We first explain in Sec. 7.1.1 why Möbius fermions offer faster convergence to the chiral limit than the original version of domain wall fermions. The Möbius fermion action is then introduced in Sec. 7.1.2 following the concrete implementation of Ref. [34]. We also discuss the resulting effective four-dimensional operator. Last, in Sec. 7.1.3 we derive the Möbius conserved vector currents and partially-conserved axial currents.

---

<sup>39</sup>The only exception is GW fermions, and in particular, overlap fermions (see Sec. 4.5).

### 7.1.1 Why Möbius fermions

Möbius domain wall fermions [74] are a generalization of domain wall fermions that are more efficient for numerical computations. In the limit  $N_5 \rightarrow \infty$ , the original version of domain wall fermions and Möbius fermions both correspond to the same chirally symmetric fermion action (this statement will be made precise below). In other words, at finite  $N_5$  they differ by small residual chiral symmetry breaking effects on the order of the residual mass.

It is easiest to understand the above facts by first following the steps in Sec. 4.5 to show the relationship between domain wall fermions in the  $N_5 \rightarrow \infty$  limit and overlap fermions, and the most general lattice chiral fermions, those that satisfy the Ginsparg-Wilson relation, Eq. (4.48).

In Sec. 4.5 we considered  $D_{GW}(N_5)$ , the approximate GW operator obtained from domain wall fermions at finite  $N_5$ , and expressed it in Eq. (4.49) in terms of the transfer matrix  $T$  of Eq. (4.26). An alternative expression for this transfer matrix which will be convenient for what follows is

$$T = \frac{1 - H}{1 + H} , \quad (7.1)$$

where the hermitian kernel is  $H = H_S = \gamma_5 D_S$ , with

$$D_S = \frac{a_5 D_W(M)}{2 + a_5 D_W(M)} . \quad (7.2)$$

Following Ref. [34] in this subsection, the notation for the Wilson kernel is  $D_W(M) = -D(M)$  with  $D(M)$  in Eq. (3.2), namely,  $D_W(M) = -D_K + W - M$ . We have re-introduced the lattice spacing in the fifth dimension,  $a_5$  (which is typically set equal to 1 in numerical simulations). For  $a_5 = 1$  one can prove Eq. (7.1) using Eq. (4.26) and<sup>40</sup>

$$2B^{\frac{1}{2}}K^{-1} = 2 \begin{pmatrix} B & 0 \\ -C^\dagger & 1 \end{pmatrix} = (2 + D_W^\dagger(M)) + \gamma_5 D_W(M) , \quad (7.3a)$$

$$2B^{\frac{1}{2}}K^\dagger = 2 \begin{pmatrix} 1 & C \\ 0 & B \end{pmatrix} = (2 + D_W^\dagger(M)) - \gamma_5 D_W(M) . \quad (7.3b)$$

With Eq. (7.1) at hand,  $D_{GW}(N_5)$  can be reexpressed as

$$D_{GW}(N_5; H) = \frac{1}{2} (1 + \gamma_5 \tilde{\epsilon}(N_5; H)) , \quad (7.4)$$

where

$$\tilde{\epsilon}(N_5; H) = \frac{(1 + H)^{N_5} - (1 - H)^{N_5}}{(1 + H)^{N_5} + (1 - H)^{N_5}} , \quad (7.5)$$

and  $H = H_S$ . For  $N_5 \rightarrow \infty$ , the approximate sign function  $\tilde{\epsilon}(N_5; H)$  tends to the sign function  $\epsilon(H)$ .<sup>41</sup>

<sup>40</sup>As in Sec. 3, we work in units of the four-dimensional lattice spacing. For  $a_5 \neq 1$  see Ref. [21].

<sup>41</sup>For the precise statement, see Sec. 7.2.1 below.

Notice that the Shamir kernel  $D_S$  resembles a conformal transformation on the Wilson operator  $D_W(0) = -D_K + W$ , with transformation parameters that depend on  $M$  and  $a_5$ . Similarly, a general conformal transformation of  $D_W(0)$  on the real axis can be written as

$$D_M = \frac{(b+c)D_W(M)}{2+(b-c)D_W(M)} = \alpha D_S, \quad (7.6)$$

where the three real parameters of the conformal transformation are functions of the three parameters  $b$ ,  $c$ , and  $M$ . This transformation is also called a Möbius transformation, hence the name. The original formulation of domain wall fermions can be thought of as a special case of Möbius fermions, one with  $b = a_5$  and  $c = 0$  and, usually,  $a_5 = 1$  as well.<sup>42</sup> More interesting is the simple rescaling [74]  $\alpha = (b+c)/a_5$  in the second equation while simultaneously keeping  $a_5 = b-c$  fixed, which we will discuss shortly, assuming  $a_5 > 0$  and  $\alpha > 0$ . If moreover we let  $b = b(s)$  and  $c = c(s)$  depend on the coordinate in the fifth dimension, more general possibilities follow, like the “optimal” domain wall fermions discussed in Sec. 7.3.

The simple rescaling in Eq. (7.6) leaves the sign function in Eqs. (4.51) and (4.53) unchanged if  $N_5 \rightarrow \infty$ . However if  $N_5$  is finite, the approximations to the sign function for  $H_S$  and for  $H_M = \gamma_5 D_M$  will differ. To see how much they differ we should investigate the violations of the Ginsparg-Wilson relation for  $m = 0$  and finite  $N_5$ . An obvious way is to simply quantify the violation of the Ginsparg-Wilson relation (4.48) induced by finite  $N_5$ ,

$$2\gamma_5 \Delta(N_5; H) \equiv \gamma_5 D_{GW} + D_{GW} \gamma_5 - 2D_{GW} \gamma_5 D_{GW} = \frac{1}{2} \gamma_5 (1 - \tilde{\epsilon}(N_5; H)^2). \quad (7.7)$$

Notice that  $\sum_{x,y} \bar{q}(x) 2\gamma_5 [\Delta(N_5; H)]_{xy} q(y)$  is the variation of the four-dimensional effective action  $\sum_{x,y} \bar{q}(x) [D_{GW}(N_5; H)]_{xy} q(y)$  under the corresponding approximate Lüscher chiral symmetry  $\delta \bar{q}(x) = \bar{q}(x) \gamma_5$ ,  $\delta q(x) = \sum_y \gamma_5 [1 - 2D_{GW}(N_5; H)]_{xy} q(y)$  [35]. It can be shown [74] that  $\Delta(N_5; H)$  is a quantity of order  $O(m_{\text{res}})$ , and hence  $\tilde{\epsilon}(N_5; H)$  differs from  $\epsilon(H)$  by  $O(m_{\text{res}})$  for any  $H$ .

Given an eigenvalue  $\lambda$  of  $H_S$ , at a qualitative level we identify three spectral regions for the approximate sign function:

$$\tilde{\epsilon}(N_5; H_M) = \tilde{\epsilon}(N_5; \alpha H_S) \approx \begin{cases} N_5 \alpha \lambda, & \alpha |\lambda| \ll 1/N_5, \\ \pm 1, & 1/N_5 \ll \alpha |\lambda| \ll N_5, \\ N_5 / (\alpha \lambda), & \alpha |\lambda| \gg N_5. \end{cases} \quad (7.8)$$

Notice the symmetry under  $\lambda \rightarrow 1/\lambda$  of these spectral regions, which can be traced back to the behavior of Eq. (7.1) under  $H \rightarrow 1/H$ . We see that  $\tilde{\epsilon}(N_5; \alpha \lambda)$  is a good approximation of the sign function  $\epsilon(\lambda) = \pm 1$  provided that  $\alpha |\lambda|$  is neither too small nor too large. By contrast, in the regions  $\alpha |\lambda| \ll 1/N_5$  and  $\alpha |\lambda| \gg N_5$  we obtain

<sup>42</sup>Another special case is  $b = c$ , where  $D_M$  reduces to the familiar Wilson kernel of the overlap operator up to a multiplicative factor [75].

poor approximations of the sign function, hence these spectral regions will dominate the residual breaking of chiral symmetry, including in particular  $m_{\text{res}}$ .

We may take the number of modes satisfying  $\alpha|\lambda| \ll 1/N_5$  as a rough measure of the residual chiral symmetry breaking coming from the near-zero spectrum. If the spectral density in the relevant range is roughly constant, this number will be inversely proportional to  $\alpha N_5$ . At fixed  $N_5$ , the residual chiral symmetry breaking can therefore be reduced by switching to the Möbius kernel  $H_M$  and increasing  $\alpha$ . Stated differently, we may keep the residual breaking of chiral symmetry roughly the same by simultaneously lowering  $N_5$  and increasing  $\alpha$  keeping their product fixed. This allows reaching a given target quality of chiral symmetry for smaller  $N_5$ , hence at smaller cost, which explains why Möbius fermions are more efficient for numerical computations [74].

The value of  $\alpha$  cannot be increased indefinitely, however, because this will populate the region  $\alpha|\lambda| \gg N_5$  where  $\tilde{\epsilon}(N_5; \alpha\lambda)$  again becomes a poor approximation of  $\epsilon(\lambda)$ . Finding the optimal value of  $\alpha$  requires numerical experimentation. In practice,  $\alpha = 2$  was found to be a reasonable choice [34].

### 7.1.2 The Möbius fermion operator

Having established the relationship between the Möbius version and the original version of domain wall fermions in Sec. 7.1.1, we next turn to the five-dimensional action and fermion propagators for Möbius fermions. We define physical four-dimensional quark fields just as before, through the fields on the boundaries of the fifth dimension, Eq. (3.31). With these relations and similar ones for propagators into the bulk fifth dimension, we will also obtain conserved vector currents and partially-conserved axial currents for Möbius domain wall fermions.

The five-dimensional Möbius action closely resembles the domain-wall fermion action:

$$S_M^5 = \bar{\psi} D_M^5 \psi, \quad (7.9)$$

where  $D_M^5 = D_M^5(N_5, m)$  is

$$D_M^5 = \begin{pmatrix} \tilde{D} & -P_L & 0 & 0 & \cdots & 0 & 0 & 0 & mP_R \\ -P_R & \tilde{D} & -P_L & 0 & \cdots & 0 & 0 & 0 & 0 \\ 0 & -P_R & \tilde{D} & -P_L & \cdots & 0 & 0 & 0 & 0 \\ \vdots & \vdots & \ddots & \ddots & \ddots & \vdots & \vdots & \vdots & \vdots \\ 0 & 0 & 0 & 0 & \cdots & -P_R & \tilde{D} & -P_L & 0 \\ 0 & 0 & 0 & 0 & \cdots & 0 & -P_R & \tilde{D} & -P_L \\ mP_L & 0 & 0 & 0 & \cdots & 0 & 0 & -P_R & \tilde{D} \end{pmatrix}, \quad (7.10)$$

and

$$\tilde{D} = D_-^{-1} D_+, \quad (7.11a)$$

$$D_+ = bD_W + 1, \quad (7.11b)$$

$$D_- = 1 - cD_W. \quad (7.11c)$$

In this subsection we follow the RBC/UKQCD conventions [34] for the Möbius operator, which differ from Ref. [74] by an explicit factor of  $D_-$ . These conventions also differ from the conventions of Sec. 3 for the domain wall operator, Eq. (3.30), in the flipping of the chiral projectors, hence the boundaries supporting the LH and RH chiral modes are also flipped, as well as by an overall minus sign, including for the Wilson-Dirac operator as already mentioned above.

The four-dimensional projection of the five-dimensional Möbius operator can be related to the corresponding (approximate) GW operator. For the derivation, see Appendix A of Ref. [34]. The result is

$$D_{GW}(N_5, m) = [\mathcal{P}^{-1} D_M^5(N_5, 1)^{-1} D_M^5(N_5, m) \mathcal{P}]_{11}, \quad (7.12)$$

where the indices  $[\cdot]_{ss'}$  refer to the matrix structure in the fifth direction,<sup>43</sup> and  $D_{GW}(N_5, m)$  is the corresponding massive GW operator defined in Eq. (4.53), except with  $\tilde{\epsilon}(N_5; H_M)$  replacing  $\epsilon(H_M)$ . We have introduced a permutation matrix,

$$\mathcal{P} = \begin{pmatrix} P_L & P_R & 0 & \dots & 0 & 0 & 0 \\ 0 & P_L & P_R & \dots & 0 & 0 & 0 \\ \vdots & \vdots & & \ddots & & \vdots & \vdots \\ 0 & 0 & 0 & \dots & P_L & P_R & 0 \\ 0 & 0 & 0 & \dots & 0 & P_L & P_R \\ P_R & 0 & 0 & \dots & 0 & 0 & P_L \end{pmatrix}. \quad (7.13)$$

With the help of  $\mathcal{P}$ , the four-dimensional quark fields introduced in Eq. (3.31) can be reexpressed as

$$q = (\mathcal{P}^{-1} \psi)_{s=1}, \quad \bar{q} = (\bar{\psi} \mathcal{R} \mathcal{P})_{s=1}. \quad (7.14)$$

We see that the role of the permutation matrix is to move the RH quark field, which here lives originally near the  $s = N_5$  boundary, to the  $s = 1$  boundary. The end result is that, in the operator  $D_M^5(N_5, m) \mathcal{P}$ , the two chiral components of the light domain wall quark both live near the  $s = 1$  boundary.

With Eq. (7.12) at hand, it is a straightforward exercise to relate  $D_{GW}(N_5, m)$  back to the domain wall propagator for the effective four-dimensional quark field,  $D_{\text{eff}}^{-1}(N_5, m)$ . Generalizing Eq. (4.46) to  $m \neq 0$ , we subtract a contact term from the propagator  $D_{GW}^{-1}(N_5, m)$  and divide by a factor  $(1 - m)$ , obtaining<sup>44</sup>

$$\begin{aligned} D_{\text{eff}}^{-1}(N_5, m) &\equiv \frac{1}{1 - m} (D_{GW}^{-1}(N_5, m) - 1) \\ &= \frac{1}{1 - m} [\mathcal{P}^{-1} D_M^5(N_5, m)^{-1} (D_M^5(N_5, 1) - D_M^5(N_5, m)) \mathcal{P}]_{11}. \end{aligned} \quad (7.15)$$

The subtraction term in parentheses is explicitly

$$[D_M^5(N_5, 1) - D_M^5(N_5, m)]_{ss'} = (1 - m)(P_L \delta_{s, N_5} \delta_{s', 1} + P_R \delta_{s, 1} \delta_{s', N_5}), \quad (7.16)$$

<sup>43</sup>As in Sec. 3 the fifth coordinate takes values  $s = 1, 2, \dots, N_5$ .

<sup>44</sup>Let us denote the five-dimensional matrix occurring on the right-hand side of Eq. (7.12) by  $\mathcal{M}$ , so that the equation becomes  $D_{GW}(N_5, m) = [\mathcal{M}]_{11}$ . Using the UDL decomposition introduced in Ref. [34] it can then be shown that  $D_{GW}^{-1}(N_5, m) = [\mathcal{M}^{-1}]_{11}$ .

hence  $[(D_M^5(N_5, 1) - D_M^5(N_5, m))\mathcal{P}]_{ss'} = (1 - m)[\mathcal{R}\mathcal{P}]_{ss'}$  for  $s' = 1$ , where  $\mathcal{R}$  is the reflection on the fifth coordinate introduced in Sec. 3.2. This gives

$$D_{\text{eff}}^{-1}(N_5, m) = [\mathcal{P}^{-1}D_M^5(N_5, m)^{-1}\mathcal{R}\mathcal{P}]_{11}. \quad (7.17)$$

Noting Eq. (7.14), it follows that Eq. (7.17) reproduces the usual domain wall four-dimensional propagator, Eq. (4.40). Thus, the four-dimensional domain wall or Möbius propagator  $D_{\text{eff}}^{-1}$  already encodes the usual contact term subtraction of the GW propagator, which implies that for  $m = 0$  it anti-commutes with  $\gamma_5$  in the limit  $N_5 \rightarrow \infty$ .

### 7.1.3 Möbius conserved currents

To obtain formulae for the (partially) conserved vector and axial currents, we have two options. The first option is to invoke Noether's theorem, as we have done in Sec. 4.1. The essence of the method is to promote the global symmetry transformation parameter  $\omega^a$  to a spacetime dependent one,  $\omega^a(x)$ . In the continuum, because the action is invariant under the global flavor transformation where  $\omega^a$  is constant, the variation must then take the form  $\delta S = \int d^d x J_\mu^a(x) \partial_\mu \omega^a(x)$ , which defines the current  $J_\mu^a(x)$  as the coefficient of  $\partial_\mu \omega^a(x)$ . Conservation of the current then follows by partial integration, while the ensuing Ward-Takahashi identities follow by performing the corresponding change of variables that leaves the partition function invariant.

Unlike in the continuum, on the lattice there can be more than one way of expressing  $\delta S$  as  $\sum_x \omega^a(x) D_\mu J_\mu^a(x)$  where  $D_\mu$  is a difference operator. Indeed we have already made use of this freedom in Sec. 4.1 to express  $j_5(x, s)$  and  $\Delta_5$  in a slightly different way from Ref. [20] (keeping  $\Delta_5 j_5(x, s)$  the same). When the Dirac operator has an infinite range, as in the case of the Möbius operator of Eq. (7.10), it gets significantly more complicated to figure out how to best express  $\delta S$  as a difference operator acting on a current. The reason is that the current and/or the difference operator must now also have an infinite range.

Instead, we will use here the alternative method. We first promote the global symmetry to a local one by introducing an external, fictitious flavor gauge field. The conserved current is then defined as the infinitesimal response to this gauge field [74, 34], while current conservation follows from gauge invariance of the partition function in the presence of the external flavor gauge field.

We start with the conserved vector current (for the domain wall case, see Eq. (4.10)). We proceed as follows. All (four-dimensional) links are replaced by

$$U_\mu(x) \rightarrow U_\mu(x) \times e^{i\lambda^a A_\mu^a(x)}, \quad (7.18)$$

where  $A_\mu^a(x)$  is the fictitious four-dimensional gauge potential which will be set to zero at the end of our manipulations, and  $\lambda^a$  is a generator of the vector flavor symmetry. The linearized variation of the flavor gauge field  $A_\mu^a(x)$  under a gauge transformation is  $\delta A_\mu^a(x) = \omega^a(x + \hat{\mu}) - \omega^a(x)$ . As a result, the difference operator occurring in the lattice continuity equation will always be the nearest-neighbor backward difference operator.

In order to obtain the conserved vector current we take the variation of the five-dimensional Möbius action with respect to  $A_\mu^a(x)$ . Using Eq. (7.11) we find

$$\begin{aligned}
\mathcal{V}_\mu^a(x) &\equiv -i\delta_{A_\mu^a(x)}\bar{\Psi}D_M^5\Psi & (7.19) \\
&= -i\sum_{s,z,y}\bar{\Psi}(z,s)\left[\delta_{A_\mu^a(x)}\tilde{D}\right]_{z,y}\Psi(y,s) \\
&= \sum_{s,z,y}\bar{\Psi}(z,s)\left[\frac{1}{D_-}c\lambda^aV_\mu(x)\frac{1}{D_-}D_+ + \frac{1}{D_-}b\lambda^aV_\mu(x)\right]_{z,y}\Psi(y,s) \\
&= \sum_{s,z,y}\bar{\Psi}(z,s)\left[\frac{1}{D_-}\lambda^aV_\mu(x)\left(c\frac{1}{D_-}D_+ + b\right)\right]_{z,y}\Psi(y,s) \\
&= (b+c)\sum_{s,z,y}\bar{\Psi}(z,s)\left[\frac{1}{D_-}\lambda^aV_\mu(x)\frac{1}{D_-}\right]_{z,y}\Psi(y,s),
\end{aligned}$$

where the usual (finite-range) kernel for the Wilson fermion conserved current acts within the four-dimensional layers, and is given by (compare Eq. (4.5))

$$\begin{aligned}
\lambda^a[V_\mu(x)]_{z,y} &= -i[\delta_{A_\mu^a(x)}D_W]_{z,y} & (7.20) \\
&= -\lambda^a\left(\frac{1+\gamma_\mu}{2}U_\mu(x)\delta_{z,x}\delta_{x+\hat{\mu},y} - \frac{1-\gamma_\mu}{2}U_\mu^\dagger(x)\delta_{z+\hat{\mu},x}\delta_{x,y}\right).
\end{aligned}$$

In contrast to Refs. [74, 34], Eq. (7.19) is a very simple, compact result. In the case of domain wall fermions,  $b = 1$ ,  $c = 0$ , it reduced to the result found in Sec. 4.1 up to an overall minus sign.

At first sight the factors of  $D_-^{-1}$  in (7.19) seem like an added computational expense. However, we can multiply  $D_M^5$  on the right or left by  $D_-$  before computing the propagators that sandwich the current in a physical quark line diagram. Thus in practice the conserved current can be implemented in essentially the same way as for Wilson (or domain wall) fermions. For an insertion of  $\mathcal{V}_\mu^a(x)$  into a physical quark line we have, using Eqs. (7.14) and (7.19), and denoting fermion contractions in a given gauge field background with expectation values,

$$\begin{aligned}
C_\mu^a(x,y,z) &= \langle q(z)\mathcal{V}_\mu^a(x)\bar{q}(y)\rangle & (7.21) \\
&= (b+c)\sum_{s,z',y'}\langle q(z)\bar{\Psi}(z',s)\rangle\left[\frac{1}{D_-}\lambda^aV_\mu(x)\frac{1}{D_-}\right]_{z',y'}\langle\Psi(y',s)\bar{q}(y)\rangle \\
&= (b+c)\sum_{s,z',y'}[\mathcal{P}^{-1}(D_M^5)^{-1}]_{z,1;z',s}\left[\frac{1}{D_-}\lambda^aV_\mu(x)\frac{1}{D_-}\right]_{z',y'}[(D_M^5)^{-1}\mathcal{R}\mathcal{P}]_{y',s;y,1} \\
&= (b+c)\sum_{s,z',y'}[\mathcal{P}^{-1}(D_-D_M^5)^{-1}]_{z,1;z',s}[\lambda^aV_\mu(x)]_{z',y'}[(D_M^5D_-)^{-1}\mathcal{R}\mathcal{P}]_{y',s;y,1}.
\end{aligned}$$

Since  $D_-$  and  $\tilde{D}$  commute,  $D_-\tilde{D} = \tilde{D}D_- = D_+$ , it follows that  $D_-D_M^5$  and  $D_M^5D_-$  are both finite-range operators. These operators are also related via the  $\gamma_5$ -hermiticity properties which are similar to those discussed in Sec. 3.2, for example,  $D_M^5D_- = \gamma_5\mathcal{R}(D_-D_M^5)^\dagger\gamma_5\mathcal{R}$ .

In order to obtain the partially conserved axial current we first construct the five-dimensional conserved current, which is defined in a similar manner by taking the variation with respect to a five-dimensional gauge potential,  $(A_\mu^a(x, s), A_5^a(x, s))$ . The result for the four-dimensional components is identical to the above except there is no sum over the fifth dimension,

$$j_\mu^a(x, s) = (b + c) \sum_{z, y} \bar{\Psi}(z, s) \left[ \frac{1}{D_-} \lambda^a V_\mu(x) \frac{1}{D_-} \right]_{z, y} \Psi(y, s) . \quad (7.22)$$

Because of the different conventions we adopted for the Möbius operator (compare Eqs. (3.30) and (7.10)) the current in the fifth direction is slightly different from Eq. (4.6). Instead, we now have

$$j_5^a(x, s) = \begin{cases} -\bar{\psi}(x, s) P_L \lambda^a \psi(x, s + 1) + \bar{\psi}(x, s + 1) P_R \lambda^a \psi(x, s) , & 1 \leq s < N_5 , \\ m \bar{\psi}(x, N_5) P_L \lambda^a \psi(x, 1) - m \bar{\psi}(x, 1) P_R \lambda^a \psi(x, N_5) , & s = N_5 . \end{cases} \quad (7.23)$$

As in Sec. 4.1, the only current which depends on the quark mass  $m$  is  $j_5^a(x, N_5)$ .

The rest of the construction is the same as in Sec. 4.1. The five-dimensional continuity equation is again Eq. (4.7). The axial current is defined via Eq. (4.14) as before, and its partial conservation equation is again given by Eq. (4.15) with the right-hand side defined via Eqs. (4.16) and (4.17). Importantly, the calculation of the residual mass is same as for standard domain wall fermions [74, 34] (see Sec. 5.2).

In Refs. [34, 76] a somewhat different approach is followed to construct the currents, but in the end they are equivalent to the ones defined here. Instead of taking the variation with respect to external gauge links of the five-dimensional Möbius operator, as we have done above (see in particular Eq. (7.19)), in Refs. [34, 76] one takes the variation of the (approximate) GW operator, Eq. (7.12). Since this effective four-dimensional operator is expressed directly in terms of the five-dimensional Möbius operator, it is possible to consider its variation with respect to both four-dimensional and five-dimensional flavor gauge transformations; the latter are needed in order to construct the partially conserved axial currents using Eq. (4.14), which in turn leads to the domain-wall fermion version of the PCAC relation in Eq. (4.15). The application of a (linearized) gauge transformation to the external flavor gauge fields then yields the usual conservation law (or Ward-Takahashi identity), and it is straightforward to identify the currents themselves. The procedure is somewhat involved, and we refer the interested reader to Appendix A of Ref. [34] and the lattice proceedings Ref. [76].

## 7.2 Further symmetry considerations

In this subsection we revisit two topics already discussed earlier, and expand their scope using ingredients introduced in our discussion of Möbius fermions in the previous subsection. In Sec. 7.2.1 we extend the scope of the proof of chiral symmetry restoration given in Sec. 4.2, while in Sec. 7.2.2 we establish the symmetry features of the phase diagram, a subject we have already encountered in Sec. 6.1 and Sec. 6.2. The discussion of improvements will be resume in Sec. 7.3.

### 7.2.1 Chiral symmetry restoration revisited

In Sec. 4.2 we proved the restoration of chiral symmetry for  $N_5 \rightarrow \infty$  within the original formulation of domain wall fermions, assuming a domain wall height  $0 < M < 1$ . This implies that  $B$  (Eq. (4.23)) is a positive operator, as are the various transfer matrices introduced there. In the range  $1 < M < 2$  the operator  $B$  can have negative eigenvalues, and the same is true for the transfer matrices.<sup>45</sup> While we expect such negative eigenvalues to be rare (see Sec. 5.1.1), in a proof of chiral symmetry restoration their role has to be addressed.

Here we will extend the proof of chiral symmetry restoration to the entire range of domain wall height  $0 < M < 2$ , as well as to general values of the Möbius parameters  $b$  and  $c$ . As a measure of chiral symmetry violation for finite  $N_5$  we will use Eq. (7.7) with  $H = H_M$ .

As follows from the discussion in Sec. 7.1.1, in the limit  $N_5 \rightarrow \infty$  the approximate sign function  $\tilde{\epsilon}(N_5, \lambda)$  of Eq. (7.5) tends to  $\epsilon(\lambda) = \pm 1$  for arbitrary (real)  $\lambda$ , except for  $\lambda = 0$  or  $\lambda = \pm\infty$ . Let us examine these two exceptional cases.

In order for  $H_M$  to have an eigenvalue  $\lambda = 0$ , the numerator in Eq. (7.6) must vanish, which implies that  $D_W(M)$  has a zero mode. This is the same condition we have already encountered in Sec. 4.2. For an eigenvalue  $\lambda = \pm\infty$  of  $H_M$ , the denominator in Eq. (7.6) must vanish, which implies that  $D_W(M)$  has an eigenvalue equal to  $2/(c - b)$ , or equivalently, that  $\det(2 + (b - c)D_W(M)) = 0$ . Either one of these special cases can be satisfied only on a measure zero subset of the gauge field configuration space. Using this observation, we can now complete the proof of chiral symmetry restoration in essentially the same way as we did in Sec. 4.2, by showing that the ensemble average of any correlation function that contains an insertion of  $1 - \tilde{\epsilon}(N_5; H)^2$  vanishes for  $N_5 \rightarrow \infty$ .

According to Eq. (7.1), an eigenvalue  $+1$  of the transfer matrix  $T$  corresponds to a zero eigenvalue of  $H_S$ , while an eigenvalue  $-1$  of the transfer matrix corresponds to eigenvalues  $\lambda = \pm\infty$  of  $H_S$ . These statements remain true if we generalize the definition of  $T$  by replacing  $H_S$  with  $H_M$  in Eq. (7.1). Eigenvalues  $\pm 1$  of the transfer matrix both give rise to zero eigenvalues of the transfer matrix hamiltonian  $H_T$ , which is defined in terms of  $\log T^2$  (see Eq. (4.50)). We have already seen in Sec. 6.7 that, for the original formulation of domain wall fermions, the dominant chiral symmetry violations for very large but finite  $N_5$  come from the (near-)zero spectrum of  $H_T$ . This behavior generalizes to Möbius fermions, as it is consistent with the roles of the spectral ranges in Eq. (7.8): transfer matrix eigenvalues near  $+1$  correspond to the range  $\alpha\lambda \ll 1/N_5$  for the eigenvalues of  $H_M$ , while transfer matrix eigenvalues near  $-1$  correspond to  $\alpha\lambda \gg N_5$ . Once again the underlying reason is the behavior of the transfer matrix in Eq. (7.1) and the approximate sign function in Eq. (7.5) under  $H \rightarrow 1/H$ .

---

<sup>45</sup>Notice that when  $B$  has negative eigenvalues,  $K$  and  $K^\dagger$  have to be defined via suitable analytic continuations. Hence Eqs. (4.26) and (4.27) no longer imply that  $T$  and  $\tilde{T}$  are positive. But  $T$  remains a hermitian matrix, and  $T$  and  $\tilde{T}$  still share the same spectrum.

## 7.2.2 Symmetry of the phase diagram

Symmetry features of the phase diagram were discussed in Sec. 6.1 and Sec. 6.2. Here we give a fuller discussion of the symmetry of the phase diagram for the original formulation of domain wall fermions with variable  $a_5$ , as well as for Möbius fermions. We verify that the corresponding chiral zero mode spectrum and effective four-dimensional operators respect this symmetry.

We start with the Wilson operator in  $d$  dimensions. Using the same notation as in Sec. 7.1 for the Wilson operator, and adding a superscript  $d$  to denote  $d$ -dimensional quantities, the  $d$ -dimensional Wilson operator is

$$D_W^d(M) = -D_K^d + W^d - M = D_h^d + d - M , \quad (7.24)$$

where as usual  $M = -m_0$ , and  $D_h^d$  contains the hopping terms which can be read off from Eqs. (4.1) and (4.2). It is easy to see that under the change of variables

$$\psi(x) \rightarrow \epsilon_d(x)\psi(x) , \quad \bar{\psi}(x) \rightarrow -\epsilon_d(x)\bar{\psi}(x) , \quad (7.25)$$

where  $\epsilon_d(x) = (-1)^{x_1+\dots+x_d}$ , the Wilson operator transforms as

$$D_W^d(M; x, y) \rightarrow -\epsilon_d(x)D_W^d(M; x, y)\epsilon_d(y) = D_W^d(M'; x, y) , \quad (7.26)$$

where

$$M' = 2d - M . \quad (7.27)$$

This result follows since the (nearest neighbor) hopping terms are invariant under the transformation (7.25), whereas the same-site terms flip sign. Hence the phase diagram is symmetric with respect to the axis  $M = -m_0 = d$ .

We next turn to the original formulation of domain wall fermions except with variable lattice spacing  $a_5$  in the fifth direction. The transformation (7.25) now takes  $M$  to

$$M' = 8 + \frac{2}{a_5} - M , \quad (7.28)$$

hence the phase diagram is symmetric with respect to the axis  $M = 4 + 1/a_5$ .

Let us check that the chiral spectrum of domain wall fermions is consistent with this symmetry (see *e.g.* Ref. [21]). On a semi-infinite fifth dimension, the condition for having a chiral zero mode at a given corner of the Brillouin zone is

$$|1 + a_5(2n - M)| < 1 . \quad (7.29)$$

As in Sec. 3.1, the number of components of the 4-momentum equal to  $\pi$  is  $0 \leq n \leq 4$ , while the remaining  $4 - n$  components are equal to zero. In momentum space, the transformation (7.25) interchanges  $p_\mu = 0$  with  $p_\mu = \pi$ . Hence it induces the transformation  $n \rightarrow n'$  where

$$n' = 4 - n . \quad (7.30)$$

Under the combined replacement  $(M, n) \rightarrow (M', n')$  we have

$$1 + a_5(2n' - M') = -(1 + a_5(2n - M)) . \quad (7.31)$$

The overall minus sign on the right-hand side can be traced to the factor of  $(-1)^s$  contained in  $\epsilon_5(x, s)$ . Condition (7.29) is seen to be invariant under this combined replacement, which confirms that the zero modes spectrum respects the symmetry of the phase diagram. For  $a_5 = 1$ , Table 1 is reproduced.

For Möbius fermions, it is more convenient to use the original formulation of Ref. [74] with the Möbius operator  $D_{BNO} = D_- D_M^5$  (see Eq. (7.10)). The Möbius parameters can be expressed as  $b = (a_5/2)(\alpha + 1)$  and  $c = (a_5/2)(\alpha - 1)$ . The transformation (7.28) of the mass parameter is now supplemented by a transformation of the scaling parameter,

$$\alpha' = \alpha^{-1} . \quad (7.32)$$

We then have

$$-\epsilon_4 \left( 1 + a_5 \frac{1 \pm \alpha'}{2} D_W(M') \right) \epsilon_4 = \pm \alpha^{-1} \left( 1 + a_5 \frac{1 \pm \alpha}{2} D_W(M) \right) . \quad (7.33)$$

Using also that  $\epsilon_5 = \epsilon_5(x, s) = \epsilon_4(x)(-1)^s$  it follows that

$$D_{BNO}(M', \alpha') = -\alpha^{-1} \epsilon_5 D_{BNO}(M, \alpha) \epsilon_5 . \quad (7.34)$$

Thus, in this formulation, the symmetry of the phase diagram under the interchange  $(M, \alpha) \rightarrow (M', \alpha')$  can be realized via the change of variables

$$\psi(x, s) \rightarrow \epsilon_5(x, s) \psi(x, s) , \quad \bar{\psi}(x, s) \rightarrow -\alpha^{-1} \epsilon_5(x, s) \bar{\psi}(x, s) . \quad (7.35)$$

The original domain wall formulation is recovered for  $\alpha = 1$ , where the transformations reduce to what we already had before.

For the Möbius operator, the condition for having a zero mode at a given corner of the Brillouin zone is  $|R| < 1$  where

$$R = \frac{1 + b(2n - M)}{1 - c(2n - M)} = \frac{2 + a_5(1 + \alpha)(2n - M)}{2 + a_5(1 - \alpha)(2n - M)} . \quad (7.36)$$

The transformations (7.28) and (7.30) of  $M$  and  $n$  are again supplemented by the transformation (7.32) of the scaling parameter  $\alpha$ . We find

$$\frac{2 + a_5(1 + \alpha')(2n' - M')}{2 + a_5(1 - \alpha')(2n' - M')} = - \frac{2 + a_5(1 + \alpha)(2n - M)}{2 + a_5(1 - \alpha)(2n - M)} . \quad (7.37)$$

The minus sign on the right-hand side is similar to Eq. (7.31). The condition  $|R| < 1$  is thus invariant under the combined transformation  $(M, \alpha, n) \rightarrow (M', \alpha', n')$ , thereby proving that the zero mode spectrum respects the symmetry of the phase diagram.

Finally, let us check that the approximate GW operator  $D_{GW}(N_5)$  of Eq. (4.49b) also respects the symmetry of the phase diagram. We will do this for the general Möbius case since the original domain wall formulation is obtained by setting  $\alpha = 1$ . The transfer matrix (7.1) with  $H = H_M = \gamma_5 D_M$  can be expressed as (see Eq. (7.6) and notice also Eq. (7.3))

$$T = \left( (2 + a_5 D_W^\dagger(M)) + \gamma_5 \alpha a_5 D_W(M) \right)^{-1} \left( (2 + a_5 D_W^\dagger(M)) - \gamma_5 \alpha a_5 D_W(M) \right) . \quad (7.38)$$

Transforming  $M$  and  $\alpha$  simultaneously gives

$$\begin{aligned} -\epsilon_4 \left( (2 + a_5 D_W^\dagger(M)) \pm \gamma_5 a_5 \alpha D_W(M) \right) \epsilon_4 &= \\ &= \pm \gamma_5 (\alpha')^{-1} \left( (2 + a_5 D_W^\dagger(M')) \pm \gamma_5 \alpha' a_5 D_W(M') \right) \gamma_5, \end{aligned} \quad (7.39)$$

where we have use  $\gamma_5$  hermiticity of  $D_W$ . Using Eq. (7.38) it follows that

$$\epsilon_4 T(M, \alpha) \epsilon_4 = -\gamma_5 T(M', \alpha') \gamma_5. \quad (7.40)$$

Finally using this result in Eq. (4.49b) and noting that  $N_5$  is always even we obtain

$$\epsilon_4 D_{GW}(N_5; M, \alpha) \epsilon_4 = \gamma_5 D_{GW}(N_5; M', \alpha') \gamma_5. \quad (7.41)$$

Thus, the symmetry of the phase diagram under the combined interchange  $(M, \alpha) \rightarrow (M', \alpha')$  can be realized by transforming the effective four-dimensional fields according to  $q(x) \rightarrow \epsilon_4(x) \gamma_5 q(x)$ ,  $\bar{q}(x) \rightarrow \bar{q}(x) \gamma_5 \epsilon_4(x)$ .

### 7.3 “Optimal” domain wall fermions

The Zolotarev approximation of a GW operator is defined by replacing the sign function  $\epsilon(H)$  in Eq. (4.51) with  $\bar{\epsilon}(N; H)$ . Here  $\bar{\epsilon}(N; x) = x R_N(x^2)$ , where  $R_N(\lambda)$  is the Zolotarev rational approximation of  $1/\sqrt{\lambda}$ , defined by the requirement that for given  $N$  and interval  $0 < \lambda_{\min} < \lambda < \lambda_{\max}$ ,  $R_N(\lambda)$  is the rational polynomial approximation of degree  $N$  that minimizes the maximal deviation  $|R_N(\lambda) - 1/\sqrt{\lambda}|$  over the interval  $\lambda_{\min} \leq \lambda \leq \lambda_{\max}$ .

The so-called optimal domain wall fermion operator [77] is defined by the requirement that the effective four-dimensional operator is the approximate overlap operator obtained by replacing  $\epsilon(H)$  in Eq. (4.51) with  $\bar{\epsilon}(N_5; H)$ , with  $H = H_W$  the standard Wilson kernel. This operator can be realized as a special case of Möbius fermions, provided that we allow the coefficients  $b$  and  $c$  in Eq. (7.6) to depend on the fifth coordinate [74]. We note that while  $\lambda_{\max}$  can be taken to be some  $O(1)$  number that depends mildly on the domain wall height  $M$  [77], the choice of  $\lambda_{\min}$  is more tricky, and sensitive to the presence of near-zero modes of the Wilson kernel [78].

While these optimal domain wall fermions do in general lead to a smaller residual mass at fixed  $N_5$ , this does not necessarily mean that they represent a better choice compared to other options, and notably, compared to the Möbius domain-wall fermions of Sec. 7.1.

First, assuming that the residual mass is on the order of  $10^{-3}$  or less in lattice units, in practice it is used as part of the light quark mass(es), thereby “turning the bug into a feature,” as far as the residual mass itself is concerned. The relevant question thus becomes how do chiral symmetry violations in *other* observables compare. Also, if we set some value of the residual mass as our target, the practical question is not quite how to achieve it at the smallest possible  $N_5$ , but, rather, how to achieve it at the smallest possible cost, as measured for example by the average number of applications of the four-dimensional Wilson operator required by the solver. For more details, see Ref. [74] (see also Ref. [78]).

## 7.4 Changing the Wilson kernel

Replacing the standard nearest-neighbor Wilson kernel in Eq. (3.30) by an improved kernel was proposed by several authors. We discuss here two proposals.

### 7.4.1 Improved exponential damping

Motivated by the calculation of the one loop wave function of the domain wall quark (Sec. 5.1.2), kernels that yield more efficient exponential suppression of the wave function in perturbation theory were discussed in Ref. [41].

The basic idea is that the wave function of the domain wall quark is controlled by the maximum of  $e^{-\alpha(p)}$  over the Brillouin zone, where in the case of the standard Wilson kernel  $\alpha(p)$  was determined by Eq. (3.20). Let us consider a more general kernel,

$$\tilde{D}(p) = i \sum_{\mu} \gamma_{\mu} f(p_{\mu}) - r \tilde{W}(p) + M, \quad (7.42)$$

where  $r > 0$  is the Wilson parameter and  $f(p_{\mu})$  and  $\tilde{W}(p)$  will be specified below. Then Eq. (3.20) generalizes to

$$2 \cosh \alpha(p) = \frac{1 + \tilde{b}^2(p) + \sum_{\mu} f^2(p_{\mu})}{\tilde{b}(p)}, \quad (7.43)$$

where now  $\tilde{b}(p) = 1 - M + r \tilde{W}(p)$ . By judiciously selecting  $f(p_{\mu})$ ,  $r$ , and  $\tilde{W}(p)$  it may then be possible to reduce the maximum of  $e^{-\alpha(p)}$  over the Brillouin zone when the domain wall height  $M$  is tuned to its optimal tadpole improved value (Sec. 5.1.1).

To keep the kernels relatively economic, only kernels with beyond nearest neighbor couplings along straight lines were considered. Specifically, the point  $x$  was allowed to couple at most to  $x \pm 2\hat{\mu}$ , and then at most to  $x \pm 3\hat{\mu}$  in each direction. The kernel with next-nearest neighbor couplings has  $\tilde{W}(p) = W_2(p)$ , where

$$W_n(p) = \sum_{\mu} (1 - \cos(p_{\mu}))^n, \quad (7.44)$$

while  $f(p_{\mu})$  was taken to be  $\sin(p_{\mu})$  times a linear function of  $\cos(p_{\mu})$ . For the kernel with next-next-nearest neighbor couplings,  $\tilde{W}(p) = W_3(p)$  was taken, while  $f(p_{\mu})$  was equal to  $\sin(p_{\mu})$  times a quadratic function of  $\cos(p_{\mu})$ . The maximum of  $e^{-\alpha(p)}$  over the Brillouin zone was then determined numerically.

For the kernel with next-nearest neighbor couplings, it was found that the maximum of  $e^{-\alpha(p)}$  can be lowered from 0.5 (its value for the standard nearest neighbor kernel, see Sec. 5.1.2) to about 0.25, while maintaining a dispersion relation with reasonably small  $O(p^3)$  discretization effects. For the kernel with next-next-nearest neighbor couplings, the maximum of  $e^{-\alpha(p)}$  can be lowered to roughly 0.1 if the dispersion relation is constrained to be  $p + O(p^5)$  and the kernel's parameters are all  $O(1)$ . In this example the exponential suppression factor of  $1/2^s$  in the one-loop wave function (5.5) would thus be replaced by  $\sim 1/10^s$ .

We leave it to the reader to estimate the relative cost of such improved kernels compared to the standard Wilson kernel for fixed size of the residual breaking of chiral symmetry. Of course, the improvement of the wave function predicted by perturbation theory would have to be tested via nonperturbative numerical experimentation, which, however, has not been done to date for these kernels.

## 7.4.2 Hypercubic fermions

An alternative strategy is to use an approximate solution of the GW relation for the Wilson kernel. This approach was proposed for both GW (or overlap) fermions and for domain wall fermions [79, 80]. It is easy to follow the logic of this approach in the case of GW fermions. Throughout, we will assume that all relevant operators satisfy  $\gamma_5$ -hermiticity.

Given an exact or approximate GW operator  $\tilde{D}$ , one defines a new GW operator by taking the kernel  $H$  in Eq. (4.51) to be

$$\tilde{H} = \gamma_5(2\tilde{D} - 1) . \quad (7.45)$$

If  $\tilde{D}$  is already an exact GW operator, it follows from the GW relation together with  $\gamma_5$ -hermiticity that  $\tilde{H}^2 = 1$ . Hence  $\epsilon(\tilde{H}) = \tilde{H}$ , and using  $\tilde{H}$  as the kernel in Eq. (4.51) reproduces the original GW operator  $\tilde{D}$ .

If  $\tilde{D}$  is only an approximate solution of the GW relation then  $\epsilon(\tilde{H}) \neq \tilde{H}$ . However, for a good approximation we still expect that  $\tilde{H}^2 \approx 1$ . Writing  $\epsilon(\tilde{H}) = \tilde{H}/|\tilde{H}| = \tilde{H}/(\tilde{H}^2)^{1/2}$  we then expect that it should be easier to construct  $(\tilde{H}^2)^{-1/2}$  numerically, because the eigenvalues of  $\tilde{H}$  should be closer to unity in comparison with, say, the standard Wilson kernel.

For domain wall fermions, one expects that the convergence of  $\tilde{\epsilon}(N_5; H)$  to  $\epsilon(H)$  with increasing  $N_5$  will be faster if in Eq. (3.30) (and thus also in Eq. (7.2)) one replaces the standard Wilson kernel by an approximate GW operator  $\tilde{D}$ . Equivalently, at fixed  $N_5$ , the replacement of the standard Wilson kernel by an approximate GW operator is expected to yield improved chiral behavior.

A particular family of approximate GW solutions goes under the name of ‘‘hypercubic fermions.’’ One requires that the approximate GW operator  $\tilde{D}(x, y)$  be such that it couples two sites  $x$  and  $y$  only if there is a unit hypercube to which both sites belong. In comparison with the overlap operator with the standard Wilson kernel, the GW operator with a hypercubic fermion kernel given by Eq. (7.45) is expected to have several advantages. First, as already explained, it should be easier to achieve good numerical approximations of the sign function  $\epsilon(\tilde{H})$ . In addition, one expects improved locality, rotational symmetry, and scaling behavior. The obvious price is that the hypercubic fermion kernel  $\tilde{H}$  connects each lattice site to  $3^4$  neighboring sites (itself included), which makes its application more costly. For more details, including numerical tests, see Refs. [79, 80].

## 7.5 Deflation

The near-zero modes of the Wilson kernel (or any other kernel for that matter) slow down the convergence to the chiral limit of domain wall fermions. For a GW operator, near-zero modes of its kernel cause difficulties in the numerical evaluation of the (operator) sign function  $\epsilon(H)$  in Eq. (4.51) or (4.53). Let  $\hat{\epsilon}(H)$  be some unspecified numerical approximation of  $\epsilon(H)$ . Typically,  $\hat{\epsilon}(\lambda)$  will provide a good approximation of the sign function  $\epsilon(\lambda)$  when  $\lambda$  lies within some bounded interval  $0 < \lambda_{\min} \leq |\lambda| \leq \lambda_{\max}$ . But when  $|\lambda| < \lambda_{\min}$  the approximation  $\hat{\epsilon}(\lambda)$  breaks down.<sup>46</sup>

Of course, one could do better by lowering  $\lambda_{\min}$ , so that the interval where  $\hat{\epsilon}(\lambda)$  provides a good approximation reaches closer to zero. But suppose that, for a typical gauge field configuration in an ensemble, there are only a few kernel eigenvalues which are smaller than some reasonable  $\lambda_{\min}$ . In that case, achieving a good approximation of  $\epsilon(\lambda)$  for these near-zero eigenvalues by further lowering  $\lambda_{\min}$  can be very costly. Deflation provides an alternative solution. In effect, a small eigenvalue  $\lambda < \lambda_{\min}$  gets replaced by an  $O(1)$  eigenvalue. As long as the sign of  $\lambda$  is preserved by the deflated eigenvalue,  $\epsilon(\lambda)$  will be reproduced much more easily.

Deflation works as follows. Starting from some kernel  $H$  in Eq. (4.51), we replace  $H$  by a deflated version

$$\hat{H} = H + \sum_{i=1}^n (\epsilon(\lambda_i) - \lambda_i) |i\rangle \langle i| . \quad (7.46)$$

Here  $|i\rangle$  denotes an eigenvector of  $H$  with eigenvalue  $\lambda_i$ . The sum runs over the  $n$  eigenvectors with smallest  $|\lambda_i|$ . For simplicity we assumed that all the affected eigenvalues are deflated to  $\pm 1$ .

In order to apply deflation to the overlap operator one first finds the  $n$  smallest eigenvalues of the Wilson kernel by some minimization method, and constructs the projection of the sign function on this subspace,  $\sum_{i=1}^n \epsilon(\lambda_i) |i\rangle \langle i|$ . Then effectively one needs to approximate  $\epsilon(H_W)$  only on the orthogonal subspace, for which a more comfortable value of  $\lambda_{\min}$  can be used.

The use of deflation for domain wall fermions was proposed in Refs. [62, 81]. For definiteness, we follow Ref. [81]. The domain wall operator is modified in such a way that in the approximate GW operator at finite  $N_5$ , Eq. (7.4),  $H_S$  gets deflated according to Eq. (7.46). Now, an eigenvalue  $\lambda_i$  yields in the approximate sign function of Eq. (7.5) a factor of

$$\tilde{\epsilon}(N_5; \lambda_i) = \frac{(1 + \lambda_i)^{N_5} - (1 - \lambda_i)^{N_5}}{(1 + \lambda_i)^{N_5} + (1 - \lambda_i)^{N_5}} . \quad (7.47)$$

The effect of the deflated kernel (7.46) is to trade  $\tilde{\epsilon}(N_5; \lambda_i)$  with  $\tilde{\epsilon}(N_5; \pm 1)$  for the relevant eigenvalues. Clearly, if  $|\lambda_i| \ll 1$  then the convergence of  $\tilde{\epsilon}(N_5; \pm 1)$  to  $\epsilon(\lambda_i)$  will be much faster than the convergence of  $\tilde{\epsilon}(N_5; \lambda_i)$ , thereby suppressing any chiral symmetry violating effects from the corresponding eigenvector. For small-scale numerical tests of these deflation methods see Refs. [62, 81].

<sup>46</sup>See the chapter of the *LQCD@50* book on overlap fermions by DeGrand [15].

We recall (Sec. 6) that both overlap and domain-wall fermions live in the supercritical phase between the two rightmost “fingers” in Fig. 6, in which the mobility edge  $\lambda_c$  is strictly positive. At fixed value of the lattice spacing, a larger  $\lambda_c$  will yield a more local (exact or approximate) GW operator.

When deflation is applied to the Wilson kernel of the overlap operator, in principle this doesn’t change the overlap operator itself; it merely affects the numerical approximation used. By contrast, modifying the kernel of domain wall fermions by deflation, as described above, gives rise to a different domain-wall fermion operator for any finite  $N_5$ . However, as long as the mobility edge is  $O(1)$ , all the deflated near-zero modes will be exponentially localized on the lattice scale. Hence, locality of the full domain-wall fermion operator, and of the effective four-dimensional operator of Eq. (4.49), are both maintained.

## 8 Epilogue

When Kaplan introduced domain wall fermions [9], his original goal was to find a method to define anomaly-free chiral gauge theories on the lattice – a long-standing problem in lattice gauge theory. However, it gradually became clear that the presence of an opposite-chirality fermion on the “far” wall represents a major obstacle for this program.

In the following years, important progress towards the construction of chiral gauge theories was made by Narayanan and Neuberger [24, 82], but the seriousness of the open issues remained debated [83].

The next major step came after the invention of the overlap operator by Neuberger [18], and the realization that the overlap operator satisfies the Ginsparg-Wilson relation, which in turn leads to a modified form of chiral symmetry on the lattice [35]. Using these algebraic ingredients as a starting point, Lüscher successfully constructed anomaly-free abelian chiral gauge theories, while requiring one new algebraic constraint on the fermion spectrum beyond the familiar anomaly-cancellation condition [84]. As for nonabelian chiral gauge theories, he was able to define them to all orders in lattice perturbation theory [85, 86]. Going beyond lattice perturbation theory it was shown that Witten’s global anomaly is reproduced [87], but it is unknown if additional non-perturbative obstructions occur within this formulation.

Kaplan has continued to work on his original proposal with various collaborators, aiming to find a way to extend the dynamical four-dimensional gauge field into the fifth dimension in such a way that the opposite-chirality fermion on the far wall would hopefully be decoupled from the resulting four-dimensional theory. This line of research remains active to date [88, 89, 90]. In brief, the emerging picture is that this goal can be achieved in the topologically trivial sector, if the topological charge is defined in terms of the zero modes of the overlap operator (see Sec. 6.3). For example, one can use gradient flow to extend the four-dimensional gauge field from the boundary into the five-dimensional bulk, and for  $N_5 \rightarrow \infty$  the gauge field will die out before reaching the far wall. However, the same is not true in topologically non-trivial sectors: the chiral fermion on the far wall and/or the bulk degrees of

freedom cannot be fully decoupled [88, 91, 92]. Whether or not such a construction can account for the observed universe remains to be seen.<sup>47</sup>

As for QCD and similar vector-like theories, the presence of the two chiralities is a welcome feature: quarks are Dirac fermions that contain both a RH and a LH component. Alongside with Wilson and staggered fermions, which were introduced in the early days of lattice gauge theory, domain wall fermions have become one of the standard methods for large-scale lattice QCD calculations.

This introduction has focused on the formulation of domain wall fermions and not on the physical results obtained with it.<sup>48</sup> The only observable we have considered in detail is the residual mass, which serves as a measure of the good (yet imperfect) chiral properties of domain wall fermions. That a residual mass exists does not represent in itself a problem because quarks are not massless, so long as the residual mass is smaller than the (bare) mass required for the light quarks.

Since the first works [93, 37] it was clear that domain wall fermions are indispensable for light quark physics where chiral symmetry (alongside flavor structure) is important. This is particularly true when operators protected by chiral symmetry in the continuum mix with chiral symmetry-breaking operators in lattice calculations using discretizations that explicitly break chiral symmetry. For example, in studies of neutral kaon mixing and decay, which are important for understanding CP violation in the Standard Model, such artifacts are difficult or practically impossible to remove, while calculations with domain wall fermions go through like their continuum counterparts as far as mixing and renormalization are concerned once the residual mass has been taken into account [94, 70]. Power divergences, if present, are suppressed relative to Wilson fermions by  $O(am_{\text{res}})$ .

As described in the last section, state of the art lattice QCD simulations are now done with the Möbius action, as well as with the original version of domain wall fermions, for a wide variety of topics [34, 70, 95, 96], including chiral symmetry restoration at non-zero temperature [97, 98] and heavy meson (quark) decays [99, 100, 101]. So far, most computations using domain wall fermions for charm and bottom quarks have been performed on 2+1 flavor ensembles, so they are partially-quenched. These calculations have shown that domain wall fermions can be used effectively for charm quark physics if the lattice spacing is sufficiently small,  $a^{-1} \gtrsim 2$  GeV [101, 100, 102]. Dynamical simulations with 2+1+1 flavors of physical quarks, including charm, but with heavier-than-physical pions have begun [103] and have been used for important measurements like contributions to the muon anomaly [95, 96]. Ensembles with dynamical charm and physical masses are planned for the near future [103].

Overlap fermions have not been widely used in dynamical simulations (*i.e.*, gauge field ensemble generation). The reasons include their cost, as well as the need for a complicated special algorithm in order to change the topological charge in a dynamical overlap simulation. We note an early dynamical overlap simulation by JLQCD which

---

<sup>47</sup>For other approaches to the construction of lattice chiral gauge theories see for example Ref. [32] and references therein.

<sup>48</sup>We did not cover chiral perturbation theory for domain wall fermions. For references, see Ref. [46, 45, 47, 34].

was restricted to the topological charge  $Q = 0$  sector [104].<sup>49</sup>

Compared to lattice QCD simulations with Wilson or staggered fermions, the obvious shortcoming of domain wall fermions is the added cost of the extra fifth dimension. However, experience suggests that domain wall fermions often display smaller discretization effects for the same lattice spacing. This improved scaling can offset much of their extra cost since in general the cost of lattice calculations grows with a large power of the inverse lattice spacing as the continuum limit is approached. While it is difficult to carry out a systematic study of this question, it is suggestive that the very good chiral symmetry of domain wall fermions together with their simple flavor structure must be responsible for this behavior. For example, recent calculations of the hadronic contributions to the muon anomalous magnetic moment appear to bear out these expectations [95, 96, 105, 106, 107].

**Acknowledgments.** We thank Maarten Golterman for extensive discussions and comments. We also thank Tom DeGrand and David Kaplan for comments. TB is partially supported by the US Department of Energy under grant DE-SC0010339. YS is supported by the Israel Science Foundation under grant no. 1429/21.

## References

- [1] L.H. Karsten and J. Smit, *Lattice Fermions: Species Doubling, Chiral Invariance, and the Triangle Anomaly*, *Nucl. Phys. B* **183** (1981) 103.
- [2] H.B. Nielsen and M. Ninomiya, *Absence of Neutrinos on a Lattice. 1. Proof by Homotopy Theory*, *Nucl. Phys. B* **185** (1981) 20.
- [3] H.B. Nielsen and M. Ninomiya, *Absence of Neutrinos on a Lattice. 2. Intuitive Topological Proof*, *Nucl. Phys. B* **193** (1981) 173.
- [4] A. Pelissetto, *LATTICE NONLOCAL CHIRAL FERMIONS*, *Annals Phys.* **182** (1988) 177.
- [5] L.H. Karsten, *Lattice Fermions in Euclidean Space-time*, *Phys. Lett. B* **104** (1981) 315.
- [6] M. Golterman, *Lattice chiral gauge theories*, *Nucl. Phys. B Proc. Suppl.* **94** (2001) 189 [[hep-lat/0011027](#)].
- [7] M. Golterman, *Staggered fermions*, 2406.02906.
- [8] MILC collaboration, *Nonperturbative QCD Simulations with 2+1 Flavors of Improved Staggered Quarks*, *Rev. Mod. Phys.* **82** (2010) 1349 [[0903.3598](#)].
- [9] D.B. Kaplan, *A Method for simulating chiral fermions on the lattice*, *Phys. Lett. B* **288** (1992) 342 [[hep-lat/9206013](#)].

---

<sup>49</sup>See the companion chapter of the *LQCD@50* book by DeGrand [15].

- [10] T. DeGrand and C.E. Detar, *Lattice methods for quantum chromodynamics*, World Scientific (2006).
- [11] J. Smit, *Introduction to Quantum Fields on a Lattice*, vol. 15, Cambridge University Press (2003), 10.1017/9781009402705.
- [12] C. Gattringer and C.B. Lang, *Quantum chromodynamics on the lattice*, vol. 788, Springer, Berlin (2010), 10.1007/978-3-642-01850-3.
- [13] D.B. Kaplan, *Chiral Symmetry and Lattice Fermions*, in *Les Houches Summer School: Session 93: Modern perspectives in lattice QCD: Quantum field theory and high performance computing*, pp. 223–272, 12, 2009 [0912.2560].
- [14] F. Niedermayer, *Exact chiral symmetry, topological charge and related topics*, *Nucl. Phys. B Proc. Suppl.* **73** (1999) 105 [hep-lat/9810026].
- [15] T. DeGrand, *The Ginsparg-Wilson relation and overlap fermions*, 2512.07743.
- [16] P.H. Ginsparg and K.G. Wilson, *A Remnant of Chiral Symmetry on the Lattice*, *Phys. Rev. D* **25** (1982) 2649.
- [17] Y. Shamir, *Chiral fermions from lattice boundaries*, *Nucl. Phys. B* **406** (1993) 90 [hep-lat/9303005].
- [18] H. Neuberger, *Exactly massless quarks on the lattice*, *Phys. Lett. B* **417** (1998) 141 [hep-lat/9707022].
- [19] K. Jansen and M. Schmaltz, *Critical momenta of lattice chiral fermions*, *Phys. Lett. B* **296** (1992) 374 [hep-lat/9209002].
- [20] V. Furman and Y. Shamir, *Axial symmetries in lattice QCD with Kaplan fermions*, *Nucl. Phys. B* **439** (1995) 54 [hep-lat/9405004].
- [21] Y. Shamir, *Reducing chiral symmetry violations in lattice QCD with domain wall fermions*, *Phys. Rev. D* **59** (1999) 054506 [hep-lat/9807012].
- [22] M. Lüscher, *Construction of a Selfadjoint, Strictly Positive Transfer Matrix for Euclidean Lattice Gauge Theories*, *Commun. Math. Phys.* **54** (1977) 283.
- [23] R. Narayanan and H. Neuberger, *Chiral determinant as an overlap of two vacua*, *Nucl. Phys. B* **412** (1994) 574 [hep-lat/9307006].
- [24] R. Narayanan and H. Neuberger, *Chiral fermions on the lattice*, *Phys. Rev. Lett.* **71** (1993) 3251 [hep-lat/9308011].
- [25] P. Hernandez, K. Jansen and M. Lüscher, *Locality properties of Neuberger's lattice Dirac operator*, *Nucl. Phys. B* **552** (1999) 363 [hep-lat/9808010].
- [26] Y. Kikukawa, *Locality bound for effective four-dimensional action of domain wall fermion*, *Nucl. Phys. B* **584** (2000) 511 [hep-lat/9912056].

- [27] M.F.L. Golterman, K. Jansen and D.B. Kaplan, *Chern-Simons currents and chiral fermions on the lattice*, *Phys. Lett. B* **301** (1993) 219 [[hep-lat/9209003](#)].
- [28] Y. Shamir, *Anomalies and chiral defects fermions*, *Nucl. Phys. B* **417** (1994) 167 [[hep-lat/9310006](#)].
- [29] C.G. Callan, Jr. and J.A. Harvey, *Anomalies and Fermion Zero Modes on Strings and Domain Walls*, *Nucl. Phys. B* **250** (1985) 427.
- [30] H. Neuberger, *Vector - like gauge theories with almost massless fermions on the lattice*, *Phys. Rev. D* **57** (1998) 5417 [[hep-lat/9710089](#)].
- [31] M. Golterman and Y. Shamir, *Propagator Zeros and Lattice Chiral Gauge Theories*, *Phys. Rev. Lett.* **132** (2024) 081903 [[2311.12790](#)].
- [32] M. Golterman and Y. Shamir, *Constraints on the symmetric mass generation paradigm for lattice chiral gauge theories*, *Phys. Rev. D* **113** (2026) 014503 [[2505.20436](#)].
- [33] Y. Kikukawa and T. Noguchi, *Low-energy effective action of domain wall fermion and the Ginsparg-Wilson relation*, *Nucl. Phys. B Proc. Suppl.* **83** (2000) 630 [[hep-lat/9902022](#)].
- [34] RBC, UKQCD collaboration, *Domain wall QCD with physical quark masses*, *Phys. Rev. D* **93** (2016) 074505 [[1411.7017](#)].
- [35] M. Lüscher, *Exact chiral symmetry on the lattice and the Ginsparg-Wilson relation*, *Phys. Lett. B* **428** (1998) 342 [[hep-lat/9802011](#)].
- [36] M. Golterman, S.R. Sharpe and R.L. Singleton, Jr., *Effective theory for quenched lattice QCD and the Aoki phase*, *Phys. Rev. D* **71** (2005) 094503 [[hep-lat/0501015](#)].
- [37] T. Blum and A. Soni, *Domain wall quarks and kaon weak matrix elements*, *Phys. Rev. Lett.* **79** (1997) 3595 [[hep-lat/9706023](#)].
- [38] T. Blum et al., *Quenched lattice QCD with domain wall fermions and the chiral limit*, *Phys. Rev. D* **69** (2004) 074502 [[hep-lat/0007038](#)].
- [39] S. Aoki and Y. Taniguchi, *One loop calculation in lattice QCD with domain wall quarks*, *Phys. Rev. D* **59** (1999) 054510 [[hep-lat/9711004](#)].
- [40] S. Aoki, T. Izubuchi, Y. Kuramashi and Y. Taniguchi, *Perturbative renormalization factors of quark bilinear operators for domain wall QCD*, *Phys. Rev. D* **59** (1999) 094505 [[hep-lat/9810020](#)].
- [41] Y. Shamir, *New domain wall fermion actions*, *Phys. Rev. D* **62** (2000) 054513 [[hep-lat/0003024](#)].

- [42] G.P. Lepage and P.B. Mackenzie, *On the viability of lattice perturbation theory*, *Phys. Rev. D* **48** (1993) 2250 [[hep-lat/9209022](#)].
- [43] J.C. Collins, *Renormalization : An Introduction to Renormalization, the Renormalization Group and the Operator-Product Expansion*, vol. 26 of *Cambridge Monographs on Mathematical Physics*, Cambridge University Press, Cambridge (1984), 10.1017/9781009401807.
- [44] CP-PACS collaboration, *Chiral properties of domain wall quarks in quenched QCD*, *Phys. Rev. D* **63** (2001) 114504 [[hep-lat/0007014](#)].
- [45] RBC-UKQCD collaboration, *Physical Results from 2+1 Flavor Domain Wall QCD and SU(2) Chiral Perturbation Theory*, *Phys. Rev. D* **78** (2008) 114509 [[0804.0473](#)].
- [46] S.R. Sharpe, *Future of Chiral Extrapolations with Domain Wall Fermions*, in *Workshop on Domain Wall Fermions at Ten Years*, 6, 2007 [[0706.0218](#)].
- [47] RBC, UKQCD collaboration, *Continuum Limit Physics from 2+1 Flavor Domain Wall QCD*, *Phys. Rev. D* **83** (2011) 074508 [[1011.0892](#)].
- [48] S. Aoki, *New Phase Structure for Lattice QCD with Wilson Fermions*, *Phys. Rev. D* **30** (1984) 2653.
- [49] S. Aoki, *A Solution to the U(1) Problem on a Lattice*, *Phys. Rev. Lett.* **57** (1986) 3136.
- [50] N. Kawamoto and J. Smit, *Effective Lagrangian and Dynamical Symmetry Breaking in Strongly Coupled Lattice QCD*, *Nucl. Phys. B* **192** (1981) 100.
- [51] S.R. Sharpe and R.L. Singleton, Jr, *Spontaneous flavor and parity breaking with Wilson fermions*, *Phys. Rev. D* **58** (1998) 074501 [[hep-lat/9804028](#)].
- [52] M. Golterman and Y. Shamir, *Localization in lattice QCD*, *Phys. Rev. D* **68** (2003) 074501 [[hep-lat/0306002](#)].
- [53] R.G. Edwards, U.M. Heller and R. Narayanan, *Spectral flow, chiral condensate and topology in lattice QCD*, *Nucl. Phys. B* **535** (1998) 403 [[hep-lat/9802016](#)].
- [54] F. Berruto, R. Narayanan and H. Neuberger, *Exact local fermionic zero modes*, *Phys. Lett. B* **489** (2000) 243 [[hep-lat/0006030](#)].
- [55] S. Aoki and Y. Taniguchi, *Chiral properties of domain wall fermions from eigenvalues of four-dimensional Wilson-Dirac operator*, *Phys. Rev. D* **65** (2002) 074502 [[hep-lat/0109022](#)].

- [56] M. Golterman and Y. Shamir, *Localization in lattice QCD (with emphasis on practical implications)*, *Nucl. Phys. B Proc. Suppl.* **129** (2004) 149 [hep-lat/0309027].
- [57] A.J. McKane and M. Stone, *Localization as an alternative to Goldstone's theorem*, *Annals Phys.* **131** (1981) 36.
- [58] M. Golterman, Y. Shamir and B. Svetitsky, *Mobility edge in lattice QCD*, *Phys. Rev. D* **71** (2005) 071502 [hep-lat/0407021].
- [59] M. Golterman, Y. Shamir and B. Svetitsky, *Localization properties of lattice fermions with plaquette and improved gauge actions*, *Phys. Rev. D* **72** (2005) 034501 [hep-lat/0503037].
- [60] RBC, UKQCD collaboration, *Localization and chiral symmetry in three flavor domain wall QCD*, *Phys. Rev. D* **77** (2008) 014509 [0705.2340].
- [61] I. Horvath, *Ginsparg-Wilson relation and ultralocality*, *Phys. Rev. Lett.* **81** (1998) 4063 [hep-lat/9808002].
- [62] R.G. Edwards and U.M. Heller, *Domain wall fermions with exact chiral symmetry*, *Phys. Rev. D* **63** (2001) 094505 [hep-lat/0005002].
- [63] Y. Aoki et al., *Domain wall fermions with improved gauge actions*, *Phys. Rev. D* **69** (2004) 074504 [hep-lat/0211023].
- [64] B. Svetitsky, Y. Shamir and M. Golterman, *Localization of lattice fermions: Lessons for overlap*, *PoS LAT2005* (2006) 129 [hep-lat/0508015].
- [65] Y. Iwasaki and T. Yoshie, *Renormalization Group Improved Action for SU(3) Lattice Gauge Theory and the String Tension*, *Phys. Lett. B* **143** (1984) 449.
- [66] QCD-TARO collaboration, *Renormalization group flow of SU(3) lattice gauge theory: Numerical studies in a two coupling space*, *Nucl. Phys. B* **577** (2000) 263 [hep-lat/9911033].
- [67] P.M. Vranas, *Gap Domain Wall Fermions*, *Phys. Rev. D* **74** (2006) 034512 [hep-lat/0606014].
- [68] JLQCD collaboration, *Lattice gauge action suppressing near-zero modes of  $H(W)$* , *Phys. Rev. D* **74** (2006) 094505 [hep-lat/0607020].
- [69] D. Renfrew, T. Blum, N. Christ, R. Mawhinney and P. Vranas, *Controlling Residual Chiral Symmetry Breaking in Domain Wall Fermion Simulations*, *PoS LATTICE2008* (2008) 048 [0902.2587].
- [70] RBC, UKQCD collaboration, *Direct CP violation and the  $\Delta I = 1/2$  rule in  $K \rightarrow \pi\pi$  decay from the standard model*, *Phys. Rev. D* **102** (2020) 054509 [2004.09440].

- [71] RBC, UKQCD collaboration,  $\Delta I=3/2$  and  $\Delta I=1/2$  channels of  $K \rightarrow \pi\pi$  decay at the physical point with periodic boundary conditions, *Phys. Rev. D* **108** (2023) 094517 [2306.06781].
- [72] E.-H. Chao and N. Christ, Calculating the two-photon exchange contribution to  $KL \rightarrow \mu + \mu^-$  decay, *Phys. Rev. D* **110** (2024) 054514 [2406.07447].
- [73] G.E. McGlynn, *Advances in Lattice Quantum Chromodynamics*, Ph.D. thesis, Columbia U., 2016. 10.7916/D8T72HD7.
- [74] R.C. Brower, H. Neff and K. Orginos, The Möbius domain wall fermion algorithm, *Comput. Phys. Commun.* **220** (2017) 1 [1206.5214].
- [75] A. Boriçi, *Truncated overlap fermions: The Link between overlap and domain wall fermions*, *NATO Sci. Ser. C* **553** (2000) 41 [hep-lat/9912040].
- [76] UKQCD collaboration, *Conserved currents for Möbius Domain Wall Fermions*, *PoS LATTICE2014* (2015) 087.
- [77] T.-W. Chiu, *Optimal domain wall fermions*, *Phys. Rev. Lett.* **90** (2003) 071601 [hep-lat/0209153].
- [78] TWQCD collaboration, *Chiral Symmetry and the Residual Mass in Lattice QCD with the Optimal Domain-Wall Fermion*, *Phys. Rev. D* **86** (2012) 094508 [1205.6151].
- [79] W. Bietenholz, *Solutions of the Ginsparg-Wilson relation and improved domain wall fermions*, *Eur. Phys. J. C* **6** (1999) 537 [hep-lat/9803023].
- [80] W. Bietenholz, *Optimised Dirac Operators on the Lattice: Construction, Properties and Applications*, *Fortsch. Phys.* **56** (2008) 107 [hep-lat/0611030].
- [81] K. Jansen and K.-i. Nagai, *Reducing residual mass effects for Domain-Wall fermions*, *JHEP* **12** (2003) 038 [hep-lat/0305009].
- [82] R. Narayanan and H. Neuberger, *A Construction of lattice chiral gauge theories*, *Nucl. Phys. B* **443** (1995) 305 [hep-th/9411108].
- [83] M.F.L. Golterman and Y. Shamir, *The Relation between the waveguide and overlap implementations of Kaplan's domain wall fermions*, *Phys. Lett. B* **353** (1995) 84 [hep-lat/9501035].
- [84] M. Lüscher, *Abelian chiral gauge theories on the lattice with exact gauge invariance*, *Nucl. Phys. B* **549** (1999) 295 [hep-lat/9811032].
- [85] M. Lüscher, *Weyl fermions on the lattice and the nonAbelian gauge anomaly*, *Nucl. Phys. B* **568** (2000) 162 [hep-lat/9904009].
- [86] M. Lüscher, *Lattice regularization of chiral gauge theories to all orders of perturbation theory*, *JHEP* **06** (2000) 028 [hep-lat/0006014].

- [87] O. Bär and I. Campos, *Global anomalies in chiral gauge theories on the lattice*, *Nucl. Phys. B* **581** (2000) 499 [hep-lat/0001025].
- [88] D.M. Grabowska and D.B. Kaplan, *Nonperturbative Regulator for Chiral Gauge Theories?*, *Phys. Rev. Lett.* **116** (2016) 211602 [1511.03649].
- [89] D.B. Kaplan, *Chiral Gauge Theory at the Boundary between Topological Phases*, *Phys. Rev. Lett.* **132** (2024) 141603 [2312.01494].
- [90] D.B. Kaplan and S. Sen, *Weyl Fermions on a Finite Lattice*, *Phys. Rev. Lett.* **132** (2024) 141604 [2312.04012].
- [91] M. Golterman and Y. Shamir, *Conserved currents in five-dimensional proposals for lattice chiral gauge theories*, *Phys. Rev. D* **109** (2024) 114519 [2404.16372].
- [92] D.B. Kaplan and S. Sen, *Regulated chiral gauge theory and the strong CP problem*, 2412.02024.
- [93] T. Blum and A. Soni, *QCD with domain wall quarks*, *Phys. Rev. D* **56** (1997) 174 [hep-lat/9611030].
- [94] Y. Aoki et al., *Continuum Limit of  $B_K$  from 2+1 Flavor Domain Wall QCD*, *Phys. Rev. D* **84** (2011) 014503 [1012.4178].
- [95] RBC, UKQCD collaboration, *Update of Euclidean windows of the hadronic vacuum polarization*, *Phys. Rev. D* **108** (2023) 054507 [2301.08696].
- [96] RBC, UKQCD collaboration, *Long-Distance Window of the Hadronic Vacuum Polarization for the Muon  $g-2$* , *Phys. Rev. Lett.* **134** (2025) 201901 [2410.20590].
- [97] M. Cheng, N.H. Christ, M. Li, R.D. Mawhinney, D. Renfrew, P. Hegde et al., *The finite temperature QCD using 2 + 1 flavors of domain wall fermions at  $N(t) = 8$* , *Phys. Rev. D* **81** (2010) 054510 [0911.3450].
- [98] A. Tomiya, G. Cossu, S. Aoki, H. Fukaya, S. Hashimoto, T. Kaneko et al., *Evidence of effective axial  $U(1)$  symmetry restoration at high temperature QCD*, *Phys. Rev. D* **96** (2017) 034509 [1612.01908].
- [99] JLQCD collaboration,  *$B \rightarrow D^* \ell \nu \ell$  semileptonic form factors from lattice QCD with Möbius domain-wall quarks*, *Phys. Rev. D* **109** (2024) 074503 [2306.05657].
- [100] RBC/UKQCD collaboration, *Exclusive semileptonic  $B_s \rightarrow K \ell \nu$  decays on the lattice*, *Phys. Rev. D* **107** (2023) 114512 [2303.11280].

- [101] P.A. Boyle, L. Del Debbio, A. Juttner, A. Khamseh, J.T. Tsang and O. Witzel, *Heavy Domain Wall Fermions: The RBC and UKQCD charm physics program*, *EPJ Web Conf.* **175** (2018) 13013 [1712.00862].
- [102] Z. Bai, N.H. Christ, J.M. Karpie, C.T. Sachrajda, A. Soni and B. Wang, *Long-distance contribution to  $\varepsilon K$  from lattice QCD*, *Phys. Rev. D* **109** (2024) 054501 [2309.01193].
- [103] R. Mawhinney, *RBC-UKQCD DWF Ensembles*, Lattice 2024, Liverpool, August, 2024.
- [104] JLQCD collaboration, *Two-flavor QCD simulation with exact chiral symmetry*, *Phys. Rev. D* **78** (2008) 014508 [0803.3197].
- [105] C. Aubin, T. Blum, M. Golterman and S. Peris, *Muon anomalous magnetic moment with staggered fermions: Is the lattice spacing small enough?*, *Phys. Rev. D* **106** (2022) 054503 [2204.12256].
- [106] M. Cè et al., *Window observable for the hadronic vacuum polarization contribution to the muon  $g-2$  from lattice QCD*, *Phys. Rev. D* **106** (2022) 114502 [2206.06582].
- [107] FERMILAB LATTICE, HPQCD,, MILC collaboration, *Hadronic Vacuum Polarization for the Muon  $g-2$  from Lattice QCD: Long-Distance and Full Light-Quark Connected Contribution*, *Phys. Rev. Lett.* **135** (2025) 011901 [2412.18491].